Photophysical Properties of Anthracenic Metal Organic Frameworks

Jennifer Marie Hay

Thesis submitted to the faculty of the Virginia Polytechnic Institute and State University
in partial fulfillment of the requirements for the degree of

Master of Science
In
Chemistry

Amanda J. Morris, Chair
Karen J. Brewer
Brian E. Hanson

September 24th, 2014
Blacksburg, VA

Keywords: Luminescence, Metal Organic Frameworks, Photophysics

Photophysical Properties of Anthracenic Metal Organic Frameworks

Jennifer Marie Hay

Abstract: Luminescent metal organic frameworks (MOFs) are promising new materials with applications as sensors, photocatalysts, and other luminescent devices. Although MOFs retain the chemical and physical properties of their constituents, the properties of the MOF are often altered from those of its building blocks, making rational design and synthesis difficult.

Anthracene is a polyaromatic hydrocarbon whose photophysical properties have been found to be easily tuned through structural modifications. The tunability of anthracene makes it an ideal candidate for use in luminescent devices, such as photoprobes and organic light emitting diodes.

MOFs designed with π conjugated molecules like anthracene ligands possess similar photophysical properties such as absorption and fluorescence in the UV and visible spectrum. In hopes of better understanding how the photophysical properties of the organic ligand is altered upon incorporation into a MOF, the spectroscopic properties of anthracenedicarboxylic acids were studied before and after integration into zinc based MOFs.

Steady state and time resolved measurements were performed on three anthracenedicarboxylic acids: 9,10-anthracenedicarboxylic acid, 2,6-anthracendicarboxylic acid, and 1,4-anthracenedicarboxylic acid. The position of the carboxylic acid groups on anthracene was found to effect the position and structure of the absorption and emission spectra. The difference in the spectra is attributed to the

perturbation by the acid groups on certain electronic transitions with dipole moments across two of the three axes of anthracene. The position of the acid groups had different effects on the fluorescence quantum yields and lifetimes of the three anthracenic acids studied.

Two of the linkers were synthesized into MOFs through a solvothermal reaction with zinc nitrate, to form PCN-13, from 9,10-anthracenedicarboxylic acid, and $[Zn(C_{16}H_8O_4)(H_2O)]_n$, from 2,6-anthracenedicarboxylic acid. The luminescent properties of the two MOFs were studied and compared to those of the free based linker. Incorporation of the luminescent anthracenedicarboxylic acids into Zn based MOFs were found to either increase or decrease the luminescent properties of the ligands.

Acknowledgements

I would like to thank my advisor, Dr. Amanda Morris, whose support has made this work possible. Thank you for your encouraging words and guidance. You have been the most influential professional mentor that has made an impression on me. You have helped me to grow both professionally and as an individual.

I would like to thank my husband, Christian, who has been by my side through some very trying times in the past and continued to support me throughout my graduate career. Words cannot describe how thankful I am for your constant support and love. Without you I would not have been able to accomplish so much.

To my parents, William and Sarah Hay, I would also like to express my extreme appreciation for their support and guidance throughout the years. I am beyond grateful to have such amazing people, not just in my life, but as my parents as well. You two have provided me with every opportunity possible, and have supported me in all my decisions.

I would like to express my gratitude for all of the help provided by Dr. William Maza. Without your guidance, contributions, and willingness to teach me, I would not have been able to accomplish so much in the lab.

I would also like to thank my committee members Dr. Karen Brewer and Dr. Brian Hanson whose patience and support has been critical to this work. Thank you for your guidance me throughout the years and for believing in my ability to succeed.

Attribution

Throughout this research project, multiple peers have guided my work. Chapter 2 summarizes the results on the three anthracenic acids and will soon be submitted for publication. A brief description of their contributions towards this publication has been added here.

Chapter 2: Systematic Investigation of the Excited State Properties Anthracenedicarboxylic Acids

Chapter 2 will be submitted to *The Journal of Physical Chemistry A*

Dr. William Maza, currently a post-doc in Dr. Amanda Morris' group, provided guidance and direction in the experimental design and analysis of the data presented in Chapter 2. He has also contributed by attaining the fluorescence lifetimes of the three acids in various solvents.

Robert Chapleski, a graduate student in Dr. Diego Troya's group, performed coordinate scan DFT calculations on the anthracenedicarboxylic acids.

Table of contents

List of Figures

List of Tables

Chapter 1: Ligand Centered Excited State Properties of Metal Organic Frameworks

1.1 Luminescent Metal Organic Frameworks

Metal organic frameworks (MOFs) are porous inorganic-organic hybrid materials with a wide range of potential applications in gas storage[1], catalysis[2], sensors[3], and separations[4]. These crystalline solids are comprised of inorganic clusters connected by functionalized organic molecules to form a 3D porous network. The chemical and physical properties of MOFs arise from the individual building blocks, which allows them to be tuned for specific applications by appropriate choice of metal and organic ligand. Postsynthetic modification provides additional means of controlling the structure and properties of these materials, affording an even wider range of possible uses.[5]

Luminescent MOFs can be designed for applications as sensors[6], photocatalysts[7], sensitizers[8], and for use in optoelectronics[9-10] , often through the incorporation of luminescent organic linkers and/or metals. Photo-excitation a MOF results in a complex that is more reactive towards electron or proton transfer and more readily undergoes chemical reactions.[7, 11] The rational design of MOFs for photophysical applications requires an understanding of how the excited state properties of the individual components, organic ligand and metal ions, are effected once incorporated into a MOF. Knowledge of the dynamics of the excited state is essential to understanding photophysical and photochemical processes and how these processes are affected by the local environment.

Recently interest in luminescent MOFs for the sensing of gases and vapours has increased because of the advantages these materials provide over current sensors. Due to their highly porous

nature, MOFs absorb analytes in greater concentrations within the system than external environment, allowing for better and possibly more sensitive detection of gases and vapours.[12] Luminescent MOFs for sensing are often comprised of rigid aromatic linkers, which provides $\pi^* \rightarrow \pi$ or $n^* \rightarrow \pi$ based emission which is susceptible to quenching or enhanced luminescence, through interactions with guest species.

Luminescent MOFs have found further applications as photocatalysts in part due to their porosity, resulting in more available catalytic sites than nonporous catalysts. They also provide the tunability, whereupon the wavelength of excitation can be adjusted by organic linker conjugation and functionalization, and they become better oxidants and reductants upon photoexcitation. The ease with which MOFs may be recovered and reused provides an additional advantage for their use as heterogeneous photcatatalysts.

Ideally luminescent MOFs may be rationally designed by selective choice of an organic linker with desired emissive properties, but often the photophysical properties of the organic backbone is effected by the new environment within the MOF. Reports show linker based emission of MOFs is less structured and broadened, with increased fluorescence lifetime, τ_{fl}, and quantum yields, Φ_{fl} due to the more rigid environment, aggregation effects, or metal-ligand interactions.[13] Although the photophysics of MOFs and their constituents has been studied throughout the literature, a better understanding of their structure-property relationships is still lacking. This chapter is an accumulation of the relevant literature pertaining to excited state processes within MOFs and how they differ from their individual building blocks, with a focus on MOFs constructed from polyaromatic ligands.

1.2 Advantages of MOFs for Luminescent Devices.

There are a number of benefits to using MOFs for a wide range of applications due to their ease of synthesis, thermal stability, structure predictability, and structural integraty due to the strong bonds between linkers and metal clusters and ions.[14-15] Through the use of reticular synthesis MOFs may be designed with predetermined structures due the formation of secondary building units (SBUs).[16] MOF synthesis is often performed using solvothermal techniques where the organic linker and metal salt are dissolved in organic solvent(s) and heated at temperatures ranging from room temperature to 200 °C for a couple hours to a few days.[15] Alternative methods used in the synthesis of MOFs include slow evaporation methods, microwave-assisted techniques, electrochemical methods, and solvent free syntheses.[17]

Interest in fluorescent MOFs with applications as sensors and photocatalysts has flourished as researchers have explored the effects of incorporating luminescent metals, linkers, and guest molecules into MOFs.[18-20] Upon absorption of a photon, electrons are promoted to an excited state, where a number of radiation and radiationless relaxation processes can occur, including internal conversion, fluorescence, intersystem crossing, and phosphorescence. All of these processes are effected by, not only the nature of the ground and excited states of the material, but also its microenvironment (solvent and analyte molecules, temperature, etc.). In MOFs the luminescence can be generated from both the organic linker and inorganic salt with possible metal-to-ligand and ligand-to-metal charge transfer. It is therefore necessary to gain an understanding of the difference between the photophysics (quantum yields, excited state lifetimes, radiative and nonradiative rate constants, etc.) of the individual components incorporated into MOFs, and the photophysics of the MOF itself, if one hopes to design MOFs rationally.

MOFs have the highest known surface area (~3000 m^2 g^{-1}) and pore volumes (1-2 cm^3 g^{-1}), and as a result, they have been well studied for applications in gas storage.[16] It has been shown, in the work of Yahgi et al., that by functionalization of the organic ligands, it is possible to obtain isoreticular MOFs with differing pore volumes, suitable for gas storage and separations. In their work with MOFs of the zeolitic imidazole framework (ZIF) series, the pore diameter was varied from 7.1 to 15.9 Å through alteration of the imidazole linker with polar and nonpolar groups, resulting in MOFs with selective gas absorption of CO_2.[21] In a similar fashion, it is possible to design MOFs with specific excited state properties through ligand modification.

An advantage to using MOFs as sensors or photocatalysts is that they can be tuned to absorb and/or emit light of a specific energy through appropriate choice of organic linker. An example of the tunability of MOF properties through variation of the organic linker is observed in the work of Mul et al.[22] In their work they were able to effect the metal-to-ligand charge-transfer energy within the IRMOF series by substitution of different carboxylate functionalized aromatic linkers into the Zn based IRMOF series (Figure 1-1). They found that the HOMO-LUMO gap of the IRMOFs could be decreased with increased conjugation and the addition of electron donating substituents. A few of the MOFs under study, with absorption edge in the 400-314 nm range, showed photocatalytic activity towards propene oxidation, with IRMOF-8, formed from 2,6-naphthalenedicarboxylic acid, showing the highest activity.[22]

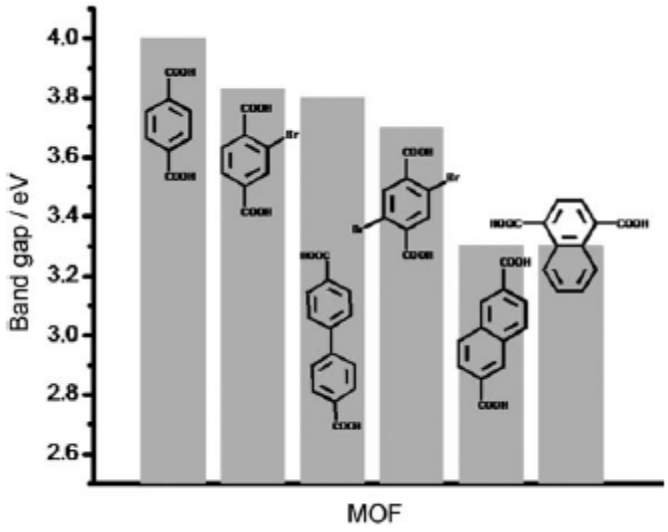

Figure 1-1. Example of tunable band gaps of the IRMOF series by substitution of aromatic linkers. (Reprinted with permission from ChemSusChem 2008, 1 (12), 981-983.)

Excited state dynamics are susceptible to environmental effects, therefore, incorporation of an organic molecule into a MOF may result in a compound with different excited state properties than molecule on its own. In some cases, incorporation of a luminescent ligand into a more rigid environment like a MOF may result in benefits like increased quantum yields and lifetimes. Such an effect is observed when tetrakis(4-carboxyphenyl)ethylene ($TCPE^{4-}$) is used as a ligand in a d^{10} metal-centered MOFs of the formulas $(Zn_2(C_{30}H_{16}O_8)(H_2O)\bullet 4DEF$ (1) and $Cd_2(C_{30}H_{16}O_8)(DEF)(C_2H_5OH)_2\bullet DEF$ (2)). The phenyl rings of tetraphenylethylene(TPE) rotate freely in dilute solutions, resulting in quenched fluorescence, but upon aggregate formation in solution or in the solid state, these rotations are hindered and emission is observed.[23] Dincă and co-workers found that MOFs **1** and **2** exhibit similar fluorescence to the solid linker, H_4TCPE, with emission maxima for the MOFs at 480 nm (**1**) and 455 nm (**2**) (Figure 1-2).[24] The fluorescence of the MOFs decay in a biexponential manner similar to the solid linker.

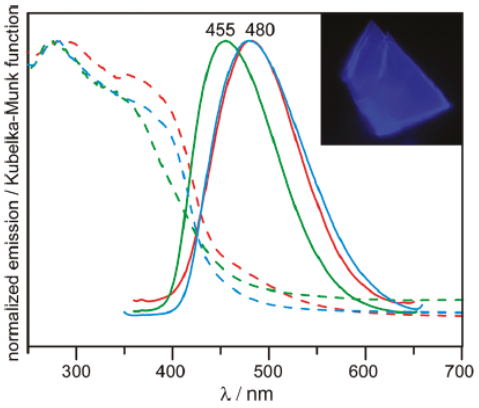

Figure 1-2. Solid state diffuse reflectance (dotted lines) and emission (solid lines) spectra of H_4TCPE (blue), **1** (red), and **2** (green), and an epifluorescence microscopy image for a crystal of **2** (inset). (Reprinted with permission from Journal of the American Chemical Society 2011, 133 (50), 20126-20129. Copyright (2014) American Chemical Society)

The emission from MOFs **1** and **2** are linker based, but results not from aggregation effects as in the solid linker, but from the rigidity of the MOF environment. Solid-state ^{1}H and ^{13}C NMR studies and DFT calculations were conducted by Dincă and co-workers[25] on the Zn based MOF to determine the dynamics of the phenyl ring systems. They found that the activation energy of the phenyl ring flip in the orthorhombic form of the MOF to be 43(6) kJ/mol, which is greater than free TPE (20 kJ/mol), and believed to be the cause of the fluorescence turn-on in the MOF.[25]

1.3 Typical Ligands Used in MOF Synthesis

Organic ligands used in MOF synthesis may range from simple molecules like terephthalic acid, used in the synthesis[26] of IRMOF-1, to complex compounds such as 5,5'-(naphthalene-2,6-diyl)diisophthalic acid, used in the synthesis[27] of a scintillating MOF. The choice of ligand is generally dependent on the intended application and/or desired topology. Ligands are

functionalized with groups capable of forming strong bonds with metals. These groups often include, but are not limited to, carboxylates[16, 28], amines[29], pyridines[30], and phosphates[31].

Figure 1-3. Common aromatic ligands of MOFs (a.) terephthalic acid (b.) 2,6-naphthacenedicarboxylic acid (c.) 9,10-anthracenedicarboxylic acid (d.) 1,3,6,8-tetrkis(p-benzoic acid)pyrene and (e.) 5,10,15,20-tetra(4-pyridyl) porphyrin.

Chromophoric organic ligands are generally aromatic, containing conjugated π-systems.[32] Electrons within the π-system of the ligand will, upon absorption of a photon with enough energy, be excited into a higher electronic state than S_0. Once in an excited electronic state, the excess energy is dispelled through radiative relaxation processes, resulting in luminescence or phosphorescence. MOFs which exhibit interesting photophysics are often composed of aromatic organic linkers such as benzene and benzene systems (azobenzene[33], naphthalene[22], anthracene[34], pyrene[35], etc.) and porphyrins[36-38] (Figure 1-3). Incorporation of photoactive ligands into MOFs yields a crystalline structure with dimensions large enough to absorb a significant quantity of light, yet small enough that excited states may migrate to the MOF/surroundings interface where interactions with the surrounding media can occur.[39-40]

Multidentate carboxylate groups are most often used as connecting groups in MOF synthesis because they form a variety of rigid SBUs with the metal ions and provide stability and increase the ability to predict the topology of the overall framework.[41-43] MOFs have also been constructed from monodentate chelating groups like 4,4'-bipyridine (bpy) and 4,4'-bipyridyl (bipy), but coordination through these sorts of functionalities often result in less predictable topologies which are often interpenetrated due to the unpredictable nature of the coordination sphere, and are known to collapse into non-porous structures upon activation.[16, 43-46] MOFs constructed from bpy and bipy ligands often have large pores, which often results in a highly

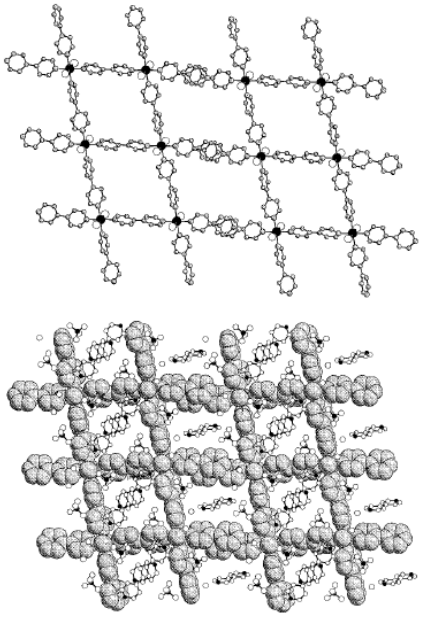

Figure 1-4. Non-interpenetrated framework of $Ni(4,4'\text{-bpy})_{2.5}(H_2O)_2\cdot(ClO_4)_2\cdot 1.5(4,4'\text{-bpy})\cdot 2H_2O$, showing 4,4'-bpy, water, and perchlorate within the pores. (Reprinted with permission from Inorg. Chem., 1997, 36 (20), pp 4292–4293. Copyright (2014) American Chemical Society)

interpenetrated network. One example of interpenetrated bpy networks was observed with Ag(4,4'-bpy)·NO_3, which is composed of three interpenetrated chains cross-linked in a near orthogonal geometry.[45] Yaghi et al. has shown that it is possible to prevent interpenetrated structures through the inclusion of hydrogen-bonded guest aggregates within the pores of the

MOF. The use of space filling guests, like hydrogen-bonded hydrate ions and bpy aggregates, were shown to prevent interpenetrated frameworks in the case of Ni(4,4'-bpy)$_{2.5}$(H_2O)$_2$·(ClO_4)$_2$·1.5(4,4'-bpy)·2H_2O (Figure 1-4).[44]

Absorption and emission processes in MOFs composed of aromatic linkers can occur through electronic interactions between the ligand and the metal clusters or they may be primarily ligand or metal based. In aromatic ligands like those listed above, the electronic transitions between the HOMO and LUMO are $\pi \rightarrow \pi^*$ based. Once incorporated into a MOF, the HOMO and LUMO may still reside on the π-system or, as a result of orbital overlap and electronic effects due to functional groups and chelation, the frontier orbitals may reside on the metal or metal clusters. An a example of a shift in the location of the HOMO and LUMO from purely linker based to linker and metal, is observed when 2,2'-dihydroxy-[1,1']-binaphthalene-3,3'-dicarboxylic acid (H_2bna) is integrated into Cd(II) or Zn(II) based MOFs.[47] Wong et al. found that the luminescence of the MOF was more intense than solid H_2Bna and longer lived due to ligand complexation with d^{10} metal-hydroxy (or oxy) clusters, which provides stability to the ligand, resulting in fewer pathways of radiationless decay. Theoretical calculations showed that the HOMO and LUMO of the ligand are associated with the π-system of the naphthalene derivative but, in the case of the MOF, the HOMO still resides on the ligand but the LUMO is d^{10}-metal-oxygen based resulting in ligand-to-metal charge transfer (LMCT) emission.

Aromatics molecules containing heteroatoms provide another characteristic transition, n → π*, when the non-bonding orbitals are higher in energy than the π orbitals of the conjugated system, the n → π* will be the lowest lying transition. In the case of 1,3,5-benzenetricarboxylic acid (H_3BTC), a common ligand in MOF synthesis[48-50], the lowest energy transition in the absorption spectrum is the n → π* transition, with the π → π* transition appearing at shorter wavelengths. Fang et al. have incorporated BTC into Zn and Cd frameworks and found the emission is π*→ n based and red-shifted relative to the free based linker.[48] The similar shape and location of the fluorescence of the Zn and Cd BTC MOFs are very similar to free H_3BTC, suggesting that the emission is primarily linker based with little perturbation resulting from coordination to the metal sites.

Phosphorescent MOFs are promising candidates for sensing materials because intersystem crossing from an excited singlet to triplet state results in a large bathochromic shift between the absorption and emission, which simplifies device configuration by reducing the interference of the excitation beam.[51] Phosphorescent metal complexes, like $Ru(bpy)_3$, have been incorporated into the MOFs because of the ability of the complex to absorb light over a broad range of wavelengths and because the dynamics of the ^{3}MLCT excited states are well understood. Kent et al. incorporated Ru(II)-bpy building blocks into a series of Zn based MOFs of the molecular formulas $[ZnL_1]\cdot 2DMF\cdot 4H_2O$ (MOF-1) and $[Zn(L_2\text{-}H_2)]\cdot 3H_2O$ (MOF-2), where L_1 is $[Ru[4,4'\text{-}(CO_2)_2\text{-}bpy]_2(bpy)]^{2-}$ and L_2-H_2 is $[Ru[4,4'\text{-}bpy)]_2(CN)_2]^{4-}$.[40] MOFs 1 and 2 exhibited light harvesting abilities due to the Ru(II)-bpy building blocks, and were capable of long-range electron migration to the MOF/solution interface where oxidative or reductive quenching could occur through interactions with 1,4-benzoquinone (oxidative quencher) or N,N,N',N'-tetramethylbenzidine (reductive quencher). The introduction of the cationic quencher methylene blue was found to

amplify the quenching of emission of MOF-2 by 7000 fold compared to quenching of free $Ru(bpy)_2CN_2$.[51]

Luminescent ligands capable of excited state electron or proton transfer provide interesting photophysical properties when incorporated into a MOF. Organic ligands capable of excited state intramolecular proton transfer (ESIPT) have been incorporated into MOFs to tune the emission.[11, 52] Jayaramulu et al. synthesized a MOF of the formula $[Mg(DHT)(DMF)_2]_n$ where DHT is 2,5-dihydroxy-terephthalate, a ligand capable of proton transfer in its excited state, through the process of enol to keto tautomerization.[11] The excited state proton transfer capabilities of the MOF allowed for its emission to be "tuned" through the use of solvent molecules in both solution and in the solid state (Figure 1-5)[11]. The freebased linker H_2DHT emits in the green in polar aprotic solvents like DMF and DMSO, with maxima 510 nm. In protic solvents like ethanol, DHT emits in the blue with a maximum around 440 nm. The shift in the emission is believed to be due to additional excited state processes like ESIPT, where the blue emission is attributed to the enol isomer and the green emission is attributed to the keto isomer of free DHT. The presence of uncomplexed hydroxide groups of DHT allows the MOF to exhibit tunable emission due to ESIPT. The MOF displays a blue emission in ethanol and trifluoroacetic acid (TFA) acidified DMSO. In ethanol and acidified DMSO, DHT is present as the enol isomer due to the formation of intermolecular hydrogen bonds preventing the ESIPT process from occurring. In water and DMSO, DHT is present as the keto isomer as a result of ESIPT and exhibits yellow and green emission, respectively. In DMF the MOF emits in the blue to yellow range, suggesting that various exited state processes are involved.[11] Desolvation of the $[Mg(DHT)]_n$ framework was shown to result in selective sensing of Cu(II), due to luminescence quenching, in both DMSO and the solid state. The

MOF was shown to be reusable through the process of removing the Cu(II) ions, using the chelating agent EDTA, without framework collapse.[53]

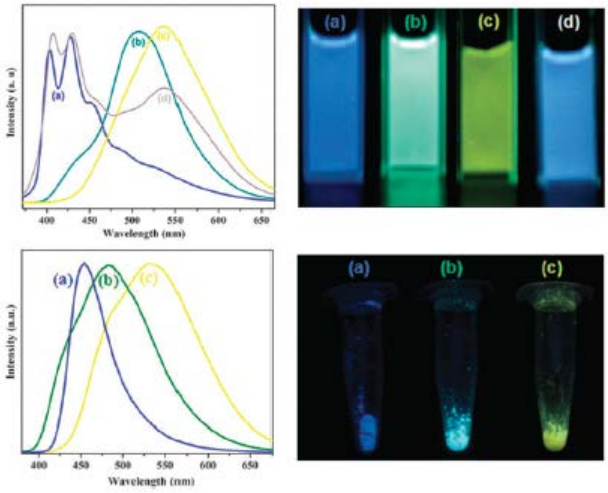

Figure 1-5. (Top) Normalized fluorescence spectra of $[Mg(DHT)(DMF)_2]_n$ and photographs of each sample under UV light; (a) ethanol, (b) DMSO, (c) water, and (d) DMF. (Bottom) Normalized fluorescence spectra of $[Mg(DHT)(DMF)_2]_n$ after grinding with solvents and photographs of each sample under UV light; (a) TFA, (b) DMSO, and (c) water. (Reproduced from Chem. Commun., 2010,46, 7906-7908 with permission of The Royal Society of Chemistry.)

1.4 Coordination and Aggregation Effects on Linker-based Luminescence in MOFs

Throughout the literature it has been shown that the emission of MOFs containing aromatic ligands is effected by metal coordination and chromophore proximity. Often the emission spectra of the MOF incorporated ligand is shifted and broadened relative to the free based linker. The following section will primarily focus on these types of effects as they pertain to stilbene, a linker that has been well studied in solution, the solid state, and upon incorporation into MOFs.

1.4.1 Stilbene MOFs. Stilbene has been incorporated into MOFs in the form of 4,4′-dicarboxylic acid and its derivatives. MOFs constructed from stilbene linkers form 3D open porous structures

with gas storage capabilities[54-56], some form interpenetrated frameworks[57-61], and others exhibit interaction with guest molecules[62-63]. The topologies and porosities of the MOF structure are dependent on the other constituents, metal ions or clusters and additional ligands, used in the synthesis. Stilbene can act as a rigid linker and provide stability through π interactions with other stilbenes or aromatic linkers, but due to its length and bent structure, interpenetration or close proximity between stilbene linkers is common in MOFs utilizing this ligand regardless of the SBU configuration and overall dimensionality.[64] Stilbene MOFs often exhibit interesting ligand based photophysical properties such as luminescence[57, 60, 65-66], tunable emission through host-guest interactions[67], and scintillation[68-69]. Although stilbenes are capable of undergoing photoisomerization, which decreases the photoluminescence quantum yield (QL) by providing a nonradiative decay pathway, incorporation of these ligands into MOFs could potentially supress this pathway by providing rigidity through linker coordination to metal sites.[70]

Stilbene has been used as a linker, by Huang et al., in the Cd based MOF [Cd(SDC)(H_2O)], where SDC = *trans*-stilbene-4,4'-dicarboxylate.[57] The MOF exhibited strong emission maximum at a wavelength of 460 nm upon excitation at 392 nm. The emission maximum of H_2SDC was observed at 466 nm with a shoulder peak at 439 nm upon excitation at 384 nm. The similar emission in the MOF relative to the free linker suggests that the emission occurs from $\pi^* \rightarrow \pi$ transitions, and the enhancement of the luminescence in the MOF compared to H_2SDC is believed to be due to the enhanced rigidity of the ligand within the MOF, resulting in fewer nonradiative relaxation pathways from S_1. Wang et al. synthesized Cd and Zn- based stilbene MOFs of the formulas [Cd(bpea)(H_2O)]$_n$ (**3**) and [Zn(bpea)(H_2O)]$_n$ (**4**), where bpea = *trans*-stilbene-4,4'-dicarboxylate.[65] Emission bands of MOF **4** were observed at λ = 435 and 459nm. The emission of **4** was more intense than that of **3** and blue-shifted and significantly more intense than the emission

observed for the free linker in the solid state (λ = 441 and 465 nm). The blue-shift is attributed differences in the orbitals involved in the emission process of the MOF relative to the free linker. Linker emission is believed to result from a $\pi^* \rightarrow \pi$ transition, whereas, upon coordination to metal ions in the MOFs, the radiative transition develops $n^* \rightarrow \pi$ character, and hence a slight blue-shift is observed in the MOF relative to the free linker. The enhancement of the luminescence is, again, believed to be a result of coordination to the metal ion, thereby reducing the intraligand nonradiative processes. The difference in emission intensity between MOFs **3** and **4** is assumed to be due to differences in the ability of the metal ions to polarize the electron density of the oxygen atoms. Stilbene has also been incorporated into Zn-based MOFs, where other ligands such as pyridine (py), 4,4'-bipyridine (4,4'-bpy), 1,2-bis(4-pyridyl)ethane (bpea/L^2), and 4-(4-((E)-2-(pyridin-4-yl)vinyl)- styryl)pyridine (L^1) are also incorporated into the framework.[60, 66] The luminescence of these MOFs have been attributed to intraligand $\pi^* \rightarrow \pi$ transitions with influences from the metal center and the coupling of electronic states between chromophores.[70]

In an effort to understand the effects of ligand coordination and local environment on the luminescent properties of stilbene MOFs, Baur et al. synthesized two stilebene/Zn MOFs with different topologies using the same starting materials, but under different reaction conditions to yield $Zn_3L_3(DMF)_2$ (**5**) and Zn_4OL_3 (**6**), where L = *trans*-4,4'-stilbene dicarboxylate.[70] MOF **5** was synthesized by solvothermal methods in DMF to yield a 2-D MOF with layers consisting of hexagonal networks of trinuclear Zn_3-$(RCO_2)_6$ SBUs connected by organic trans-4,4'-stilbenedicarboxylate links. The stilbene linkers remain planar due to the symmetry of the SBU in which the bridging carboxylate groups connect the Zn atoms through a nonplanar syn-skew geometry.[70] MOF **6** was synthesized solvothermally in DEF, which afforded a 3-D framework

with $Zn_4O(RCO_2)_6$ SBUs connected by *trans*-stilbene links, which are distorted slightly more than the linker in **5** but still remain essentially planar.

The difference in topology of MOFs **5** and **6** seemed to effect the luminescence properties of the stilbene linker, as is indicated by the differences observed in their excitation and emission

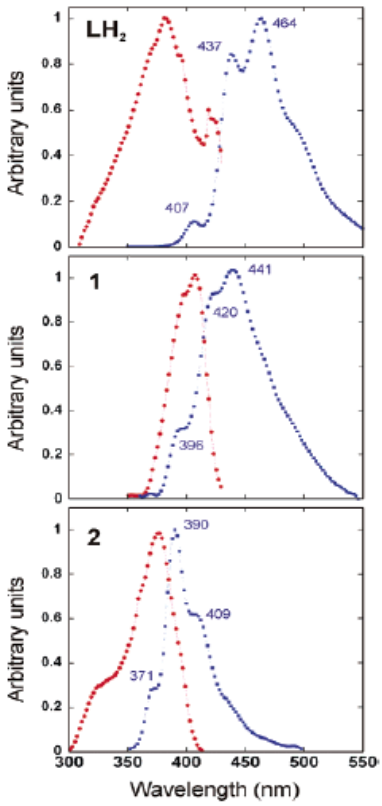

Figure 1-6. Normalized excitation (red) and emission (blue) profiles of (top) powdered trans-4,4'-stilbenedicarboxylic acid (excitation at λ = 350 nm , (middle) individual crystal of MOF 5 soaked in chloroform (excitation at λ = 350 nm), and (top) chloroform soaked crystal of MOF 6 (excitation at λ = 325 nm). Excitation spectra of all three were detected at λ = 450 nm. (Reprinted with permission from J. Am. Chem. Soc., 2007, 129 (22), pp 7136–7144. Copyright (2014) American Chemical Society)

spectra (Figure 1-6)[70]. The solid state emission spectra of the **5** and **6** have similar structure to the emission spectrum of H_2L in the solid state, suggesting that the emission of the MOFs is principally ligand-based with little influence from the Zn clusters. The nearly identical position of the emission of solid MOF **6** relative to the emission of a dilute DMF/H_2O solution of H_2L provides further evidence that the Zn_4O SBU has effectively little to no contribution to the emission of *trans*-stilbene in **6**. The structure in the emission of both MOFs is more prominent at room temperature, which suggests that the linker is rigidified within these structures.

The differences observed in the excitation and emission spectra of the two MOFs is likely influenced by a number of features such as the local environment and steric proximity of the ligands to other species within the MOFs. Though it is possible that the difference in the Zn clusters may have some influence on the electronic spectra of the two MOFs, the dominant influence is due to crystal density which effects the degree of interligand π-π interactions. The stilbene units of **5** are in a displaced face-to-face staking arrangement between layers. The arrangement allows for greater interchromophore coupling between stilbenes relative to **6**, which results in a greater red-shift and broadening in the emission spectrum of **5** compared to **6**.[70] The difference between the maxima of the excitation and emission spectra obtained for MOFs **5** and **6** is much less than is observed in dilute solutions of LH_2, which indicates that there is less reorganization between the ground and first excited states of the MOFs compared to LH_2, likely a result of the stilbene linkers becoming more rigid within the MOFs.

It was shown above by Wang et al. that the choice of metal ion or cluster can have interesting effects of the excited state processes occurring within the linker resulting in strengthened or weakened luminescence. Recently, Baur et al. examined the effects of metal ion

choice on linker based luminescence of a series of 8 isostructural homo- and heterometallic 2-D MOFs composed of *trans*-4,4'-stilbene dicarboxylate (L) and Cd, Co, Mn, and/or Zn.[64] MOFs were synthesized using solvothermal methods and DMF as the solvent, which yielded 8 MOFs of the formula $M^1{}_2M^2L_3(DMF)_2$, where MOF the homometallic structures **7**-**10** consist of (**7**) M^1 = M^2 = Zn, (**8**) = Cd, (**9**) = Mn, and (**10**) = Co, and the heterometallic structures consist of (**11**) M^1 = Zn, and M^2 = Cd, (**12**) = Mn, (**13**) = Co, and (**14**) M^1 = Co, M^2 = Mn. The isostructural MOFs exhibit trinuclear SBUs consisting of a central M^2(II) ions coordinated octahedrally, connected, through bridging carboxylate groups, to two tetrahedral-coordinated M^1(II) ions, which are also coordinated to two DMF molecules.[64] The trans-stilbene linker connects the SBUs and forms a 2-D hexagonal pinwheel network extending outwards into the a,b-plane; these 2-D layers pack in a staggered fashion to give a dense structure with pore spaces filled with DMF molecules.[64]

Steady-state fluorescence studies were conducted on MOFs **7**-**9** and **11**-**13** using an excitation wavelength of 350 nm (Figure 1-7a)[64]. Fluorescence lifetimes were measured by exciting the samples at 330 nm using a sub-nanosecond excitation pulse, and detecting the resulting emission at 440 nm, and fitting the signal decay to a model which deconvoluted the sample signal from the excitation pulse. The emission spectra of MOFs **7**-**9** and **11**-**13** exhibit fine structure and several vibronic bands similar to the vibronic structure observed in the emission of *trans*-stilbene in solution and in the solid state, indicating the emission of the MOFs are primarily ligand based. The small red-shift observed in the emission profiles of the MOFs relative to an aqueous solution of stilbenedicarboxylate sodium salt (Na_2L), is attributed to intermediate electronic coupling between stilbene units (Figure 1-7b)[64]. The emission spectrum of powdered *trans*-stilbene-4,4'-dicarboxylic acid (H_2L) is even further red-shifted than the MOFs and is significantly broadened as a result of extensive coupling between the aromatic molecules in the solid state (Figure 1-7b)[64].

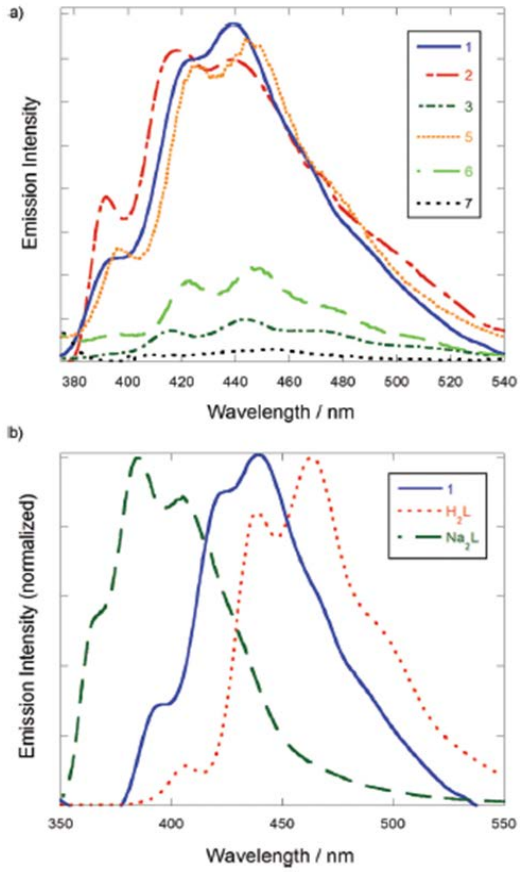

Figure 1-7. a) emission spectra of 1-3 and 5-7 MOF crystals. (b) emission spectra of MOF 1 (blue), powder H_2L (yellow), and aqueous solution of Na_2L (green). (Reproduced from Dalton Trans., 2014,43, 2925-2935 with permission of The Royal Society of Chemistry.)

Further evidence for linker based emission is suggested by the similar energies of the emission of the MOFs containing different metal ions. The Lewis acidity of Cd, Co, Mn, and Zn ions differ and as a result would be expected to perturb the electronic configuration of linker, resulting in different energies of emission, to a greater extent than is observed. The emission intensities of MOFs **7**, **8**, and **11** are greater than those observed for MOFs **9, 12**, and **13**. The reduced emission is attributed to quenching by through space electron and/or energy transfers, resulting from the close proximity of the stilbene linkers to high-spin metal ions Mn (II) and Co

(II), with S = 5/2 and S = 3/2, respectively.[64] These quenching processes do not occur in the structures containing d^{10} metal ions, Zn and Cd. The lack of emission from MOFs **10** and **14** is believed to be due to reabsorption of any weak luminescence by the higher concentrations of Co(II) ions within the structures.

Time-resolved fluorescence experiments were conducted on MOFs **1**-**3** and **5** and **6** to further probe their photophysical properties. The fluorescence lifetimes (τ) and pre-exponential factors (α) obtained by fitting the decay to $I(t)= \alpha_1 e^{-t/\tau_1} + \alpha_2 e^{-t/\tau_2}$, where t is time, are listed in Table 1-1. The fluorescence decays of MOFs **7**, **8**, **11**, and **12** were able to be fit the decay function to yield two different lifetimes, with one lifetime significantly shorter than the other indicating the presence of two different emissive states. The first, shorter lifetime is attributed to a "monomer" state, where the electronic transitions are localized within individual stilbene units. The second, longer lived emissive state is believed to result from partially aggregated or "dimer" states, the population of which occurs through excited state, through-space interchromophore coupling with the "monomer" states.[64] MOF **9** exhibited a single exponential fluorescence decay with a shorter lifetime than the other MOFs studied. The shorter fluorescence lifetime is attributed to close proximity of three Mn(II) ions per SBU, resulting in fluorescence quenching due to the reduction of the "monomer" fluorescence lifetime.

Table 1-1. Fluorescent lifetimes and pre-exponential factors of MOFs 1-6. (Data obtained from Dalton Trans., 2014,43, 2925-2935)

MOFs	***τ_1/ns***	***τ_2/ns***	***α_1/%***	***α_2/%***
7	0.76	5.88	93.1	6.9

8	0.59	3.54	92.2	7.8
9	0.37	n/a	100	n/a
11	0.64	4.39	95.4	4.6
12	0.64	6.67	88.0	12

1.4.2 Anthracene MOFs. The large π-conjugated system of anthracene makes it a good candidate in the development of luminescent materials. MOFs composed of anthracene based linkers have been studied for applications in gas separations[71], gas storage[72], as stationary phases for chemical separations[73], and as heterogeneous catalyst[74], but there are relatively few accounts of the luminescent properties of these MOFs being studied. Functionalized anthracenes have been incorporated into Zn, Cd, Mn, Co, or Ni metal based MOFs that exhibit linker-based luminescence.[34, 75-77] Luminescence of the anthracenic MOFs constructed from the d^{10} metals, Cd and Zn, were determined to be primarily a result of intraligand electronic transitions of the π*- π type.[34, 76] Metal to ligand or ligand to metal charge transfers are not observed in these cases, because Zn(II) and Cd(II) ions are both difficult to oxidize or reduce.[34, 76] One Zn based framework composed of anthracene-9,10-dicarboxylic acid and 1,4-diazabicyclo[2.2.2]octane was shown to have fluorescence dependent on solvent loading within the pores.[75]

Wang et al. found that in the case of five MOFs composed of anthracenedicarboxylic acids, dimethylformamide (DMF), 1,3-di(4-pyridyl)propane (DPP) and Zn or Cd ions, the emission of the MOFs most often resulted from intramolecular electronic transitions between anthracene ligands.[34] One of the five MOFs studied had an emission spectrum which suggested influence from

the coordinated metal ions. The five MOFs of the formulas: $[Cd_4(L_1)_2(DPP)_2(DMF)_2(SO_4)_2]_n$ (**15**), $[Zn_2(L_1)(DPP)_2Cl_2]_n$ (**16**), $[Cd(L_2)(DPP)]_n$ (**17**), $[Zn(L_2)(DPP)]_n$ (**18**), and $([Cd_2(L_2)Cl_4][((CH_3)_2NH_2]_2)_n$ (**19**), where synthesized in a solvothermal reaction with anthracene-9,10-dicarboxylic acid (H_2L_1) or anthracene-1,5-dicarboxylic acid (H_2L_2) and Cd^{II} or Zn^{II} ions.[34] The solid state emission spectra of the five MOFs and the ligands, H_2L_1 and H_2L_2, are shown in Figure 1-8[34]. All of the complexes exhibited luminescence with either the purple, green, or blue emission. MOFs **17**-**19** showed intense emission upon excitation at 386, 385, and 380 nm, respectively. **17**-**19** exhibit emission maxima at 442/485/529, 433/485/524, and 434/520 nm, respectively. Complexes **15**, and **17**-**19** show similar emissive structure to the ligands in the solid state, which indicates that the intraligand transfer π^*–π transitions are the dominant source of the emission.[34] MOF **16** has a blue shifted emission spectrum of ~70 nm, relative to H_2L_1 in the solid state. The blue shift of the emission spectrum of **16** relative to the ligand may be due to increased rigidity and asymmetry of the ligand upon complexation to the metal center, which reduces the nonradiative decay from the intraligand excited state.

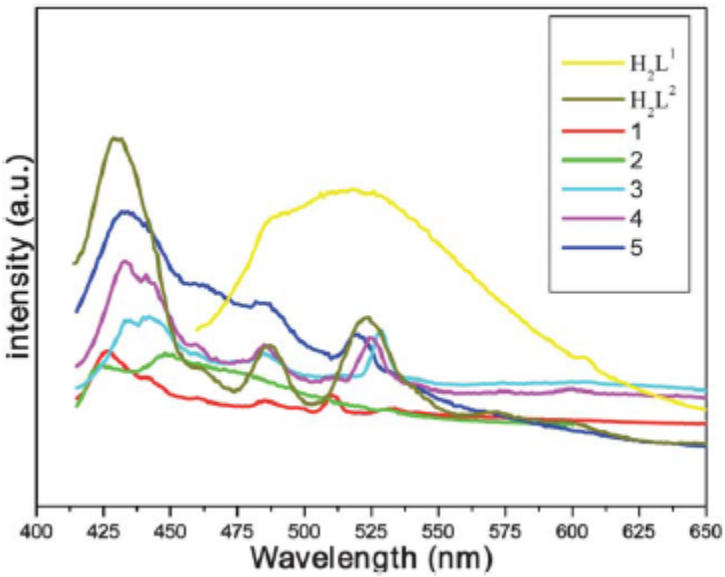

Figure 1-8. Solid state emission spectra at room temperature of H_2L_1 and H_2L_2 and complexes **1**–**5** (with excitation at λ = 444 nm for H_2L_1, 379 nm for H_2L_2, 380 nm for **1**, 336 nm for **2**, 386 nm for **3**, 383 nm for **4** and 380 nm for **5**, respectively). (Reproduced from CrystEngComm, 2011,13, 5152-5161 with permission of The Royal Society of Chemistry)

The difference in the relative emission intensities of the five MOFs studied is possibly a result of the different structures of the MOFs, and/or the degree of conjugation and inter/intramolecular interaction between ligands.

1.4.3 Phosphorescent MOFs. Phosphorescent materials have been incorporated into plasma displays, field emission displays, light-emitting diodes, and lamps to name a few.[78] Both organic and inorganic materials are currently being used for such devices, but these materials often lack tunability. MOFs, consisting of both organic and inorganic components, are highly tunable and may be designed with luminescent metals or organic linkers. The majority of phosphorescent MOFs found in the literature are prepared from lanthanides. Very few phosphorescent MOFs that don't require these expensive metals or doping have been reported.[14, 18, 51, 79-80]

Yaun et al. have reported two phosphorescent MOFs of the formulas $([Zn(tipa)Cl]\cdot NO_3\cdot 2DMF)_n$ (**20**) and $([Cd_2(tipa)_2Cl_4]\cdot 6DMF)_n$ (**21**), where tipa = tri(4-imidazolylphenyl)amine).[14] Upon excitation at 365 nm at 298 K, MOFs **20** and **21** exhibit diffuse emission with maxima centered at 414 and 401 nm, respectively (Figure 1-9a)[14]. Using the integrated sphere method with excitation at 365 nm, quantum yields were determined at 298 K to be 0.10 and 0.22 for **20** and **21**, respectively. Interestingly at a lower temperature of 77 K, the emission of **1** is hypsochromatically shifted by 18 nm to 396 nm, and the intensity of the emission of **21** at 401 nm is decreased dramatically and new band appears at 454 nm (Figure 1-9b)[14]. At the 77 K the decay of both MOFs exhibit macroscopic persistent emission after UV excitation is terminated (Figure 1-9c).[14] The emission at 77 K was able to be determined by the naked eye to be around 2 s (Figure 1-9d)[14], which is not observed at 298 K. The emission of **20** and **21** resemble that of the tipa ligand (λ_{ex} = 365 nm, λ_{em} = 420 nm)[81], and based on the long lived emission lifetimes at 77 K, the emission should be due to an excited triplet state of the ligand. Intersystem crossing to the triplet state is enhanced by lower temperature and coordination to Zn^{II} and Cd^{II} ions.[14]

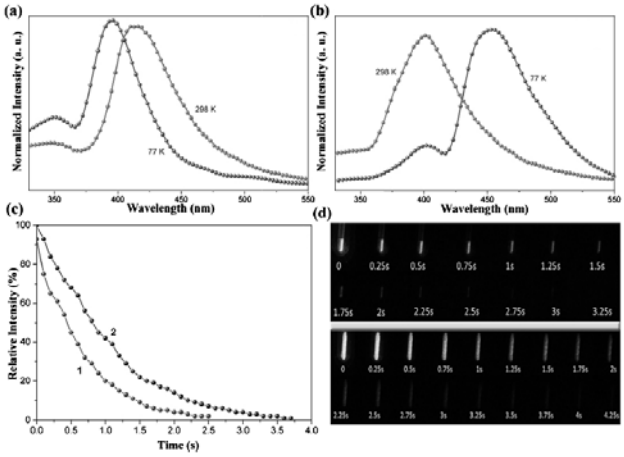

Figure 1-9. The solid-state luminescence spectra of: a) complex **20**, and b) complex **21** at 298 and 77 K upon excitation at λ_{ex}=365 nm. c) Afterglow intensity decay curves of **20** and **21**. d) After stopping the UV irradiation, the afterglow photographs of samples (**20**: upper; **21**: lower) in Suprasil quartz tubes were extracted from videos with 0.25 s intervals at 77 K. (Reprinted with permission from *Chemistry – A European Journal* 2014, 20 (32), 10093-10098)

Some MOF materials have been found to exhibit both fluorescence and phosphorescence emission at room temperature and very low temperatures. Chen et al. prepared a MOF with such properties of the formula $[(Ag_4I_4(bix)]_n$ **20**, where bix = 1,4-bis(imidazole-1-ylmethyl)benzene.[80] Excitation at 380 nm of complex **20** at both room temperature and 10 K results in emission bands at 448 nm and 523 nm. Upon excitation at 10 K, the intensity of the higher energy band at 448 nm is reduced and the intensity of the lower energy band is increased, suggesting that the two bands result from different excited states. To test this assumption emission lifetimes of these two bands were determined at 10 K. Both decay curves for the emission at 448 and 523 nm were satisfyingly fit to a biexponential function to give lifetimes τ_1 = 7.580 x 10^{-9} s (16.31%), τ_2 = 6.662 x 10^{-10} s (83.96%) and τ_1 = 3.402 x 10^{-4} s (44.26%), τ_2 = 1.264 x 10^{-3} s (56.57%), respectively. The decay of the 448 nm band is on the order of nanoseconds, suggesting fluorescence emission, whereas the decay of the 523 nm band is much slower, on the order of milliseconds, suggesting the emission is phosphorescent. The free ligand exhibits an emission band at 444 nm when excited at 380 nm, which resembles the higher energy band of **20**. This resemblance suggests that the higher energy band of **20** is due to intraligand $\pi \rightarrow \pi^*$ transitions, and the lower energy band is possible due to metal-ligand charge transfer with perturbation from metal-metal interactions.[80]

1.5 MOFs with Sensitizing Ligands

Luminescent lanthanide MOFs are highly sensitive to their microenvironment which is why they are some of the most well studied MOF sensors, which have been used in the detection of gases, vapors, temperature, and pH.[82] Sensitizing luminescent lanthanide metals with organic ligands, which act as "antenna" have been studied extensively.[20, 82-89] Lanthanides typically exhibit f-f type transitions with small extinction coefficients, and when sensitized with organic ligands, strong f-f emission can be observed upon excitation of the ligand.[90] Bo et al. have synthesized two europium based MOFs sensitized with either 5-methylisophthalate (mip) ions or 5-*tert*-butylisophthalate anions (tip) with the formulas $[Eu(OH)(mip)]_n$ (**mip-Eu**) and $[Eu(tip_{1.5}]_{2n}$ (**tip-Eu**).[20] The excitation spectra, monitored at 614 nm, of **mip-Eu** and **tip-Eu** show characteristic sharp lines due to $4f^6$-$4f^6$ transitions as well as a broad band centered about 308 nm. The broad band is likely a result of a ligand to metal energy transfer resulting from excited state orbital overlap between the ligand and the 4f orbitals of the lanthanides. The MOFs exhibited characteristic Eu^{3+} emission by excitation at 308 nm providing further evidence of energy transfer between the ligand and lanthanides.

In certain lanthanide MOFs the ligand may also play a role in the depopulation of the excited states. Silva et al. have shown that a MOF constructed from 2,5-pyridinedicarboxylate, lanthanum, and/or europium exhibited characteristic lanthanide emission upon UV excitation of the ligand (λ = 310 nm), as well as excitation of the lanthanide band (λ = 393 nm).[85] The quantum yield of emission is much greater under UV excitation (43%) than under direct lanthanide excitation (4%), and is nearly double the calculated quantum efficiency (23%) calculated on the assumption that only radiative and nonradiative processes are involved in the depollution of the $^5D_0$ excited state. The large difference between the calculated efficiency and the observed efficiency upon UV excitation at 393 nm suggests that other processes besides radiative and

nonradiative decay are involved in population/depopulation of the $^5D_0$ state due to interaction with the ligand.[85]

1.6 Research of Goals

It has been shown that the luminescence of a MOF is dependent on the organic and inorganic building blocks that form the framework. The majority of photoactive MOFs, not composed from lanthanides, are designed with aromatic linkers. The photophysical properties of the linker in a MOF are often altered, relative to the solid or liquid state, by the new environment within the framework. The excited state processes that occur upon absorption of a photon are perturbed by the different environment within the MOF, which results in shifted and broadened spectra, as well as altered quantum yields and lifetimes, relative to the free ligand. The following chapters will discuss the difference in the photophysical properties of three anthracenedicarboxylic acids: 9,10-antrhacenedicarboxylic acid, 2,6-anthracenedicarboxylic acid, and 1,4-anthracenedicarboxylic acid. The effects of carboxylic acid group location on the photophysics of anthracene will be discussed in further detail. Finally the effects on the photophysics of 9,10-anthracenedicarboxylic acid and 2,6-anthracenedicarboxylic acid upon incorporation into Zn based MOFs will be discussed.

1.7 References

1. Li, H.; Eddaoudi, M.; Groy, T. L.; Yaghi, O. M., Establishing Microporosity in Open Metal−Organic Frameworks: Gas Sorption Isotherms for Zn(BDC) (BDC = 1,4-Benzenedicarboxylate). *Journal of the American Chemical Society* **1998,** *120* (33), 8571-8572.
2. Zhou, S.; Kong, Z.-G.; Wang, Q.-W.; Li, C.-B., Synthesis, structure and photocatalytic property of a novel 3D (3,8)-connected metal–organic framework based on a flexible triphosphonate and a pentanuclear Cu(II) unit. *Inorganic Chemistry Communications* **2012,** *25* (0), 1-4.

3. Dou, Z.; Yu, J.; Cui, Y.; Yang, Y.; Wang, Z.; Yang, D.; Qian, G., Luminescent Metal–Organic Framework Films As Highly Sensitive and Fast-Response Oxygen Sensors. *Journal of the American Chemical Society* **2014,** *136* (15), 5527-5530.
4. Li, J.-R.; Sculley, J.; Zhou, H.-C., Metal-Organic Frameworks for Separations. *Chem. Rev. (Washington, DC, U. S.)* **2012,** *112* (2), 869-932.
5. Vermeulen, N. A.; Karagiaridi, O.; Sarjeant, A. A.; Stern, C. L.; Hupp, J. T.; Farha, O. K.; Stoddart, J. F., Aromatizing Olefin Metathesis by Ligand Isolation inside a Metal- Organic Framework. *J. Am. Chem. Soc.* **2013,** *135* (40), 14916-14919.
6. Wang, G.-Y.; Song, C.; Kong, D.-M.; Ruan, W.-J.; Chang, Z.; Li, Y., Two luminescent metal-organic frameworks for the sensing of nitroaromatic explosives and DNA strands. *Journal of Materials Chemistry A* **2014,** *2* (7), 2213-2220.
7. Zhang, C.-F.; Qiu, L.-G.; Ke, F.; Zhu, Y.-J.; Yuan, Y.-P.; Xu, G.-S.; Jiang, X., A novel magnetic recyclable photocatalyst based on a core-shell metal-organic framework Fe3O4@MIL-100(Fe) for the decolorization of methylene blue dye. *Journal of Materials Chemistry A* **2013,** *1* (45), 14329-14334.
8. Lee, D. Y.; Shin, C. Y.; Yoon, S. J.; Lee, H. Y.; Lee, W.; Shrestha, N. K.; Lee, J. K.; Han, S.-H., Enhanced photovoltaic performance of Cu-based metal-organic frameworks sensitized solar cell by addition of carbon nanotubes. *Sci. Rep.* **2014,** *4*.
9. Pramanik, M.; Patra, A. K.; Bhaumik, A., Self-assembled titanium phosphonate nanomaterial having a mesoscopic void space and its optoelectronic application. *Dalton Trans.* **2013,** *42* (14), 5140-5149.
10. Silva, C. G.; Corma, A.; Garcia, H., Metal-organic frameworks as semiconductors. *Journal of Materials Chemistry* **2010,** *20* (16), 3141-3156.
11. Jayaramulu, K.; Kanoo, P.; George, S. J.; Maji, T. K., Tunable emission from a porous metal-organic framework by employing an excited-state intramolecular proton transfer responsive ligand. *Chemical Communications* **2010,** *46* (42), 7906-7908.
12. Kreno, L. E.; Leong, K.; Farha, O. K.; Allendorf, M.; Van Duyne, R. P.; Hupp, J. T., Metal–Organic Framework Materials as Chemical Sensors. *Chemical Reviews* **2011,** *112* (2), 1105-1125.
13. Cui, Y.; Yue, Y.; Qian, G.; Chen, B., Luminescent Functional Metal–Organic Frameworks. *Chemical Reviews* **2011,** *112* (2), 1126-1162.
14. Yuan, S.; Deng, Y.-K.; Sun, D., Unprecedented Second-Timescale Blue/Green Emissions and Iodine-Uptake-Induced Single-Crystal-to-Single-Crystal Transformation in ZnII/CdII Metal–Organic Frameworks. *Chemistry – A European Journal* **2014**, n/a-n/a.
15. Rowsell, J. L. C.; Yaghi, O. M., Metal–organic frameworks: a new class of porous materials. *Microporous and Mesoporous Materials* **2004,** *73* (1–2), 3-14.
16. Yaghi, O. M.; O'Keeffe, M.; Ockwig, N. W.; Chae, H. K.; Eddaoudi, M.; Kim, J., Reticular synthesis and the design of new materials. *Nature* **2003,** *423* (6941), 705-714.
17. Dey, C.; Kundu, T.; Biswal, B. P.; Mallick, A.; Banerjee, R., Crystalline metal-organic frameworks (MOFs): synthesis, structure and function. *Acta Crystallographica Section B* **2014,** *70* (1), 3-10.
18. Zhang, C.-J.; Wang, M.-S.; Guo, G.-C., Crystal structure and photoluminescent properties of a Ag(I)-carboxylate coordination compound: Luminescence modulation by a π-conjugated ancillary ligand. *Inorganic Chemistry Communications* **2013,** *35* (0), 76-78.
19. Tanaka, D.; Horike, S.; Kitagawa, S.; Ohba, M.; Hasegawa, M.; Ozawa, Y.; Toriumi, K., Anthracene array-type porous coordination polymer with host-guest charge transfer interactions in excited states. *Chemical Communications* **2007,** (30), 3142-3144.

20. Bo, Q.-B.; Zhang, H.-T.; Wang, H.-Y.; Miao, J.-L.; Zhang, Z.-W., Anhydrous Lanthanide MOFs and Direct Photoluminescent Sensing for Polyoxometalates in Aqueous Solution. *Chemistry – A European Journal* **2014,** *20* (13), 3712-3723.
21. Banerjee, R.; Furukawa, H.; Britt, D.; Knobler, C.; O'Keeffe, M.; Yaghi, O. M., Control of Pore Size and Functionality in Isoreticular Zeolitic Imidazolate Frameworks and their Carbon Dioxide Selective Capture Properties. *Journal of the American Chemical Society* **2009,** *131* (11), 3875-3877.
22. Gascon, J.; Hernández-Alonso, M. D.; Almeida, A. R.; van Klink, G. P. M.; Kapteijn, F.; Mul, G., Isoreticular MOFs as Efficient Photocatalysts with Tunable Band Gap: An Operando FTIR Study of the Photoinduced Oxidation of Propylene. *ChemSusChem* **2008,** *1* (12), 981-983.
23. Dong, Y.; Lam, J. W. Y.; Qin, A.; Liu, J.; Li, Z.; Tang, B. Z.; Sun, J.; Kwok, H. S., Aggregation-induced emissions of tetraphenylethene derivatives and their utilities as chemical vapor sensors and in organic light-emitting diodes. *Applied Physics Letters* **2007,** *91* (1), -.
24. Shustova, N. B.; McCarthy, B. D.; Dincă, M., Turn-On Fluorescence in Tetraphenylethylene-Based Metal–Organic Frameworks: An Alternative to Aggregation-Induced Emission. *Journal of the American Chemical Society* **2011,** *133* (50), 20126-20129.
25. Shustova, N. B.; Ong, T.-C.; Cozzolino, A. F.; Michaelis, V. K.; Griffin, R. G.; Dincă, M., Phenyl Ring Dynamics in a Tetraphenylethylene-Bridged Metal–Organic Framework: Implications for the Mechanism of Aggregation-Induced Emission. *Journal of the American Chemical Society* **2012,** *134* (36), 15061-15070.
26. Hailian, L.; Mohamed, E.; Keeffe, M. O.; Yaghi, O. M., Design and synthesis of an exceptionally stable and highly porous metal-organic framework. *Nature* **1999,** *402* (6759), 276-279.
27. Perry Iv, J. J.; Feng, P. L.; Meek, S. T.; Leong, K.; Doty, F. P.; Allendorf, M. D., Connecting structure with function in metal-organic frameworks to design novel photo- and radioluminescent materials. *Journal of Materials Chemistry* **2012,** *22* (20), 10235-10248.
28. Logvinenko, V.; Sapchenko, S.; Fedin, V., Thermal decomposition of inclusion compounds on the base of the metal–organic framework [Zn4(dmf)(ur)2(ndc)4]. *J Therm Anal Calorim* **2014**, 1-7.
29. Jasuja, H.; Huang, Y.-g.; Walton, K. S., Adjusting the Stability of Metal–Organic Frameworks under Humid Conditions by Ligand Functionalization. *Langmuir* **2012,** *28* (49), 16874-16880.
30. Zhou, L.; Xue, Y.-S.; Xu, Y.; Zhang, J.; Du, H.-B., Two photoluminescent metal-organic frameworks based on a BODIPY-derived bipyridine ligand. *CrystEngComm* **2013,** *15* (36), 7315-7320.
31. Darling, K.; Zubieta, J., Solid state coordination chemistry of metal-azolate compounds: Structural consequences of incorporation of phosphate components in the Co(II)/4-pyridyltetrazolate/phosphate system. *Inorganica Chimica Acta* **2013,** *394* (0), 512-518.
32. Valeur, B., *Molecular Fluorescence: Principles and Applications*. WILEY-VCH Weinheim ; New York, 2002.
33. Brown, J. W.; Henderson, B. L.; Kiesz, M. D.; Whalley, A. C.; Morris, W.; Grunder, S.; Deng, H.; Furukawa, H.; Zink, J. I.; Stoddart, J. F.; Yaghi, O. M., Photophysical pore control in an azobenzene-containing metal-organic framework. *Chemical Science* **2013,** *4* (7), 2858-2864.
34. Wang, J.-J.; Hu, T.-L.; Bu, X.-H., Cadmium(ii) and zinc(ii) metal-organic frameworks with anthracene-based dicarboxylic ligands: solvothermal synthesis, crystal structures, and luminescent properties. *CrystEngComm* **2011,** *13* (16), 5152-5161.

35. Stylianou, K. C.; Heck, R.; Chong, S. Y.; Bacsa, J.; Jones, J. T. A.; Khimyak, Y. Z.; Bradshaw, D.; Rosseinsky, M. J., A Guest-Responsive Fluorescent 3D Microporous Metal−Organic Framework Derived from a Long-Lifetime Pyrene Core. *Journal of the American Chemical Society* **2010,** *132* (12), 4119-4130.
36. Johnson, J. A.; Chen, S.; Reeson, T. C.; Chen, Y.-S.; Zeng, X. C.; Zhang, J., Direct X-ray Observation of Trapped CO2 in a Predesigned Porphyrinic Metal–Organic Framework. *Chemistry – A European Journal* **2014,** *20* (25), 7632-7637.
37. Zhao, M.; Ou, S.; Wu, C.-D., Porous Metal–Organic Frameworks for Heterogeneous Biomimetic Catalysis. *Accounts of Chemical Research* **2014,** *47* (4), 1199-1207.
38. Xie, M.-H.; Yang, X.-L.; Zou, C.; Wu, C.-D., A SnIV–Porphyrin-Based Metal–Organic Framework for the Selective Photo-Oxygenation of Phenol and Sulfides. *Inorganic Chemistry* **2011,** *50* (12), 5318-5320.
39. Kent, C. A.; Liu, D.; Ito, A.; Zhang, T.; Brennaman, M. K.; Meyer, T. J.; Lin, W., Rapid energy transfer in non-porous metal-organic frameworks with caged Ru(bpy)32+ chromophores: oxygen trapping and luminescence quenching. *Journal of Materials Chemistry A* **2013,** *1* (47), 14982-14989.
40. Kent, C. A.; Liu, D.; Ma, L.; Papanikolas, J. M.; Meyer, T. J.; Lin, W., Light Harvesting in Microscale Metal–Organic Frameworks by Energy Migration and Interfacial Electron Transfer Quenching. *Journal of the American Chemical Society* **2011,** *133* (33), 12940-12943.
41. Rosi, N. L.; Eddaoudi, M.; Kim, J.; O'Keeffe, M.; Yaghi, O. M., Advances in the chemistry of metal-organic frameworks. *CrystEngComm* **2002,** *4* (68), 401-404.
42. Yaghi, O. M.; Li, G.; Li, H., Selective binding and removal of guests in a microporous metal-organic framework. *Nature* **1995,** *378* (6558), 703-706.
43. Kim, J.; Chen, B.; Reineke, T. M.; Li, H.; Eddaoudi, M.; Moler, D. B.; O'Keeffe, M.; Yaghi, O. M., Assembly of Metal−Organic Frameworks from Large Organic and Inorganic Secondary Building Units: New Examples and Simplifying Principles for Complex Structures ▵. *Journal of the American Chemical Society* **2001,** *123* (34), 8239-8247.
44. Yaghi, O. M.; Li, H.; Groy, T. L., A Molecular Railroad with Large Pores: Synthesis and Structure of Ni(4,4‘-bpy)2.5(H2O)2(ClO4)2·1.5(4,4‘-bpy)·2H2O†. *Inorganic Chemistry* **1997,** *36* (20), 4292-4293.
45. Yaghi, O. M.; Li, H., T-Shaped Molecular Building Units in the Porous Structure of Ag(4,4‘-bpy)·NO3. *Journal of the American Chemical Society* **1996,** *118* (1), 295-296.
46. Blake, A. J.; Champness, N. R.; Hubberstey, P.; Li, W.-S.; Withersby, M. A.; Schröder, M., Inorganic crystal engineering using self-assembly of tailored building-blocks. *Coordination Chemistry Reviews* **1999,** *183* (1), 117-138.
47. Zheng, S.-L.; Yang, J.-H.; Yu, X.-L.; Chen, X.-M.; Wong, W.-T., Syntheses, Structures, Photoluminescence, and Theoretical Studies of d10 Metal Complexes of 2,2‘-Dihydroxy-[1,1‘]binaphthalenyl-3,3‘-dicarboxylate. *Inorganic Chemistry* **2003,** *43* (2), 830-838.
48. Fang, Q.; Zhu, G.; Xue, M.; Sun, J.; Sun, F.; Qiu, S., Structure, Luminescence, and Adsorption Properties of Two Chiral Microporous Metal−Organic Frameworks. *Inorganic Chemistry* **2006,** *45* (9), 3582-3587.
49. Chen, W.; Wang, J.-Y.; Chen, C.; Yue, Q.; Yuan, H.-M.; Chen, J.-S.; Wang, S.-N., Photoluminescent Metal−Organic Polymer Constructed from Trimetallic Clusters and Mixed Carboxylates. *Inorganic Chemistry* **2003,** *42* (4), 944-946.

50. Tomar, K., Assembly of an eight connected porous Cd(II) framework with octahedral and cubo-octahedral cages: Sorption and luminescent properties. *Inorganic Chemistry Communications* **2013,** *37* (0), 127-131.
51. Kent, C. A.; Liu, D.; Meyer, T. J.; Lin, W., Amplified Luminescence Quenching of Phosphorescent Metal–Organic Frameworks. *Journal of the American Chemical Society* **2012,** *134* (9), 3991-3994.
52. Kanoo, P.; Ghosh, A. C.; Cyriac, S. T.; Maji, T. K., A Metal–Organic Framework with Highly Polar Pore Surfaces: Selective CO2 Adsorption and Guest-Dependent On/Off Emission Properties. *Chemistry – A European Journal* **2012,** *18* (1), 237-244.
53. Jayaramulu, K.; Narayanan, R. P.; George, S. J.; Maji, T. K., Luminescent Microporous Metal–Organic Framework with Functional Lewis Basic Sites on the Pore Surface: Specific Sensing and Removal of Metal Ions. *Inorganic Chemistry* **2012,** *51* (19), 10089-10091.
54. Wei, W.; Xia, Z.; Wei, Q.; Xie, G.; Chen, S.; Qiao, C.; Zhang, G.; Zhou, C., A heterometallic microporous MOF exhibiting high hydrogen uptake. *Microporous and Mesoporous Materials* **2013,** *165* (0), 20-26.
55. Wang, X.-S.; Ma, S.; Rauch, K.; Simmons, J. M.; Yuan, D.; Wang, X.; Yildirim, T.; Cole, W. C.; López, J. J.; Meijere, A. d.; Zhou, H.-C., Metal−Organic Frameworks Based on Double-Bond-Coupled Di-Isophthalate Linkers with High Hydrogen and Methane Uptakes. *Chemistry of Materials* **2008,** *20* (9), 3145-3152.
56. Zheng, S.-T.; Zuo, F.; Wu, T.; Irfanoglu, B.; Chou, C.; Nieto, R. A.; Feng, P.; Bu, X., Cooperative Assembly of Three-Ring-Based Zeolite-Type Metal–Organic Frameworks and Johnson-Type Dodecahedra. *Angewandte Chemie International Edition* **2011,** *50* (8), 1849-1852.
57. Kun-Lin, H.; Yan-Ting, H.; Mei, H., [Cd(SDC)(H2O)]: a 3-D hybrid open framework with an interpenetrated (4,4) topology and double-strand helicates (SDC=4,4'-stilbenedicarboxylate). *Journal of Coordination Chemistry* **2008,** *61* (17), 2735-2742.
58. Yang, J.; Ma, J.-F.; Liu, Y.-Y.; Batten, S. R., Four-, and six-connected entangled frameworks based on flexible bis(imidazole) ligands and long dicarboxylate anions. *CrystEngComm* **2009,** *11* (1), 151-159.
59. Zhang, L.; Yao, Y.-L.; Che, Y.-X.; Zheng, J.-M., Hydrothermal Synthesis of a Series of Interpenetrated Metal−Organic Frameworks Based on Long Multicarboxylate and Long Heterocyclic Aromatic Ligands. *Crystal Growth & Design* **2010,** *10* (2), 528-533.
60. Huang, K.-L.; Liu, X.; Liang, G.-M., Second-ligand-dependent multi-fold interpenetrated architectures of two 3-D metal(II)–organic coordination polymers. *Inorganica Chimica Acta* **2009,** *362* (5), 1565-1570.
61. Deng, Z.-P.; Huo, L.-H.; Wang, H.-Y.; Gao, S.; Zhao, H., A series of three-dimensional lanthanide metal-organic frameworks with biphenylethene-4,4[prime or minute]-dicarboxylic acid: Hydrothermal syntheses and structures. *CrystEngComm* **2010,** *12* (5), 1526-1535.
62. Cheng, A.-L.; Liu, N.; Yue, Y.-F.; Jiang, Y.-W.; Gao, E.-Q.; Yan, C.-H.; He, M.-Y., Unprecedented 3D entanglement of 1D zigzag coordination polymers leading to a robust microporous framework. *Chemical Communications* **2007,** (4), 407-409.
63. Cheng, A.-L.; Ma, Y.; Zhang, J.-Y.; Gao, E.-Q., Towards tuning the packing and entanglement of zigzag coordination chains by terminal ligands. *Dalton Transactions* **2008,** (15), 1993-2004.
64. Bauer, C. A.; Jones, S. C.; Kinnibrugh, T. L.; Tongwa, P.; Farrell, R. A.; Vakil, A.; Timofeeva, T. V.; Khrustalev, V. N.; Allendorf, M. D., Homo- and heterometallic luminescent 2-D stilbene metal-organic frameworks. *Dalton Transactions* **2014,** *43* (7), 2925-2935.

65. Wang, H.-Y.; Gao, S.; Huo, L.-H.; Ng, S. W.; Zhao, J.-G., Three Interpenetrated Frameworks Assembly from a Long Multicarboxylate Ligand and Transition Metal. *Crystal Growth & Design* **2008,** *8* (2), 665-670.
66. Cheng, A.-L.; Ma, Y.; Sun, Q.; Gao, E.-Q., Layered and pillar-layered metal-organic frameworks based on pinwheel trinuclear zinc-carboxylate clusters. *CrystEngComm* **2011,** *13* (7), 2721-2726.
67. Yan, D.; Tang, Y.; Lin, H.; Wang, D., Tunable Two-color Luminescence and Host-guest Energy Transfer of Fluorescent Chromophores Encapsulated in Metal-Organic Frameworks. *Sci. Rep.* **2014,** *4*.
68. Allendorf, M.; Houk, R.; Bhakta, R.; Nielsen, I. B.; Doty, P., Scintillating Metal Organic Frameworks: A New Class of Radiation Detection Materials. *MRS Online Proceedings Library* **2009,** *1164*, null-null.
69. Bauer, C. A.; Allendorf, M. D.; Doty, F. P.; Simmons, B. A. Hybrid metal organic scintillator materials system and particle detector. US7985868B1, 2011.
70. Bauer, C. A.; Timofeeva, T. V.; Settersten, T. B.; Patterson, B. D.; Liu, V. H.; Simmons, B. A.; Allendorf, M. D., Influence of Connectivity and Porosity on Ligand-Based Luminescence in Zinc Metal−Organic Frameworks. *Journal of the American Chemical Society* **2007,** *129* (22), 7136-7144.
71. Duan, X.; Cai, J.; Yu, J.; Wu, C.; Cui, Y.; Yang, Y.; Qian, G., Three-dimensional copper (II) metal-organic framework with open metal sites and anthracene nucleus for highly selective C2H2/CH4 and C2H2/CO2 gas separation at room temperature. *Microporous Mesoporous Mater.* **2013,** *181*, 99-104.
72. Wen, H.-M.; Li, B.; Yuan, D.; Wang, H.; Yildirim, T.; Zhou, W.; Chen, B., A porous metal-organic framework with an elongated anthracene derivative exhibiting a high working capacity for the storage of methane. *J. Mater. Chem. A* **2014,** *2* (29), 11516-11522.
73. Hawes, C. S.; Nolvachai, Y.; Kulsing, C.; Knowles, G. P.; Chaffee, A. L.; Marriott, P. J.; Batten, S. R.; Turner, D. R., Metal-organic frameworks as stationary phases for mixed-mode separation applications. *Chem. Commun. (Cambridge, U. K.)* **2014,** *50* (28), 3735-3737.
74. Gole, B.; Bar, A. K.; Mallick, A.; Banerjee, R.; Mukherjee, P. S., An electron rich porous extended framework as a heterogeneous catalyst for Diels-Alder reactions. *Chem. Commun. (Cambridge, U. K.)* **2013,** *49* (67), 7439-7441.
75. Zhuang, J.; Friedel, J.; Terfort, A., The oriented and patterned growth of fluorescent metal–organic frameworks onto functionalized surfaces. *Beilstein Journal of Nanotechnology* **2012,** *3*, 570-578.
76. Chang, Z.; Zhang, A.-S.; Hu, T.-L.; Bu, X.-H., ZnII Coordination Poylmers Based on 2,3,6,7-Anthracenetetracarboxylic Acid: Synthesis, Structures, and Luminescence Properties. *Crystal Growth & Design* **2009,** *9* (11), 4840-4846.
77. Liu, F.; Zhang, L.; Wang, R.; Sun, J.; Yang, J.; Chen, Z.; Wang, X.; Sun, D., Five MOFs with different topologies based on anthracene functionalized tetracarboxylic acid: syntheses, structures, and properties. *CrystEngComm* **2014,** *16* (14), 2917-2928.
78. Jüstel, T.; Nikol, H.; Ronda, C., New Developments in the Field of Luminescent Materials for Lighting and Displays. *Angewandte Chemie International Edition* **1998,** *37* (22), 3084-3103.
79. Zhang, C.; Zhang, M.; Qin, L.; Zheng, H., Crystal Structures and Spectroscopic Properties of Metal–Organic Frameworks Based on Rigid Ligands with Flexible Functional Groups. *Crystal Growth & Design* **2013,** *14* (2), 491-499.

80. Chen, L.; Ma, J.; Chen, Q.; Feng, R.; Jiang, F.; Hong, M., A 2D silver-iodide-organic framework with both fluorescent and phosphorescent emissions. *Inorganic Chemistry Communications* **2012,** *15* (0), 208-211.
81. Wu, H.; Liu, H.-Y.; Liu, Y.-Y.; Yang, J.; Liu, B.; Ma, J.-F., An unprecedented 2D [rightward arrow] 3D metal-organic polyrotaxane framework constructed from cadmium and a flexible star-like ligand. *Chemical Communications* **2011,** *47* (6), 1818-1820.
82. Zhou, X.-H.; Li, L.; Li, H.-H.; Li, A.; Yang, T.; Huang, W., A flexible Eu(iii)-based metal-organic framework: turn-off luminescent sensor for the detection of Fe(iii) and picric acid. *Dalton Transactions* **2013,** *42* (34), 12403-12409.
83. Guo, L.-R.; Tang, X.-L.; Ju, Z.-H.; Zhang, K.-M.; Jiang, H.-E.; Liu, W.-S., Lanthanide metal-organic frameworks constructed by asymmetric 2-nitrobiphenyl-4,4[prime or minute]-dicarboxylate ligand: syntheses, structures, luminescence and magnetic investigations. *CrystEngComm* **2013,** *15* (44), 9020-9031.
84. Vilela, S. M. F.; Ananias, D.; Fernandes, J. A.; Silva, P.; Gomes, A. C.; Silva, N. J. O.; Rodrigues, M. O.; Tome, J. P. C.; Valente, A. A.; Ribeiro-Claro, P.; Carlos, L. D.; Rocha, J.; Almeida Paz, F. A., Multifunctional micro- and nanosized metal-organic frameworks assembled from bisphosphonates and lanthanides. *J. Mater. Chem. C* **2014,** *2* (17), 3311-3327.
85. Silva, P.; Ananias, D.; Bruno, S. M.; Valente, A. A.; Carlos, L. D.; Rocha, J.; Almeida Paz, F. A., Photoluminescent Metal–Organic Frameworks – Rapid Preparation, Catalytic Activity, and Framework Relationships. *European Journal of Inorganic Chemistry* **2013,** *2013* (32), 5576-5591.
86. Zhang, L.; Song, T.; Xu, J.; Sun, J.; Zeng, S.; Wu, Y.; Fan, Y.; Wang, L., Polymorphic Ln(III) and BPTC-based porous metal-organic frameworks with visible, NIR photoluminescent and magnetic properties. *CrystEngComm* **2014,** *16* (12), 2440-2451.
87. Wei, Z.; Gu, Z.-Y.; Arvapally, R. K.; Chen, Y.-P.; McDougald, R. N.; Ivy, J. F.; Yakovenko, A. A.; Feng, D.; Omary, M. A.; Zhou, H.-C., Rigidifying Fluorescent Linkers by Metal-Organic Framework Formation for Fluorescence Blue Shift and Quantum Yield Enhancement. *J. Am. Chem. Soc.* **2014,** *136* (23), 8269-8276.
88. Decadt, R.; Van Hecke, K.; Depla, D.; Leus, K.; Weinberger, D.; Van Driessche, I.; Van Der Voort, P.; Van Deun, R., Synthesis, Crystal Structures, and Luminescence Properties of Carboxylate Based Rare-Earth Coordination Polymers. *Inorganic Chemistry* **2012,** *51* (21), 11623-11634.
89. Rao, X.; Song, T.; Gao, J.; Cui, Y.; Yang, Y.; Wu, C.; Chen, B.; Qian, G., A Highly Sensitive Mixed Lanthanide Metal–Organic Framework Self-Calibrated Luminescent Thermometer. *Journal of the American Chemical Society* **2013,** *135* (41), 15559-15564.
90. Zhang, T.; Lin, W., Metal-organic frameworks for artificial photosynthesis and photocatalysis. *Chemical Society Reviews* **2014,** *43* (16), 5982-5993.

Chapter 2. Systematic Investigation of the Excited State Properties Anthracenedicarboxylic Acids

*Jennifer M. Hay, William A. Maza, Robert C. Chapleski, Taylor M. Gaillot, Diego Troya, and Amanda J. Morris**

Department of Chemistry, Virginia Polytechnic Institute and State University, Blacksburg, Virginia 24061, United States

This chapter will soon be submitted for publication to *Physical Chemistry A*, therefore the manuscript is formatted for submission. Jennifer Hay conceived and executed the data presented, with guidance on experimental design and interpretation from Dr. William A. Maza and Amanda J. Morris. The majority of the theoretical calculations were performed by Robert C. Chapleski with guidance from Dr. Diego Troya.

ABSTRACT : Steady state absorption and emission spectra and time resolved fluorescence measurements were obtained for three anthracenedicarboxylic acids: 9,10-anthracenedicarboxylic acid (9,10-ADCA), 2,6-anthracenedicarboxylic acid (2,6-ADCA), and 1,4-anthracenedicarboxylic acid (1,4-ADCA). The fluorescence quantum yields in polar solvents (dimethylsulfoxide, acetonitrile, dimethylformamide, and methanol) were found to be between 0.9 and 0.1, and fluorescence quantum yields between of 0.7 and 0.5 were determined in non-polar tetrahydrofuran. These quantum yields were found to decrease with decreasing solvent dielectric constant, and are dependent on the position of the acid groups on the ring system, with 1,4-ADCA exhibiting the lowest quantum yields in the solvents studied. The fluorescence lifetimes ranged between 8.5 to

23 ns in polar solvents, and between 16.3 and 11.1 ns in tetrahydrofuran. The lifetimes show an overall decrease with decreasing solvent dielectric constant, and are dependent on substituent location with 1,4-ADCA exhibiting the longest lifetimes. The radiative and nonradiative decay constants were calculated from the fluorescence quantum yields and lifetimes. Analysis and comparison of the experimentally determined radiative rate of decay to calculated rates of decay suggest that intramolecular forces are dominant contributors to the radiative rate of decay. Evaluation of the 0,0 energies and the non-radiative rate of decay indicates that while changes in the energy gap contribute to an increase in non-radiative rate of decay, the dominant contributor is an increase in the rate of intersystem crossing. The position of the carboxylic acid functional groups on the anthracene system resulted in differences in the photophysics of anthracene due to resonance, inductive effects resulting in the perturbation of the electronic transitions oriented along the longitudinal and transverse short axes of anthracene.

2.1 Introduction

The tenability and sensitivity of the excited states of organic photoactive molecules impart versatility to their potential use in a wide array of applications. These include incorporation into organic light emitting diodes[1-2] (OLEDs), organic semicondictors[3], and fluorescent probes as sensing elements[4-5]. Knowledge of the dynamics and energetics of the excited states is important to understand the photophysical and photochemical propensity of a species towards a particular application. Such knowledge also aids the rational design of derivatives whose photophysical and photochemical properties may be more adept towards the same applications than the parent structure.

Anthracene is a polyaromatic hydrocarbon whose excited state properties have been extensively researched. Its photophysical properties have been found to be easily tuned through structural

modifications, making it an ideal chromophore for use in luminescent devices. For example, anthracene has been used in the functionalization of bimesityls, resulting in tunable emission, fluorescence quantum yields and electroluminescence suitable for OLED applications.[2] Incorporation of anthracene onto polyphenyleneethynylene backbones has resulted in organic semiconductor materials with applications in solar energy harvesting.[3] Anthracenes have also been incorporated into Langmuir-Blodgett (LB) films as a photoprobe in order to characterize the molecular microenvironment of the anthracene within the films.[4] The possible applications of anthracene and its derivatives are extensive, but full realization of its potential requires a greater understanding of how microenvironment and derivatization effects its photophysical properties.

The photophysical characterization of three anthracene derivatives, 9,10-anthracenedicarboxylic acid, 2,6-anthracenendicarboxylic acid, and 1,4-anthracenedicarboxylic acid were studied in various solvents in hopes of gaining a better understanding of the effect of substituent position and specific solvent effects on the ground and excited state properties of anthracenedicarboxylic acid.

2.2 Materials and Methods

9,10-anthracenedicarboxylic acid (9,10-ADCA), 1,4-anthracenedicarboxylic acid (1,4-ADCA), and 2,6-anthracenedicarboxylic acid (2,6-ADCA) were synthesized following previously reported procedures with minimal modifications.[6-10] All other chemicals and solvents including anthracene (> 99 %), $Zn(NO_3)_2 \cdot 6\ H_2O$ (> 99 %), KOH (85 %), acetonitrile (AcCN, HPLC grade > 99.9 %), cyclohexane (HPLC grade > 99.5 %), dimethylformamide(DMF, HPLC grade > 99%), dimethyl sulfoxide (DMSO, ACS grade > 99.9 %), methanol (MeOH, HPLC grade > 99.9 %), and tetrahydrofuran (THF, ACS grade > 99 %) were used as received without further purification from Alfa Aesar, Fisher Scientific, or Sigma-Aldrich.

Synthesis of 9,10-ADC.[10] 9,10-dibromoanthracene (2.0 g, 5.96 mmol) was stirred in anhydrous diethyl ether (20 mL) and n-butyllithium (9.76 mL, 15.6 mmol, of 1.6 M hexane solution) was added dropwise to the solution. After stirring the reaction was cooled in an ice bath and gaseous CO_2 was bubbled through the solution for 1 h. The product was extracted into DI water and then acidified with sulfuric acid, and the yellow product was collected and washed with DI water. ^{1}H NMR (d-DMSO, p.p.m.) δ 8.06 (dd, 4 H, J = 6.85 MHz, J = 3.15 MHz), 7.67 (dd, 4 H, J = 6.80 MHz, J = 2.80 MHz).

Synthesis of 1,4-ADCA.[6, 8-9]

1,4-dimethylanthraquinone. 1,4-napthoquinone(18.7 g, 0.118 mol) and 2,4-hexadiene (10.0 g, 0.121 mol) in toluene was heated at 65 ºC for 4 days with stirring. The solvent was evaporated off to yield an oily brown mixture of 1,4-dimethyl-1,4-dihydro-9,10-anthraquinone. A solution of 60 g of KOH in absolute ethanol (500 mL) was cooled in an ice bath and stirred while adding a solution of 1,4-dimethyl-1,4-dihydro-9,10-anthraquinone in ethanol (2.5 L). The resulting mixture was purged with gaseous O_2 for 2 h while being cooled in an ice bath. The solvent was evaporated off, and the resulting residue was dissolved in water and the dimethyl product was extracted with toluene. Removal of the aromatic solvent, followed by recrystallization in ethanol at 4 ºC yielded pure 1,4-dimethylanthraquinone. ^{1}H NMR ($CDCl_3$, p.p.m.) δ 8.17 (dd, 2 H, J = 5.80 MHz, J = 3.4 MHz), 7.73 (dd, 2 H. J = 5.80 MHz, J = 3.40 MHz), 7.41 (s, 1 H), 2.79 (s, 6 H).

1,4-dicarboxyanthraquinone. In a 40 mL autoclave, 1,4-dimethylanthraquinone (200 mg, 0.8 mmol) was combined with an 18 % HNO_3 solution and heated 220 ºC for 3 h. After cooling, the yellow precipitate was collected and washed with water to give pure 1,4-dicarboxyanthraquinone. ^{1}H NMR (d-DMSO, p.p.m.) δ 8.16 (dd, 2 H, J = 5.80 MHz, J = 3.60 MHz), 7.95 (dd, 2 H, J = 5.80 MHz, J = 3.4 MHz), 7.85 (s, 1 H).

1,4-ADCA. Reduction of the quinone was performed using a modified procedure given by Johnson et al.[7], where metallic Zn (6.58 g, 0.10 mol) and NH_4OH (50 mL) were stirred in a round bottom flask in an ice bath as 1,4-dicarboxyanthraquinone (2.11 g, 7.13 mmol) was added slowly. Following the addition, the reaction is heated to 100 °C and stirred for 2 h. The reaction mixture was cooled to room temperature (rt) and filtered by vacuum. The filtrate was acidified with 12 M HCl to give an orange precipitate, 1,4-ADCA. ^{1}H NMR (d-DMSO, p.p.m) δ 9.47 (s, 2 H), 8.17 (dd, 2 H, J = 5.12 MHz, J = 2.60 MHz), 8.14 (s, 2 H), 7.61 (dd, 2 H, J = 5.24 MHz, J = 2.52 MHz).

Synthesis of 2,6-ADCA.[6-7, 9]

2,6-dimethylanthraquinone. In an autoclave, benzoquinone (5.0 g, 46 mmol), isoprene (11.4 g, 139 mmol), and a spatula tip of hydroquinone, were suspended in 20 mL of ethanol and heated at 130 ºC for 6 h. The autoclave was allowed to reach rt and the reaction mixture was mixed with a potassium hydroxide solution in ethanol (400 ml, 5 %) and heated for 8h at 40 ºC. Stirring was continued for 12h at room temperature. The mixture was heated again at 50 ºC for 1h and filtered to give an insoluble white cream solid, 2,6-dimethylanthraquinone.[6] ^{1}H NMR (d-DMSO) δ 8.11 (d, 2 H, J = 8.0 MHz), 8.01 (s, 1 H), 7.73 (d, 2 H, J = 8.0 MHz), 2.52 (s, 6 H).

2,6-dicarboxyanthraquinone was prepared using the same procedure used to synthesize 1,4-dicarboxyanthraquinone.[9] ^{1}H NMR (d-DMSO, p.p.m.) δ 8.67 (s, 2 H), 8.4 (d, 2 H, J = 6.40 MHz), 8.3 (d, 2 H, J = 7.60 MHz).

2,6-dicarboxyanthraquinone was reduced to 2,6-ADCA using the same modified reduction procedure given above for the 1,4-dicarboxyanthraquinone.[7] ^{1}H NMR (d-DMSO, p.p.m) δ 8.89 (s, 2 H), 8.83 (s, 2 H), 8.21 (d, 2 H, J = 8.92 MHz), 7.98 (d, 2 H, J = 8.90 MHz).

Photophysical measurements. Steady-state absorption spectra of the ADCAs were obtained using a Cary Series 5000 UV-vis NIR spectrophotometer. Steady-state fluorescence spectra were

obtained using a Cary Eclipse Fluorescence Spectrometer. Fluorescence spectra were obtained between 380-550 nm by excitation of liquid samples at 370 nm.

Fluorescence lifetime decays of the ADCAs in cyclohexane, acidic and basic DMF, MeOH, AcCN, DMSO, and THF were obtained with an Applied Photophysics model LKS.60 laser photolysis system. Samples were excited using the third harmonic of a Continuum Surelite SLI-10 Nd:YAG laser (6-8 ns pulsewidth, λ_{exc} =355 nm) directed onto the face of the samples cuvette, and the resulting fluorescence signals, collected 90° relative to the excitation pulse, were focused into a Spectrokinetic monochromator (Applied Photophysics, model 05-109, bandpass 4.65 nm/mm). A photomultiplier (Applied Photophysics) amplified the signals, which were then digitized with a HP Infinium 500 MHz digital oscilloscope (2 GS/sec sampling) and recorded on a PC running the Applied Photophysics Reaction Analyser Software package. Fluorescence lifetime decays were deconvoluted from the observed time-dependent fluorescence signal obtained at 450 nm and the instrument response function using the freeware DecayFit fluorescence decay analysis software package available online (Fluortools, www.fluortools.com).

Theoretical calculations. The radiative decay constants were calculated using the Strickler-Berg method obtained in the PHOTOCHEMCAD 2.1 software package. Ground state energy calculations, in which the dihedral angle between COOH and the ring system were varied from 0-180°, were obtained with Gaussian 09[11] using B3LYP/6-31G[12-15] density functional method.

2.3 Results and Discussion

Upon absorption of a photon of appropriate energy, a molecule can be promoted from its ground state (S_0) to an excited state of higher energy (S_n). Electronic transitions occur more rapidly (10^{-15} s) than vibronic motion (10^{-12} s)[16] therefore, excitation of a molecule to a higher electronic state occurs instantaneously compared to nuclear motion, so that this non-equilibrium excited state, or

Franck-Condon state, configuration is identical to the ground state. The excess energy of the excited state is dissipated through radiation and/or radiationless processes. Such transitions may be unimolecular or bimolecular depending on the chemical structure and environment.[17] A useful parameter used to describe such photophysical processes is quantum yield of fluorescence. The fluorescence quantum yield (Φ_{fl}), simply put, is the ratio of the number of emitted photons to the number of photons absorbed. In the absence of intermolecular deactivation processes, Φ_{fl}, is related to the radiative (k_r) and nonradiative (k_{nr}) decay rate constants by expression (1).

$$\Phi_{fl} = \frac{k_r}{k_r + k_{nr}} \tag{1}$$

where, k_{nr} is sum of the internal conversion rate constant, k_{ic}, and the intersystem crossing rate constant, k_{isc} (5).

$$k_{nr} = k_{ic} + k_{isc} \tag{2}$$

$$\tau_{fl} = \frac{1}{k_r + k_{nr}} \tag{3}$$

$$\Phi_{fl} = k_r \tau_{fl} \tag{4}$$

The rates of deactivation from S_1 are related to the lifetime of the fluorecence, τ_{fl}, using expression (3), which can be related to the fluorescence quantum yield by (4). Fluorescence quantum yields can provide useful information on the nonradiative processes that compete with fluorescence in the deactivation of the lowest singlet excited state, S_1.[18]

Anthracene displays interesting spectral properties such as intense absorption and emission spectra. The absorption spectrum is characterized by two sets of close lying bands spanning the 1) 220 nm to 280 nm range and 2) the 290 nm to 400 nm range (Figure 2-1). These band clusters correspond to two separate $\pi \rightarrow \pi^*$ transitions; the various maxima observed in these regions are vibrational in nature, whose transition moments lie in one of the three planes of the molecular axes. For example, it has been established that the transition dipole of the lowest energy transition of

anthracene occurring at ~ 386 nm is polarized along the transverse short axis, whereas the high energy transition occurring at ~ 256 nm is thought to correspond to a longitudinally polarized transition dipole.[19-21]

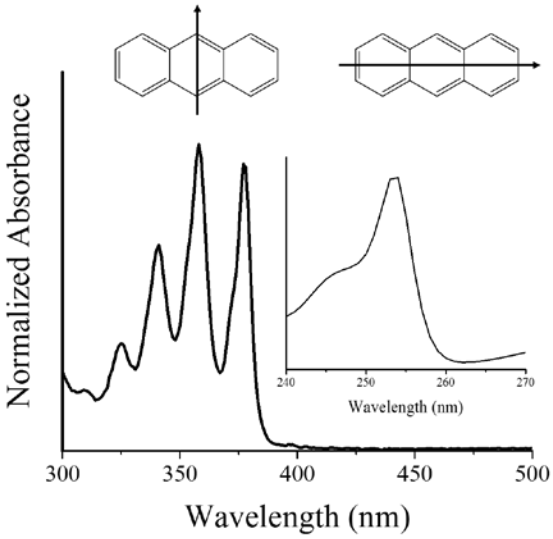

Figure 2-1. Absorbance spectrum of anthracene in THF showing the lower energy $\pi \rightarrow \pi^*$ transitions with dipoles moments oriented about the transverse short axis of anthracene, and the higher energy $\pi \rightarrow \pi^*$ transition occurring near 256 nm, whose dipole moment is polarized across the longitudinal axis of anthracene (inset).

The emission spectrum of anthracene exhibits fine structure with energy spacing between vibrational bands similar to the energy spacing between vibronic bands in the absorbance spectrum. The similar energy spacing between vibronic bands in the emission spectrum (~1350 cm^{-1} in THF) and absorbance spectrum (~1400 cm^{-1} in THF) spectrum results in a mirror image relationship between the two spectra. The observation of a mirror image relationship indicates that the energy difference between the vibrational levels are similar in the ground (S_0) and excited (S_1) electronic states. These and other spectral properties have made anthracene an excellent prototype for studying the effects of temperature[22-24], derivitization[19, 23-29], solvents[23, 25-26, 30], and quenching[27] on ground and excited state dynamics of aromatic molecules.

The excited state properties of anthracene have been extensively studied, with the molecule displaying fluorescence quantum yields in the range of 0.23 to 0.36 and fluorescence lifetimes between 5.1 and 6.8 ns depending on solvent and temperature.[18, 22, 29, 31] It has been theoretically determined that forbidden, nonradiative transitions of the S_1 to T_2 and T_1 type in anthracene become allowed transitions through the process of vibronically induced spin orbit (VISO) coupling, with the rate constant, k_{isc}, being proportional to the square of the coupling energies of the singlet and triplet states.[32] Functionalization of anthracene with electron-withdrawing carbonyl groups at the 9 position has been shown to decrease or eliminate radiative transitions from S_1, an effect that has been attributed to an increase in intersystem crossing from S_1 to a triplet $n\pi^*$ state not accessible in anthracene.[33] On this basis, the addition of carboxylic acid groups onto anthracene may result in additional excited states with triplet character, like $n\pi^*$ states, which could provide better overlap with the S_1 via the VISO mechanism. This increased overlap between S_1 and a triplet state, T_n, could increase the contribution of the rate of intersystem crossing, k_{isc} to the overall rate of nonradiative decay, k_{nr}.

Absorption and Emission Spectra. Steady state absorption and emission spectra were obtained for 9,10-, 2,6-, and 1,4-ADCA in AcCN, DMSO, MeOH, DMF, and THF. The absorbance and emission of the three acids in THF are shown in Figure 2-2. The absorbance spectra of 9,10- and 2,6-ADCA display similar vibrational structure to that of anthracene in THF. 9,10-ADCA exhibits maxima centered at 386 nm, 366 nm, 349 nm, and a shoulder at 333 nm, that are red-shifted to anthracene (Figure 2-2b). The emission of 9,10-ADCA displays a bathochromic shift and is diffuse and broad compared to the emission of anthracene. 2,6-ADAC exhibits absorption maxima at 408 nm, 386 nm, 358 nm, and 342 nm, with emission maxima at 418 nm, 443 nm, and 471 nm. The

absorbance (maxima at 369 and 398 nm with a slight shoulder at 350 nm) and emission spectra of 1,4-ADCA is broadened and red shifted relative to anthracene.

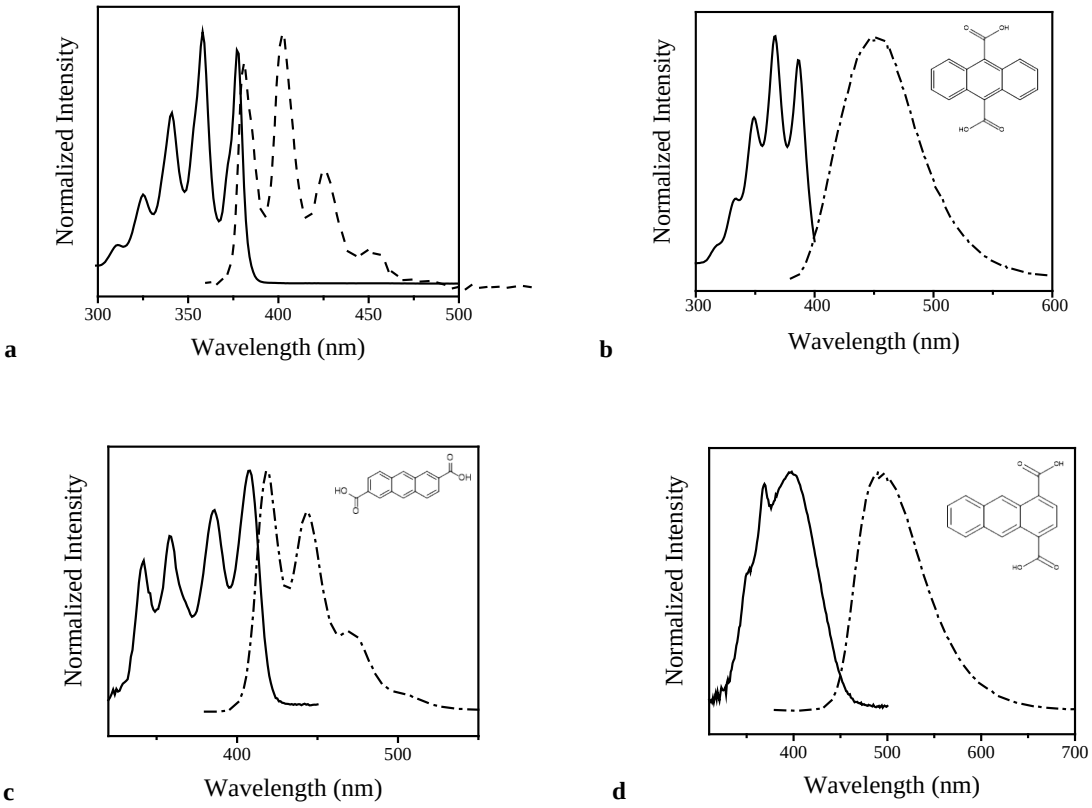

Figure 2-2. Normalized absorbance (solid lines) and emission, upon excitation a,t 370 nm (dotted lines) of **(a)** anthracene, (**b**) 9,10-ADCA, with absorption maxima centered at 386/366/349 nm and a shoulder at 333 nm, (**c**) 2,6-ADCA, with absorption maxima at 408/386/358/342 nm, and (**d**) 1,4-ADCA, with maxima at 369/398 nm and a slight shoulder at 350 nm, in THF.

A summary of the absorption and emission data is given in Table 1. Solvents and the corresponding data are listed in order of decreasing solvent dielectric constant (ε). The absorbance (λ^{abs}) and emission (λ^{em}) wavelengths listed in Table 2-1 correspond to the maxima of the higher energy and lower energy vibrational bands, respectively.

Table 2-1. Summary of Steady State Absorption and Emission Data

	Solvent	[a]ε	[b]λ_{abs} (nm)	[c]λ_{em} (nm)	Stokes (cm-1)	$E_{0,0}$ (eV)
9,10-ADCA	**DMSO**	46.7	390	455	3660	3.1
	AcCN	37.5	385	457	4090	3.1
	DMF(acid)	36.7	388	451	3600	3.1
	MeOH	32.7	385	423	2330	3.1
	THF	7.58	387	451	3670	3.1
2,6-ADCA	**DMSO**	46.7	410	425	861	3.0
	DMF(acid)	36.7	409	423, 448	809	3.0
	MeOH	32.7	401	424	1350	3.0
	THF	7.58	408	418	590	3.0
1,4-ADCA	**DMSO**	46.7	389	511	6140	2.8
	AcCN	37.5	392	517	6170	2.8
	DMF(acid)	36.7	390	531	6810	2.8
	MeOH	32.7	386	497	5790	2.9
	THF	7.58	397	490	4780	2.8

[a]ε is the dielectric constant[16], [b]λ_{abs} is the lowest energy maximum in the absorbance spectrum, and [c]λ_{em} is the highest energy maximum in the fluorescence spectrum.

The Stokes shift, given in cm^{-1}, was calculated from the difference between the λ^{em} and λ^{abs} of the absorbance and emission spectra. The largest Stokes shift (Table 2-1) is observed in 1,4-ADCA (4780 cm^{-1}) followed by 9,10-ADCA (3670 cm^{-1}) and 2,6-ADCA (590 cm^{-1}), all three of which are larger than the Stokes shift of anthracene in THF (~ 278 cm^{-1}).

The 0,0 transition energy was determined using the Planck relation (5), where λ is the wavelength at which the absorbance and emission spectra intersect.

$$E(eV) = \frac{1240\ eV\ nm}{\lambda\ (nm)} \quad (5)$$

The energies of the 0,0 transition do not vary much between solvents, but decrease in the order of 9,10-ADCA, 2,6-ADCA, and 1,4-ADCA with 0,0 energies of 3.1, 3.0, and 2.8/2.9, respectively.

Effects of Functional Group Location on Spectra. The addition of functional groups onto the anthracene ring system has been shown to effect the absorption and emission spectra.[19, 26, 34-35] For

example, in the case of 9-anthroic acid, the vibrational structure in the absorbance spectra is maintained but, due to inductive effects, the spectra is red-shifted relative to that of anthracene.[34] It is assumed that the red-shift observed in the absorbance spectra of the three acids studied here (Figure 2-1b-d) are also due to inductive effects. The magnitude of the spectral shift and the vibrational structure depend on the location of the carboxylic acid on the aromatic ring system and the extent to which the groups perturb the electronic transitions. It is known that the effects of sterics and electronics are closely related, suggesting that the dihedral angle between an aromatic system and its substituents is what will differ most between electronic states rather than changes in the bond lengths of the aromatic system.[17] The energetics of the ground state have been calculated relative to the dihedral angle between the acid groups and the anthracene rings to determine the angle that generates the most stable ground state conformation of the three acids studied (Figure 2-3,4, and 5c). An understanding of the ground state geometry of the acid groups on the ring system will provide a better understanding of the effects of the functional groups on the electronic transitions occurring in anthracene.

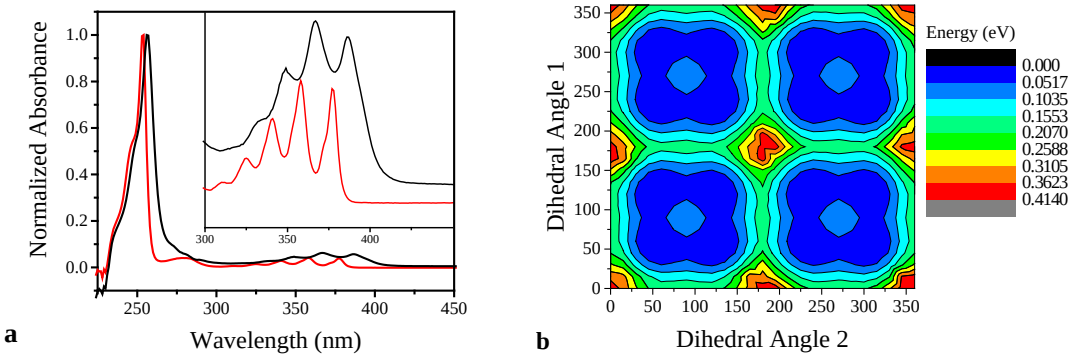

Figure 2-3. (a) Normalized absorbance of 9,10-ADCA (black) and anthracene (red) in THF. Inset shows lower energy maxima. (b) DFT calculations of ground state energy as a function of the COOH and anthracene dihedral angles.

The absorbance of 9,10-ADCA, though red-shifted, resembles that of anthracene, showing similar spectral structure in all solvents (Figure 2-3a and Appendix Figures 3-7) and similar separation between vibronic bands (~1400 cm^{-1}). The similarity in the absorbance suggests that these electronic transitions arise from similar ground state configurations compared to unsubstituted anthracene with dipole moments oriented along the parent anthracene ring system. The absence of a large perturbation to the absorbance spectra due to the COOH group is believed to be a result of poor orbital overlap between the functional group and the aromatic ring system.

It is has been suggested that, in the case of 9-anthroic acid and its esters, the steric hindrance of the *peri*-hydrogens causes the COOH group to be almost perpendicular to the ring system, thereby minimizing resonance interactions between COOH and the ring system in the ground and Franck-Condon excited states.[27, 34] DFT calculations (Figure 2-3b) show that the lowest energy conformation in the ground state of 9,10-ADCA is obtained when the acid group are at a dihedral angle of 60° relative to the planarity of the ring system. When the dihedral angle is at 0°, the ground state energy is the highest and the ring system is contorted due to steric interactions between the *peri*-hydrogens and the acid groups (Appendix Figure 22). The results of the DFT calculations indicate that it is energetically unfavorable for the acid groups and anthracene rings to be in a coplanar conformation in the ground state. Therefore, in the pseudo-perpendicular conformation, π overlap between the two is not significant enough to perturb the dipole moments of the higher or lower energy electronic transition oriented along the long and short axes of the molecule. Additionally, frontier orbital calculations of 9,10-ADCA (Appendix Figure 15) show that the HOMO and LUMO are localized on the anthracene ring and are very similar in electron density distribution to the frontier orbitals of anthracene (Appendix Figure 18). Both DFT calculations and absorption spectrum of 9,10-ADCA are in agreement with the model in which the electronic

transitions with dipole moments oriented in the direction of the short axis, result from the π-system of anthracene with no perturbation of the transition dipole moment due to the COOH groups.

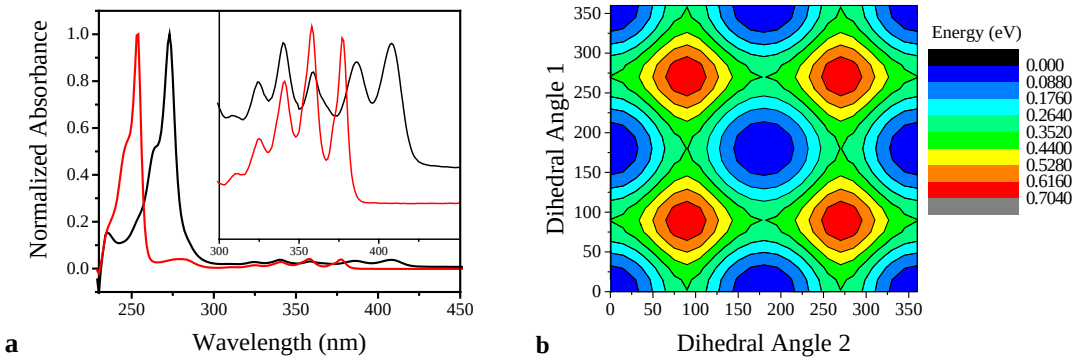

Figure 2-4. (a) Normalized absorbance of 2,6-ADCA (black) and anthracene (red) in THF. Inset shows lower energy maxima. (b) DFT calculations of ground state energy as a function of the COOH and anthracene dihedral angles of 2,6-ADCA.

The absorbance spectrum of 2,6-ADCA also exhibits anthracenic vibrational structure in all solvents studied, with no observable solvent dependence between polar and nonpolar solvents (Figure 2-4a and Appendix Figures 8-10). It was found that the higher energy band, λ = 273 nm, is shifted to a much greater extent than the lower energy bands in the absorbance spectrum of 2,6-ADCA in THF (Figure 2-4a). The higher energy band is red shifted by ~2740 cm^{-1} compared to the lower energy band which is shifted by ~2015 cm^{-1}. The lower energy bands of 2,6-ADCA shows similar but broadened vibrational structure relative to anthracene, and has absorption maxima at 408 nm, 386 nm, 358 nm, and 342 nm. Like the spectra of 9,10-ADCA, the absorbance of 2,6-ADCA is also red-shifted relative to anthracene in all solvents studied, likely due to inductive effects of the COOH groups. Interestingly, the most intense vibrational band resides on the lower energy edge of the spectrum, unlike in anthracene where the most intense band is the second to lowest energy band. Also, vibrational structure is maintained despite that the lowest

energy conformation being when the COOH groups are coplanar with the ring system, at a dihedral angle of 0°, according to DFT calculations. At such an angle, overlap of the π-orbitals between the ring system of anthracene and the COOH groups should be significant enough to allow for resonance between the rings and the acid groups, which would be expected to perturb the electronic transitions. Frontier orbital calculations of 2,6-ADCA in its lowest energy conformation ($\theta \approx 0°$) show that the HOMO and LUMO are localized almost completely on the anthracene ring system. The calculations predict that the electronic transitions occurring in the absorption spectrum of the acid would be $\pi \rightarrow \pi^*$ transitions.

It is clear from the absorbance spectrum of 2,6-ADCA in THF, that functionalization of the anthracene ring at the 2,6 position perturbs the electronic transitions with dipole moments across the longitudinal axis to a greater extent that those oriented across the short axis of anthracene. Additional evidence of these substituent effects on the absorbance spectra of anthracene has been observed in the case of 2,3,9,10-tetraphenylanthracene. The addition of phenyl substituents at the 9,10 positions had relatively no effect on the absorption spectrum, compared to anthracene, other than producing a slight red shift.[19] There is believed that the phenyl groups in the 2,3 positions approach near coplanarity with the ring system, which has a much greater effect on the higher energy absorption band (220 nm to 280 nm), shifting it to the red by ~4000 cm^{-1}, whereas the lower energy absorption band is only shifted by ~800 cm^{-1}.[19] The greater red shift of the higher energy transition relative to the lower energy transition in the absorption spectrum of 2,3,9,10-tetraphenylanthracene indicates that functionalization at the 2 and 3 position may result in greater perturbation of the transition dipole moment along the long axis than the dipole moment along the short axis. The tetraphenyl data along with the anthracenic structure evident in the absorption spectrum of 2,6-ADCA suggests that functionalization at the 2, 3, 6, and 7 positions on anthracene

mainly effect the electronic transitions with moments oriented along the longitudinal long axis with minor perturbation to the transitions oriented along the vertical short axis. Additionally, DFT calculations of the ground state frontier orbitals of 2,6-ADCA show that the HOMO and LUMO are evenly distributed on the anthracene ring, with little electron density residing on the COOH groups (Appendix Figures 20). DFT calculations and the absorption data obtained for 2,6-ADCA indicate that functionalization at the 2,6, and likely the 3,7 positions, has little effect on the transition dipole moment across the short axis, regardless of increased resonance, but perturbs the dipole oriented along the long axis to a much greater extent.

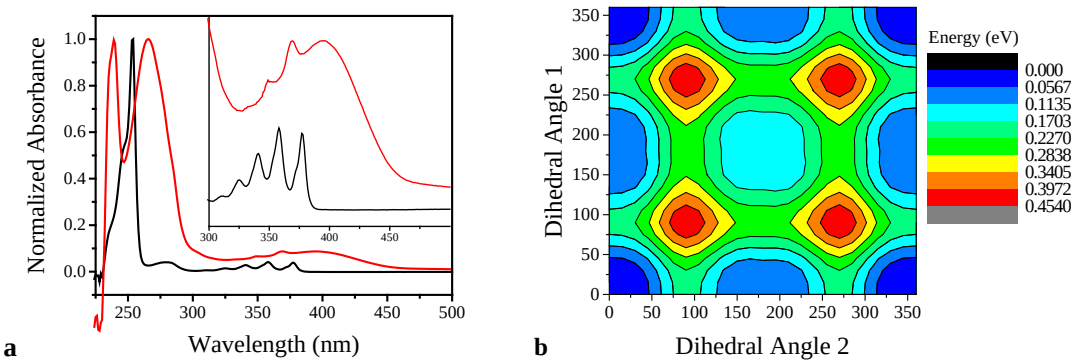

Figure 2-5. (a) Normalized absorbance of 1,4-ADCA (red) and anthracene (black) in THF. Inset shows lower energy maxima. (b) DFT calculations of ground state energy as a function of the COOH and anthracene dihedral angles of 1,4-ADCA.

The absorbance spectra of 1,4-ADCA is structureless in DMSO, but in THF (Figure 2-5a), AcCN, and MeOH, a broad band is observed around 390 nm and a higher energy shoulder is seen around 369 nm (Appendix Figures 11-14). The lack of vibrational structure and the red shift of the spectra indicate that there is additional resonance between the COOH group and the ring system, which perturbs the dipole moment of the electronic transitions along the short axis. DFT calculations (Figure 2-5b) show that the lowest energy conformation in the ground state has the dihedral angles between acid groups and ring system at 0°, making the COOHs coplanar with the

anthracene rings. Additionally, molecular orbital calculations show that the HOMO and LUMO of 1,4-ADCA are unevenly distributed over the anthracene ring unlike the symmetric distribution predicted in the case of 9,10 and 2,6-ADCA (Appendix Figures 15-17). The HOMO of 1,4-ADCA is delocalized more heavily away from the acid groups, whereas the LUMO is localized on the ring and the acid groups themselves. Such an uneven distribution of electron density would be expected to affect the anthracenic electronic transitions oriented along the long and short axes. The absorption spectrum of 1,4-ADCA indicates that the transitions with dipole moments oriented along both axes of the anthracene ring are indeed perturbed. Perturbation of the higher energy transition is evident by the shifting of the maximum around 240 nm by ~2470 cm^{-1}, as well as splitting of the higher energy maximum into two peaks which is not observed in anthracene or the other derivatives studied.

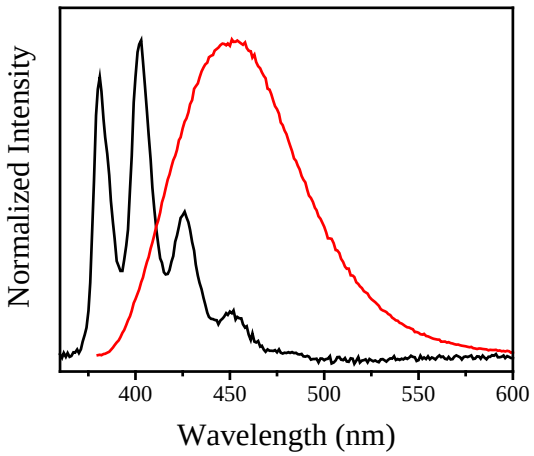

Figure 2-6. Normalized emission spectra of 9,10-ADCA (red) and anthracene (black) in THF.

The steady state emission of 9,10-ADCA, shown in Figure 2-6, is diffuse with no vibrational structure, and is greatly red-shifted, exhibiting a larger Stokes shift (3670 cm^{-1}) than is observed for anthracene, 278 cm^{-1} in THF. The magnitude of the shift does not differ

greatly between solvents differing in polarity, therefore it is assumed that the solvent dielectric of those solvents probed has little influence on the electronic transitions, $S_0 \rightarrow S_n$ and $S_1 \rightarrow S_0$.

The origin of the Stokes shift is likely due to changes in the nuclear geometry in the excited state as the rotation of the -COOH groups to a near coplanar conformation with anthracene, result in a lower energy excited state complex due to increased resonance and π overlap. This suggests that the equilibrium excited state, S_1, lies significantly lower in energy than the Franck-Condon state compared to anthracene. Another possible contribution to the large shift, originally suggested by Werner and Hercules[34] is due to differences in the potential energy functions of the ground and excited states. DFT calculations of 9,10-ADCA indicate that in the ground state the potential energy function has a minimum and maximum around $\theta = 60°$ and 0°, respectively (Figure 2-3b). It is proposed that an excited state of singlet character, S_n', exists lying below the Franck-Condon state of singlet character, S_n, and that this lowest energy accessible state has a geometric configuration in which the dihedral angle between the COOH group and anthracene rings is significantly different than that of the ground state and probably approaches $\theta = 0°$ (Figure 2-7).

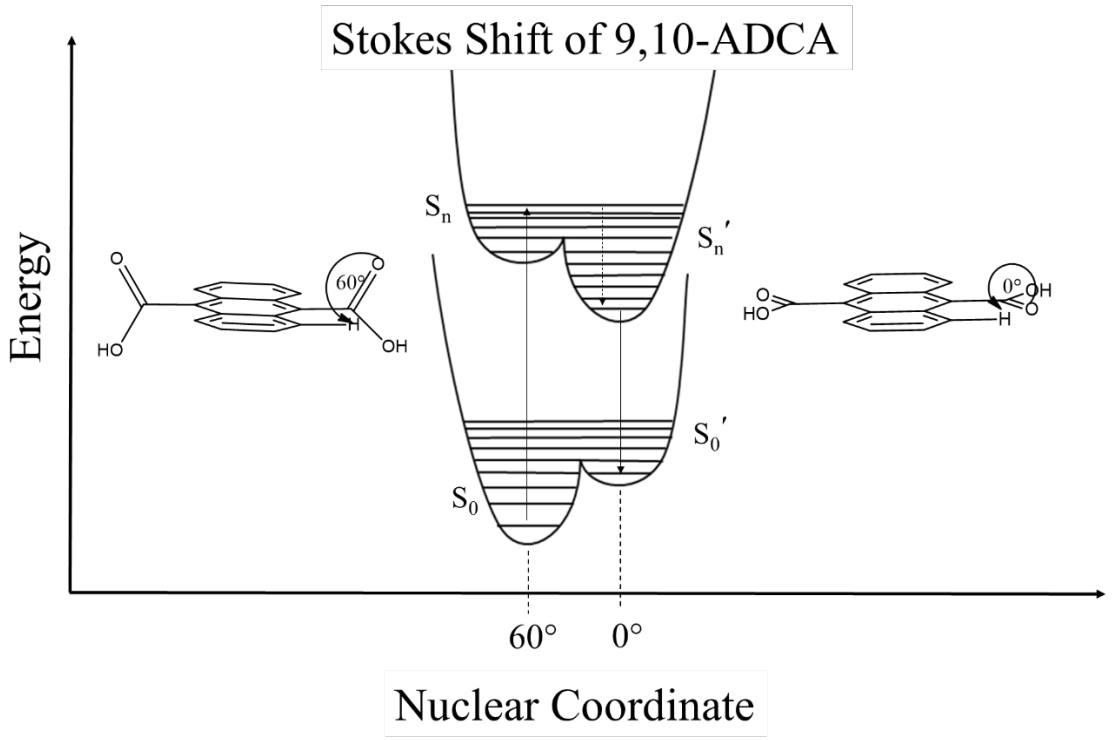

Figure 2-7. Possible relationship between ground states of different geometries (S_0 and S_0') and Franck-Condon and equilibrium excited state (S_n and S_n').

The broad and structureless emission does not seem to be the result of inhomogeneous band broadening but more likely results from CT interactions between the functional groups and the ring system in the equilibrium excited state.[27, 34] Relaxation from the Franck-Condon excited state, S_n, to the equilibrium excited state, S_n', coincides with rotation of the COOH group to near coplanarity with the anthracene ring, resulting in increased π-overlap causing homogeneous band broadening in the emission.[34]

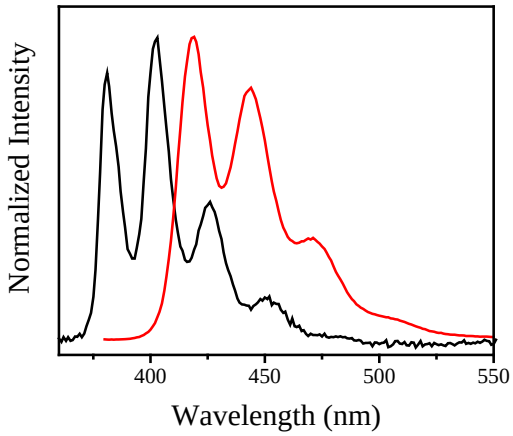

Figure 2-8. Normalized emission of 2,6-ADCA (red) and anthracene (black) in THF.

The 2,6-ADCA is the only one of the three acids studied that exhibits structured emission in all solvents (Figure 2-8 and Appendix Figures 8-10). The emission of 2,6-ADCA is the least red-shifted of the three acids when compared to anthracene and does not show any dependence on solvent polarity. The anthracenic structure of the emission suggests that the electronic transitions occurring from the excited state, S_1, have dipole moments oriented along the short axis of anthracene. In this case, the dipole moment of the excited to ground state electronic transition is directed along the short axis, with little perturbance from the carboxylic acid groups at the 2 and 6 positions. The red shift in the emission is most likely due to inductive effects of the carboxylic acid groups, with resonance providing minor contributions. The small Stokes shift (580 cm^{-1}), suggest that the nuclear configuration in the equilibrium excited state is not very different than the nuclear configuration in the ground and Franck-Condon states.

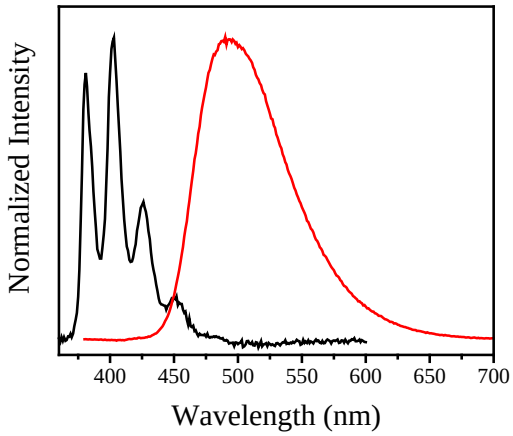

Figure 2-9. Normalized emission of 1,4-ADCA (red) and anthracene (black) in THF.

The emission spectra of 1,4-ADCA is red shifted and lacks vibrational structure in all solvents with no observable trends due to solvent polarity. The red shift, as in the case of the other derivatives studied, is most likely due to inductive effects of the COOH groups. The lack of structure is likely due to resonance with the COOH groups providing additional relaxation pathways and perturbation of the electronic transition along the short axis of anthracene.

1,4-ADCA shows the largest Stokes shift of the three acids (4780 cm^{-1}). The magnitude of the Stokes shift is indicative of a significant change in nuclear configuration between the equilibrium excited state and the Franck-Condon state. Figure 2-10 shows a simplified representation of the difference between the equilibrium excited state the Franck-Condon state for the three acids and anthracene in THF in order of increasing change in nuclear configuration between interacting states.

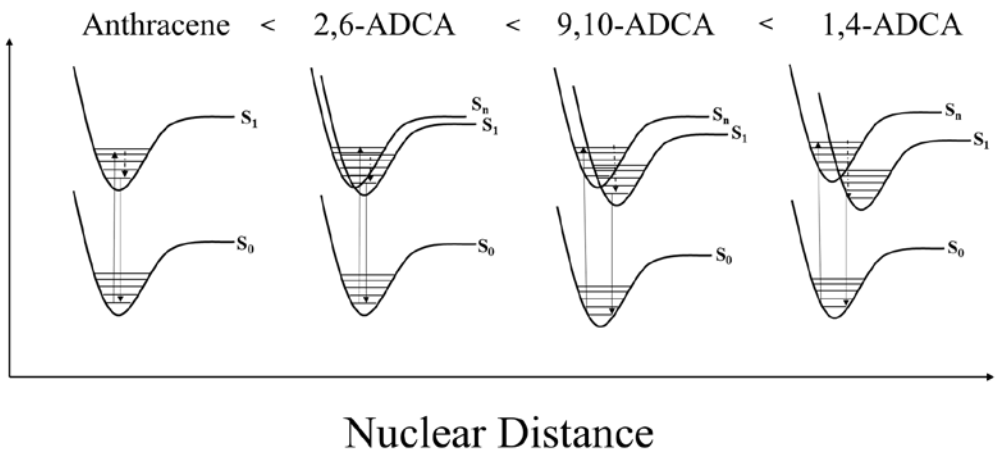

Figure 2-10. Comparison of nuclear coordinate changes between the equilibrium excited state and the ground and Franck-Condon states of the three anthracenic acids and anthracene.

Contributions to Radiative and Nonradiative Decay Constants. Fluorescence quantum yields, Φ_{fl}, and fluorescence lifetimes, τ_{fl}, of the three acids in various solvents are displayed in Table 2-2 along with the rate constants for the radiative, k_r, and nonradiative, k_{nr}, decay components of the fluorescence lifetimes. The Φ_{fl} of the three acids were determined using Eq. 6 and the Φ_{fl} of anthracene in ethanol (0.27)[16] as a reference, Φ_{ref}. The fluorescence lifetimes (τ_{fl}) were determined by deconvoluting the fluorescence decays (Figure 2-11), using DecayFit software, from the impulse signal and modeling the decays to a single exponential decay function (Eq. 7).

$$\phi_{fl} = \phi_{ref} \frac{m_s}{m_{ref}} \frac{\eta_s^2}{\eta_{ref}^2} \tag{6}$$

$$I(t) = A_1 e^{-t/\tau_{fl}} \tag{7}$$

where m_s and m_{ref} are the slopes obtained by plotting the integrated intensity of emission vs. absorbance at the excitation wavelength for both the sample and reference.

The rate constants were calculated from the experimentally determined Φ_{fl} and τ_{fl} using equations 1, 3, and 4

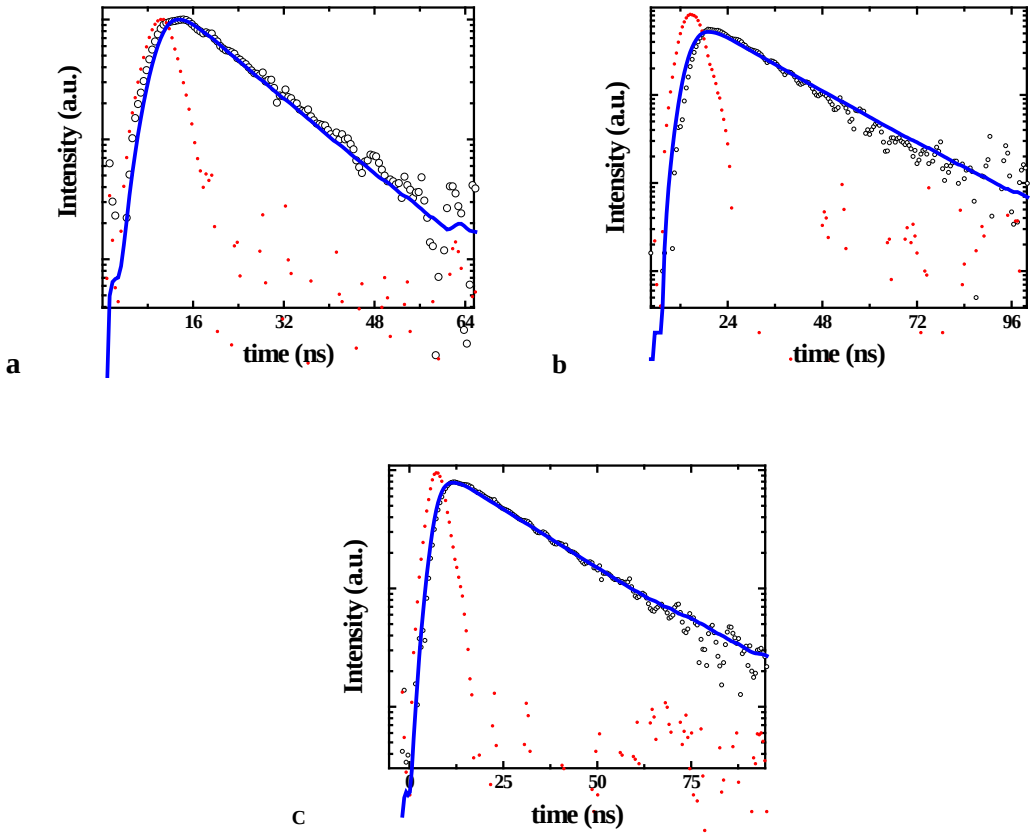

Figure 2-11. Florescence decay of 9,10-ADCA (a), 2,6-ADCA (b), and 1,4-ADCA (c) in THF, showing the impulse signal decay (red dots), the samples fluorescence decay (black circles), and the fit obtained from signal deconvolution using decay fit (blue).

Table 2-2. Summary of Fluorescence Lifetimes and Quantum Yield Data

	Solvent	[a]ε	Φ_{fl}	τ_{fl} (ns)	k_r (10^7 s^{-1})	k_{nr} (10^7 s^{-1})
Anthracene[16]	**EtOH**	25.1	0.27	5.1		
9,10-ADCA	**DMSO**	48.9	0.73 ± 0.1	11 ± 0.2	6.9 ± 0.8	2.6 ± 0.3
	AcCN	38.8	0.5 ± 0.2	12 ± 0.3	4.0 ± 1.5	4.1 ± 1.5
	DMF(acid)	37.6	0.39 ± 0.1	10 ± 0.2	3.2 ± 0.6	5.7 ± 1.0

	MeOH	33.6	0.19 ± .1	8.5 ± 0.2	2.2 ± 0.6	9.5 ± 2.5
	THF	7.52	0.71 ± 0.1	11 ± 0.5	6.4 ± 0.7	2.6 ± 0.3
2,6-ADCA	**DMSO**	48.9	0.69 ± 0.2	18 ± 0.2	3.9 ± 1.1	1.7 ± 0.5
	DMF(acid)	37.6	0.85 ± 0.2	17 ± 0.1	4.9 ± 1.1	0.9 ± 0.2
	MeOH	33.6	0.16 ± 0.1	14 ± 0.2	1.2 ± 0.4	5.9 ± 2.2
	THF	7.52	0.57 ± 0.2	15 ± 0.4	3.9 ± 1.1	2.9 ± 0.8
1,4-ADCA	**DMSO**	48.9	0.40 ± 0.10	23 ± 0.5	1.8 ± 0.4	2.6 ± 0.7
	AcCN	38.8	0.30 ± 0.04	19 ± 0.6	1.6 ± 0.2	3.7 ± 0.5
	DMF(acid)	37.6	0.10 ± 0.02	22 ± 0.6	0.5 ± 0.1	5.1 ± 1.0
	MeOH	33.6	0.21 ± 0.04	13 ± 0.2	1.6 ± 0.3	5.9 ± 1.1
	THF	7.52	0.47 ± 0.1	16 ± 0.2	2.9 ± 0.4	3.3 ± 0.5

[a]ε is the dielectric constant.[16]

The fluorescence quantum yields of the anthracenedicarboxylic acids decrease with decreasing solvent dielectric constant, with the exception of THF. 1,4-ADCA has displayed the longest lived emissive state of the three acids studied, with fluorescence lifetimes between 16 and 23 ns, compared to the other two acids whose lifetimes ranged between 9 and 18 ns. The carbonyl group is a widely known to quench fluorescence rather than enhance it, and because of a lower lying nπ* states, it is believed to effect the radiationless decay process from S_1.[33] DFT calculations show that the lowest energy ground state conformation of 1,4-ADCA is obtained when the dihedral angles between the COOH groups and the anthracene ring are at 0°, which allows for increased conjugation between the acid groups and the ring system. Frontier orbital calculations of 1,4-ADCA (S14) show more delocalization due to functional group position than with either of the two acids studied (S12-13). Both types of calculations suggest that the carboxylic acid groups will have a greater effect at the 1,4 position, than 9,10 or 2,6 positions, on the quenching of fluorescence and the rates of radiative and nonradiative decay, which is consistent with the experimental data.

An inverse correlation is observed between the 0,0 energy transition and the radiationless rate constants, in DMF and THF, which show a decrease in k_{nr} as the energy of the transition increases. According to the energy gap law, as the magnitude of the energy gap increases, k_{nr} decreases.[36]

No such correlation is observed in the other solvents studied, nor is there any correlation between k_{nr} and the solvent parameters listed above. The lack of solvent dependence suggests that while changes in the energy gap contribute to an increase in k_{nr}, the dominant contributor is an increase in k_{isc}. The increase in triplet formation, as suggested previously, is likely due to an increase in VISO coupling between singlet and triplet states.

2.4 Conclusion

Three anthracenedicarboxylic acids were synthesized and the photophysical properties probed as a function of substituent location. Differences in solvent polarity, H-bond donor and acceptor ability have little or no significant effects on the ground and excited state radiative and nonradiative decay processes of the three acids. The addition of carboxylic acid groups onto different positions on anthracene has been shown to effect the location of the ground state HOMOs and LUMOs and the electronic transitions of the anthracene system.

The results indicate that functionalization at the 9,10- and 2,6 position does not perturb the electronic transitions to the same extent as functionalization at the 1,4 position. The addition of the acid groups at the 9,10 positions has almost no effect of the electronic transition oriented along the short axis of anthracene due to sterics prohibiting orbital overlap between the COOHs and anthracene. Functionalization at the 2,6 position only slightly perturbs the electronic transitions oriented along both the longitudinal and transverse axis of anthracene, resulting in a red-shifted and broadened spectrum with differences in the intensities of the vibrational bands. In both molecules, the HOMOs and LUMOs of the ground state are localized on the anthracene ring system showing little changes due to carboxylic acid positions. 1,4-ADCA has a diffuse absorbance spectrum with significant changes to both the higher and lower energy bands, relative to anthracene. The COOH groups are oriented about the short axis, so perturbation of the short

axis transitions is expected as a result of resonance between the acid groups and the ring system. The structural differences observed in the higher energy bands is believed to be related to the unsymmetric delocalization of the HOMO and LUMOs of 1,4-ADCA. The diffuse and red-shift could be indicative of charge transfer interactions between anthracene and the acid groups in the excited state, but further studies are needed to confirm such character and its effects on the absorption spectrum.

Emission spectra of 9,10- and 1,4-ADCA are vibrationless unlike in anthracene and 2,6-ADCA. Emission from the equilibrium excited state of 9,10-ADCA is broad and diffuse due to rotation of the COOH groups resulting in perturbation of the $S_1 \rightarrow S_0$ and increased line broadening. Emission from the equilibrium excited state of 1,4-ADCA is also structureless due to perturbation by the COOH groups of the $S_1 \rightarrow S_0$ transition. The large Stokes shift of 9,10- and 1,4-ADCA suggest that the ground state and equilibrium excited state conformations of the acids are significantly different. The structured emission of 2,6-ADCA and small Stokes shift indicate that the configuration of the ground and Franck-Condon states are similar and that the dipole moment of the $S_1 \rightarrow S_0$ transition is oriented along the short axis, thereby being mostly unaffected by the functional groups.

The fluorescence quantum yields and lifetimes exhibit may exhibit a trend with solvent dielectric constant, while k_r and k_{nr} do not show a similar trend. The fluorescence quantum yields, lifetimes, and the rates of radiative and nonradiative decay do not show any observable trend with any other solvent parameters. This indicates that intramolecular, rather than intermolecular, dynamics are dominate contributors the rates of radiative and nonradiative decay. In THF and DMF, k_{nr} decreases with increased 0,0 energy gap, but no such trend is observed in the other solvents studied. This data suggests that the dominate contributor to k_{nr} is intersystem crossing to a triplet state,

likely due to increased VISO coupling. In order to truly determine whether or not intrermolecular forces are a dominant contributor to the rates of radiative and nonradiative decay, further studies in various solvents are needed.

2.5 References

1. Danel, K.; Huang, T.-H.; Lin, J. T.; Tao, Y.-T.; Chuen, C.-H., Blue-Emitting Anthracenes with End-Capping Diarylamines. *Chemistry of Materials* **2002,** *14* (9), 3860-3865.
2. Moorthy, J. N.; Venkatakrishnan, P.; Natarajan, P.; Huang, D.-F.; Chow, T. J., De Novo Design for Functional Amorphous Materials: Synthesis and Thermal and Light-Emitting Properties of Twisted Anthracene-Functionalized Bimesitylenes. *Journal of the American Chemical Society* **2008,** *130* (51), 17320-17333.
3. Swager, T. M.; Gil, C. J.; Wrighton, M. S., Fluorescence Studies of Poly(p-phenyleneethynylene)s: The Effect of Anthracene Substitution. *The Journal of Physical Chemistry* **1995,** *99* (14), 4886-4893.
4. Dutta, A. K., Characterization of Aggregates of Nonamphiphilic Anthracene Assembled in Ultrathin Supramolecular Langmuir−Blodgett Films. *Langmuir* **1997,** *13* (21), 5678-5684.
5. Nierth, A.; Kobitski, A. Y.; Nienhaus, G. U.; Jäschke, A., Anthracene−BODIPY Dyads as Fluorescent Sensors for Biocatalytic Diels−Alder Reactions. *Journal of the American Chemical Society* **2010,** *132* (8), 2646-2654.
6. Cabellero, A. G.; Croft, A. K.; Nalli, S. M., Remote aromatic stabilization in radical reactions. *Tetrahedron Letters* **2008,** *49* (22), 3613-3615.
7. Fontenot, S. A.; Cangelosi, V. M.; Pitt, M. A. W.; Sather, A. C.; Zakharov, L. N.; Berryman, O. B.; Johnson, D. W., Design, synthesis and characterization of self-assembled As2L3 and Sb2L3 cryptands. *Dalton Transactions* **2011,** *40* (45), 12125-12131.
8. Garay, R. O.; Naarmann, H.; Muellen, K., Synthesis and characterization of poly(1,4-anthrylenevinylene). *Macromolecules* **1994,** *27* (7), 1922-1927.
9. J. Arient, J. P., Nitration and Oxidation of Anthraquinone Dimethyl Derivatives. *Collection of Czechoslovak Chemical Communications* **1973,** *39* (11), 3117-3123.
10. Jones, S.; Atherton, J. C. C.; Elsegood, M. R. J.; Clegg, W., Dimethyl 9,10-anthracenedicarboxylate: a centrosymmetric transoid molecule. *Acta Crystallographica Section C* **2000,** *56* (7), 881-883.
11. Frisch, M. J.; Trucks, G. W.; Schlegel, H. B.; Scuseria, G. E.; Robb, M. A.; Cheeseman, J. R.; Scalmani, G.; Barone, V.; Mennucci, B.; Petersson, G. A.; Nakatsuji, H.; Caricato, M.; Li, X.; Hratchian, H. P.; Izmaylov, A. F.; Bloino, J.; Zheng, G.; Sonnenberg, J. L.; Hada, M.; Ehara, M.; Toyota, K.; Fukuda, R.; Hasegawa, J.; Ishida, M.; Nakajima, T.; Honda, Y.; Kitao, O.; Nakai, H.; Vreven, T.; Montgomery Jr., J. A.; Peralta, J. E.; Ogliaro, F.; Bearpark, M. J.; Heyd, J.; Brothers, E. N.; Kudin, K. N.; Staroverov, V. N.; Kobayashi, R.; Normand, J.; Raghavachari, K.; Rendell, A. P.; Burant, J. C.; Iyengar, S. S.; Tomasi, J.; Cossi, M.; Rega, N.; Millam, N. J.; Klene, M.; Knox, J. E.; Cross, J. B.; Bakken, V.; Adamo, C.; Jaramillo, J.; Gomperts, R.; Stratmann, R. E.; Yazyev, O.; Austin, A. J.; Cammi, R.; Pomelli, C.; Ochterski, J. W.; Martin, R. L.; Morokuma, K.; Zakrzewski, V. G.; Voth, G. A.; Salvador, P.; Dannenberg, J. J.; Dapprich, S.; Daniels, A. D.; Farkas, Ö.; Foresman, J. B.; Ortiz, J. V.; Cioslowski, J.; Fox, D. J. *Gaussian 09*, Gaussian, Inc.: Wallingford, CT, USA, 2009.

12. Becke, A. D., Density-functional thermochemistry. III. The role of exact exchange. *The Journal of Chemical Physics* **1993,** *98* (7), 5648-5652.
13. Lee, C.; Yang, W.; Parr, R. G., Development of the Colle-Salvetti correlation-energy formula into a functional of the electron density. *Physical Review B* **1988,** *37* (2), 785-789.
14. Miehlich, B.; Savin, A.; Stoll, H.; Preuss, H., Results obtained with the correlation energy density functionals of becke and Lee, Yang and Parr. *Chemical Physics Letters* **1989,** *157* (3), 200-206.
15. Stephens, P. J.; Devlin, F. J.; Chabalowski, C. F.; Frisch, M. J., Ab Initio Calculation of Vibrational Absorption and Circular Dichroism Spectra Using Density Functional Force Fields. *The Journal of Physical Chemistry* **1994,** *98* (45), 11623-11627.
16. Valeur, B., *Molecular Fluorescence : Principles and Applications*. Wiley-VCH: Weinheim, New York, 2002.
17. Martin Klessinger, J. M., *Excited States and Photochemistry of Organic Molecules*. VCH Publishers, Inc.: New York, New York, 1995.
18. Dawson, W. R.; Windsor, M. W., Fluorescence yields of aromatic compounds. *The Journal of Physical Chemistry* **1968,** *72* (9), 3251-3260.
19. Jones, R. N., The Ultraviolet Absorption Spectra of Anthracene Derivatives. *Chemical Reviews* **1947,** *41* (2), 353-371.
20. Sidman, J. W., Electronic and Vibrational States of Anthracene. *The Journal of Chemical Physics* **1956,** *25* (1), 115-121.
21. Platt, J. R., Classification of Spectra of Cata-Condensed Hydrocarbons. *The Journal of Chemical Physics* **1949,** *17* (5), 484-495.
22. Eastman, J. W., The dependence of fluorescence on solvent and temperature. *Spectrochimica Acta Part A: Molecular Spectroscopy* **1970,** *26* (7), 1545-1557.
23. Greiner, G., The unusual temperature dependence of the fluorescence intensity and lifetime of anthracene in ethanol. *Journal of Photochemistry and Photobiology A: Chemistry* **2000,** *137* (1), 1-7.
24. Bennett, R. G.; McCartin, P. J., Radiationless Deactivation of the Fluorescent State of Substituted Anthracenes. *The Journal of Chemical Physics* **1966,** *44* (5), 1969-1972.
25. Werner, T. C.; Hoffman, R. M., Relation between an excited state geometry change and the solvent dependence of 9-methyl anthroate fluorescence. *The Journal of Physical Chemistry* **1973,** *77* (13), 1611-1615.
26. Jones, R. N., Some Factors Influencing the Ultraviolet Absorption Spectra of Polynuclear Aromatic Compounds. I. A General Survey1. *Journal of the American Chemical Society* **1945,** *67* (12), 2127-2150.
27. Werner, T. C.; Fisch, R.; Goodman, G., Spectral Studies on Aromatic Esters of 9-Anthroic Acid. *Spectroscopy Letters* **1974,** *7* (8), 385-393.
28. Ohta, A.; Hattori, K.; Kusumoto, Y.; Kawase, T.; Kobayashi, T.; Naito, H.; Kitamura, C., Effects of Alkoxy Substitution on the Optical Properties of 9,10-Anthraquinone and Anthracene: 2,3,6,7-Tetrapropoxy-substituted vs. 2,6-Dipropoxy-substituted Derivatives. *Chemistry Letters* **2012,** *41* (7), 674-676.
29. Boens, N.; Qin, W.; Basarić, N.; Hofkens, J.; Ameloot, M.; Pouget, J.; Lefèvre, J.-P.; Valeur, B.; Gratton, E.; vandeVen, M.; Silva, N. D.; Engelborghs, Y.; Willaert, K.; Sillen, A.; Rumbles, G.; Phillips, D.; Visser, A. J. W. G.; van Hoek, A.; Lakowicz, J. R.; Malak, H.; Gryczynski, I.; Szabo, A. G.; Krajcarski, D. T.; Tamai, N.; Miura, A., Fluorescence Lifetime

Standards for Time and Frequency Domain Fluorescence Spectroscopy. *Analytical Chemistry* **2007,** *79* (5), 2137-2149.
30. Tigoianu, I. R.; Dorohoi, D. O.; Airinei, A., Solvent influence on the electronic absorption spectra of anthracene. *Rev. Chim. (Bucharest, Rom.)* **2009,** *60* (1), 42-44.
31. Blatt, E.; Treloar, F. E.; Ghiggino, K. P.; Gilbert, R. G., Viscosity and temperature dependence of fluorescence lifetimes of anthracene and 9-methylanthracene. *The Journal of Physical Chemistry* **1981,** *85* (19), 2810-2816.
32. Gastilovich, E. A.; Klimenko, V. G.; Korol'kova, N. V.; Nurmukhametov, R. N.; Serov, S. A., Effect of the vibronically induced spin-orbit coupling of electronic ππ* states on nonradiative intersystem crossing: Anthracene. *Optics & Spectroscopy* **2008,** *105* (1), 38-45.
33. Hirayama, S., Effect of substituent on the behaviour of the excited singlet and triplet states in carbonyl derivatives of anthracene of the type 9-X[middle dot]CO[middle dot]A. *Journal of the Chemical Society, Faraday Transactions 1: Physical Chemistry in Condensed Phases* **1982,** *78* (8), 2411-2421.
34. Werner, T. C.; Hercules, D. M., Fluorescence of 9-anthroic acid and its esters. Environmental effects on excited-state behavior. *The Journal of Physical Chemistry* **1969,** *73* (6), 2005-2011.
35. Abdel-Mottaleb, M. S. A.; Galal, H. R.; Dessouky, A. F. M.; El-Naggar, M.; Mekkawi, D.; Ali, S. S.; Attya, G. M., Fluorescence and photostability studies of anthracene-9-carboxylic acid in different media. *International Journal of Photoenergy* **2000,** *2* (1), 47-53.
36. Englman, R.; Jortner, J., The energy gap law for radiationless transitions in large molecules. *Molecular Physics* **1970,** *18* (2), 145-164.

Chapter 3. Synthesis and Luminescent Properties of Two Microporous Metal Organic Frameworks

3.1 Introduction

Photoactive metal organic frameworks (MOFs) have been shown to be promising new candidates for applications as sensors[1-2], photocatalysts[3], sensitizers[4], and electroluminescent devices[5-6]. Luminescent MOFs can be constructed from fluorescent or phosphorescent lanthanides, aromatic organic molecules, or metal complexes used as linkers.[7-9] A very attractive feature of MOFs, which allow for their use in an array of applications, is that they are constructed from both organic and inorganic components. In the case of fluorescent MOFs, the luminescence may be generated from either or both the organic and inorganic counterparts resulting in both predictable and unforeseen properties and tunability previously unobserved in materials primarily composed of inorganic or organic parts.

MOFs with luminescence originating from the organic ligand are desirable because the range of their absorption and emission can be tuned through functionalization of the organic linkers prior or post MOF synthesis. This provides researchers with the ability to rationally design these materials with desired absorption and emission properties required for a particular application. Photoactive MOFs are often constructed from aromatic ligands which provide rigidity and π-based excitation and emission. Functionalization of the aromatic ligands often results in perturbation of the photo-induced electronic transitions, thereby affecting the absorption and emission energies of the material.

MOFs with ligand-based luminescence may have similar chemical and physical properties to that of the ligand, but as a result of metal coordination, solvent environment, and aggregation effects, the photophysics of the MOF differ. In this chapter, the steady state luminescence of two MOFs, $Zn_4O(H_2O)_3(C_{16}H_8O_4)_3 \cdot 2DMF$ (PCN-13)[10], and being reported for the first time, $[Zn(C_{16}H_8O_4)(H_2O)]_n$ (**1**), are compared to the steady state luminescence of their constituent linkers: 9,10-anthracenedicarboxylic acid (9,10-ADCA) and 2,6-anthracenedicarboxylic acid (2,6-ADCA). In the previous chapter the effects of carboxylic acid functional group location on the ring system on the photophysics of the organic ligands were examined. It was determined that both the absorbance and emission spectra were effected differently, depending on the location of the carboxylic acid groups. Upon construction into a MOF, the ligands photophysical properties would be expected to differ due to the change in molecular environment. Herein, I will discuss the effects of the incorporated ligand on steady state luminescence of the zinc based MOFs, PCN-13 and $[Zn(C_{16}H_8O_4)(H_2O)]_n$ (**1**).

3.2 Experimental

The synthesis of 9,10-ADCA and 2,6-ADCA have been described in the previous chapter. *Synthesis of PCN-13.* Synthesis of PCN-13 was performed as previously reported.[10] 9,10-ADCA (0.005 g, 0.019 mmol) and $Zn(NO_3)_2 \cdot 6H_2O$ (0.02 g, 0.068 mmol) was dissolved separately in 1.5 mL of dimethylformamide (DMF). The two solution were combined in a 20 mL autoclave and placed in an oven programmed to increase in temperature at a rate of 1 °C/min to 120 °C. The autoclave was left in the oven at 120 °C for 24 h. After 24 h, the autoclave was cooled to room temperature at a rate < 1 °C/min. The resulting light-brown crystals were collected by vacuum filtration, washed with DMF, and dried in a vacuum oven with no heat.

*Synthesis of [Zn($C_{16}H_8O_4$)(H_2O)]$_n$ (**1**).* 5.0 mg (1.9 x 10^{-2} mmol) of 2,6-ADCA was added to a 1 dram vial, and 5.6 mg (1.9 x 10^{-2} mmol) of $Zn(NO_3)_2 \cdot 6H_2O$ was added to a separate 1 dram vial. To each vial 583 μL of a DEF/H_2O (9:1) solution was added. The $Zn(NO_3)_2$ solution was added to the vial containing 2,6-ADCA, and the vial was capped and sonicated for 15 min. After sonication, the vial was placed in an oven set to ramp up to 120 °C at 1 °C/min. The reaction was left at 120 °C for 24 h before being cooled to room temperature at a rate of less than 1 °C/min. Yellow/brown plate crystals were collected by vacuum filtration, washed with DEF and dried under vacuum for 24 h. Once dry, the crystals were ground using a mortar and pestle and characterized using PXRD. Single crystal analysis was performed on a batch of **1**, which were left in the DEF solution until analysis could be performed.

Single Crystal X-ray Crystallographic Study. A yellow-brown plate (0.1769 x 0.1098 x 0.0195 mm^3) was centered on the goniometer of an Agilent Nova diffractometer operating with CuKα radiation. The data collection routine, unit cell refinement, and data processing were carried out with the program CrysAlisPro.[11] The Laue symmetry and systematic absences were consistent with the monoclinic space groups *C*2/*c* and *Cc*. The centric space group *C*2/*c* was chosen. The structure was solved using SHELXS-2013[12] and refined using SHELXL-2013[12] via OLEX2.[13] The final refinement model involved anisotropic displacement parameters for non-hydrogen atoms. A riding model was used for the aromatic hydrogens. The symmetry independent H-atom of the water molecule was located from the residual electron density map and the O-H distance restrained to 0.82(2) during refinement. The isotropic displacement parameter of the water H-atom was refined independently.

Steady State Luminescence Studies. Steady-state absorption spectra of the 9,10- and 2,6-ADCs were obtained using a Cary Series 5000 UV-vis NIR spectrophotometer on ~5 x 10^{-5} M DMF

solutions. Basic solutions of DMF were obtained by dissolving 1.0 g of KOH tablets in approximately 20 mL of DMF, followed by filtration to remove undissolved KOH. The basic DMF solution was titrated into 5 x 10^{-5} M DMF solutions of the linkers, and the UV-vis spectrum was monitored throughout the titration. The basic form of the linkers were determined to be present in solution once the spectra stopped shifting after the addition of many aliquots of basic DMF.

MOF steady-state Kubelka-Monk spectra were carried out on a Cary Series 5000 UV-vis NIR spectrophotometer equipped with a diffuse reflectance attachment. The MOF was ground into a fine powder using a mortar and pestle, before being placed in the sample holder.

Steady-state fluorescence spectra of 5 x 10^{-5} M basic DMF solutions of 9,10- and 2,6-ADC were obtained using a Cary Eclipse Fluorescence Spectrometer. Fluorescence spectra were obtained between 380-600 nm by excitation of liquid samples at 370 nm. MOF fluorescence spectra were collected on the same instrument using quartz slides and a light layer of vacuum grease to hold the MOF in place on the slide.

3.3 Results and Discussion

Crystal Structure Description of 1. Single X-ray crystal analysis reveals that **1** crystallizes in a monoclinic crystal system of a C1 2/c 1 space group with the molecular formula of $Zn(C_{16}H_8O_4)(H_2O)$ and formula weight of 347.61 g/mol. The unit cell consists of six 2,6-ADC molecules, each connected to four Zn atoms by the oxygens of the carboxylate groups (Figure 3-1 b). The Zn atom is complexed to four different 2,6-ADC linkers and a water molecule in a distorted triganol bipyramidal geometry (Figure 3-1a).

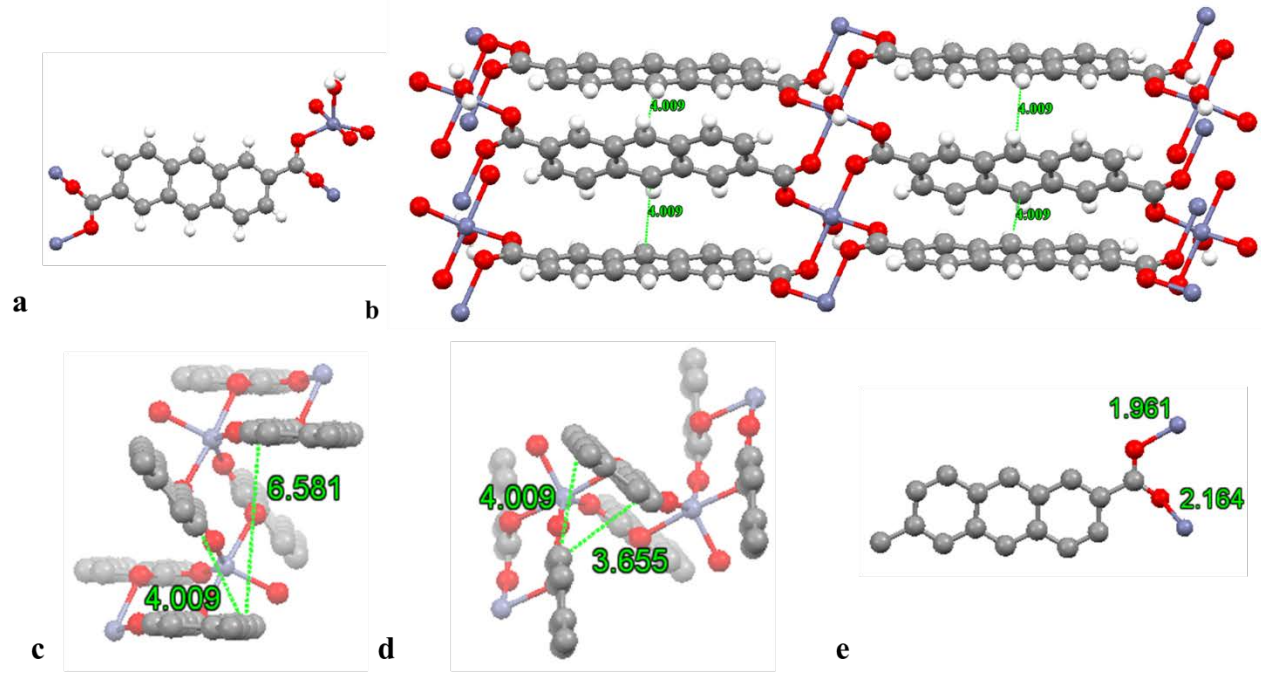

Figure 3-1. (a) Example of central Zn atom connectivity to chelated 2,6-ADC and water molecule in a distorted triganol bipyramidal geometry SBU of **1**. (b) Unit cell of **1** (view down the *b* axis) showing interchromophore distances of 4.0 Å, and further shows the connectivity of the Zn atom to four different ligands and a single water molecule. (c and d) View down the *a* axis of 1 (Hydrogens emitted for clarity) showing interchromophore distances. (e) A single 2,6-ADC molecule showing O-Zn bond lengths.

All Zn and 2,6-ADC units are equivalent, with the shortest interchromophore distances (4.01 - 3.70 Å) resulting from the interactions between the face of one 2,6-ADCA molecule with the edge of a second 2,6-ADC molecule (Figure 3-1c and d). The oxygens of the carboxylate groups are connected to different Zn atoms, with bond lengths of 1.96 and 2.16 Å.

Table 3-1, 2, and 3 show the crystal data and structure refinement parameters, bond length and angles, and hydrogen bonding lengths and angles for complex **1**, respectively.

Table 3-1. Crystal data and structure refinement for Complex **1**

IDENTIFICATION CODE	cs2061	
EMPIRICAL FORMULA	$Zn(C_{16}H_8O_4)(H_2O)$	
FORMULA WEIGHT	347.61	
TEMPERATURE	100.15 K	
WAVELENGTH	1.54184 Å	
CRYSTAL SYSTEM	Monoclinic	
SPACE GROUP	*C* 1 2/*c* 1	
UNIT CELL DIMENSIONS	*a* = 27.4992(7) Å *b* = 6.32395(17) Å *c* = 7.2090(2) Å	∠ *α* = 90°. ∠ *β* = 91.804(3)°. ∠ *γ* = 90°.
VOLUME	1253.06(6) Å^3	
Z	4	
DENSITY (CALCULATED)	1.843 Mg/m^3	
ABSORPTION COEFFICIENT	2.954 mm^{-1}	
F(000)	704	
CRYSTAL SIZE	0.1769 x 0.1098 x 0.0195 mm^3	
THETA RANGE FOR DATA COLLECTION	3.216 to 74.811°.	
INDEX RANGES	-34<=h<=33, -7<=k<=7, -9<=l<=8	
REFLECTIONS COLLECTED	11624	
INDEPENDENT REFLECTIONS	1278 [R(int) = 0.0490]	
COMPLETENESS TO THETA = 67.684°	99.9 %	
ABSORPTION CORRECTION	Gaussian	
MAX. AND MIN. TRANSMISSION	0.947 and 0.708	
REFINEMENT METHOD	Full-matrix least squares on F^2	
DATA / RESTRAINTS / PARAMETERS	1278 / 1 / 105	
GOODNESS-OF-FIT ON F²	1.057	
FINAL R INDICES [I>2SIGMA(I)]	R1 = 0.0276, wR2 = 0.0780	
R INDICES (ALL DATA)	R1 = 0.0283, wR2 = 0.0788	
EXTINCTION COEFFICIENT	n/a	
LARGEST DIFF. PEAK AND HOLE	0.420 and -0.340 e.Å^{-3}	

Table 3-2. Bond lengths [Å] and angles [°] for complex **1**.

Bond lengths [Å] for 1		Angles [°] for 1			
Zn(1)-O(1)#1	2.1645(13)	**O(1)#2-Zn(1)-O(1)#1**	175.12(6)	**C(3)-C(2)-C(4)**	120.58(16)
Zn(1)-O(1)#2	2.1645(13)	**O(2)-Zn(1)-O(1)#1**	93.55(5)	**C(4)-C(2)-C(1)**	119.27(16)
Zn(1)-O(2)#3	1.9611(12)	**O(2)#3-Zn(1)-O(1)#2**	93.55(5)	**C(2)-C(3)-C(7)**	120.44(17)
Zn(1)-O(2)	1.9611(12)	**O(2)-Zn(1)-O(1)#2**	88.11(5)	**C(5)-C(4)-C(2)**	120.49(16)
Zn(1)-O(3)	1.977(2)	**O(2)#3-Zn(1)-O(1)#1**	88.11(5)	**C(4)-C(5)-C(6)**	120.89(17)
O(1)-C(1)	1.268(2)	**O(2)-Zn(1)-O(2)#3**	140.32(8)	**C(5)-C(6)-C(7)**	118.74(16)
O(2)-C(1)	1.260(2)	**O(2)#3-Zn(1)-O(3)**	109.84(4)	**C(8)#4-C(6)-C(5)**	121.87(17)
C(1)-C(2)	1.499(2)	**O(2)-Zn(1)-O(3)**	109.84(4)	**C(8)#4-C(6)-C(7)**	119.39(17)
C(2)-C(3)	1.371(3)	**O(3)-Zn(1)-O(1)#2**	87.56(3)	**C(3)-C(7)-C(6)**	118.85(17)
C(2)-C(4)	1.427(3)	**O(3)-Zn(1)-O(1)#1**	87.56(3)	**C(8)-C(7)-C(3)**	121.61(17)
C(3)-C(7)	1.430(2)	**C(1)-O(1)-Zn(1)#1**	123.67(11)	**C(8)-C(7)-C(6)**	119.53(17)
C(4)-C(5)	1.360(2)	**C(1)-O(2)-Zn(1)**	119.36(11)	**C(7)-C(8)-C(6)#4**	121.07(17)
C(5)-C(6)	1.432(2)	**O(1)-C(1)-C(2)**	118.99(16)		

C(6)-C(7)	1.436(2)	**O(2)-C(1)-O(1)**	123.37(16)	
C(6)-C(8)#4	1.401(2)	**O(2)-C(1)-C(2)**	117.62(15)	
C(7)-C(8)	1.401(3	**C(3)-C(2)-C(1)**	120.14(16)	

Symmetry transformations used to generate equivalent atoms:
#1 -x,-y,-z+1 #2 x,-y,z-1/2 #3 -x,y,-z+1/2 #4 -x+1/2,-y+1/2,-z+1

Table 3-3. Hydrogen bonds lengths [Å] and angles [°]for **1**.

D-H...A	**d(D-H)**	**d(H...A)**	**d(D...A)**	**<(DHA)**
O(3)-H(3A)...O(1)#5	0.780(17)	1.878(19)	2.6314(19)	162(3)

Symmetry transformations used to generate equivalent atoms:
#1 -x,-y,-z+1 #2 x,-y,z-1/2 #3 -x,y,-z+1/2 #4 -x+1/2,-y+1/2,-z+1 #5 -x,y-1,-z+1/2

Figure 3-2 shows the structure of **1** looking down the a, b, and c axes. The MOF has a very compact and symmetric topology interchromophore distances of 4.0 Å. The complex has a calculated density of 1.843 Mg/m^3 and no solvent molecules are present within the crystal structure. Each 2,6-ADC molecule is connected to four separate Zn centers through the carboxylate functional groups.

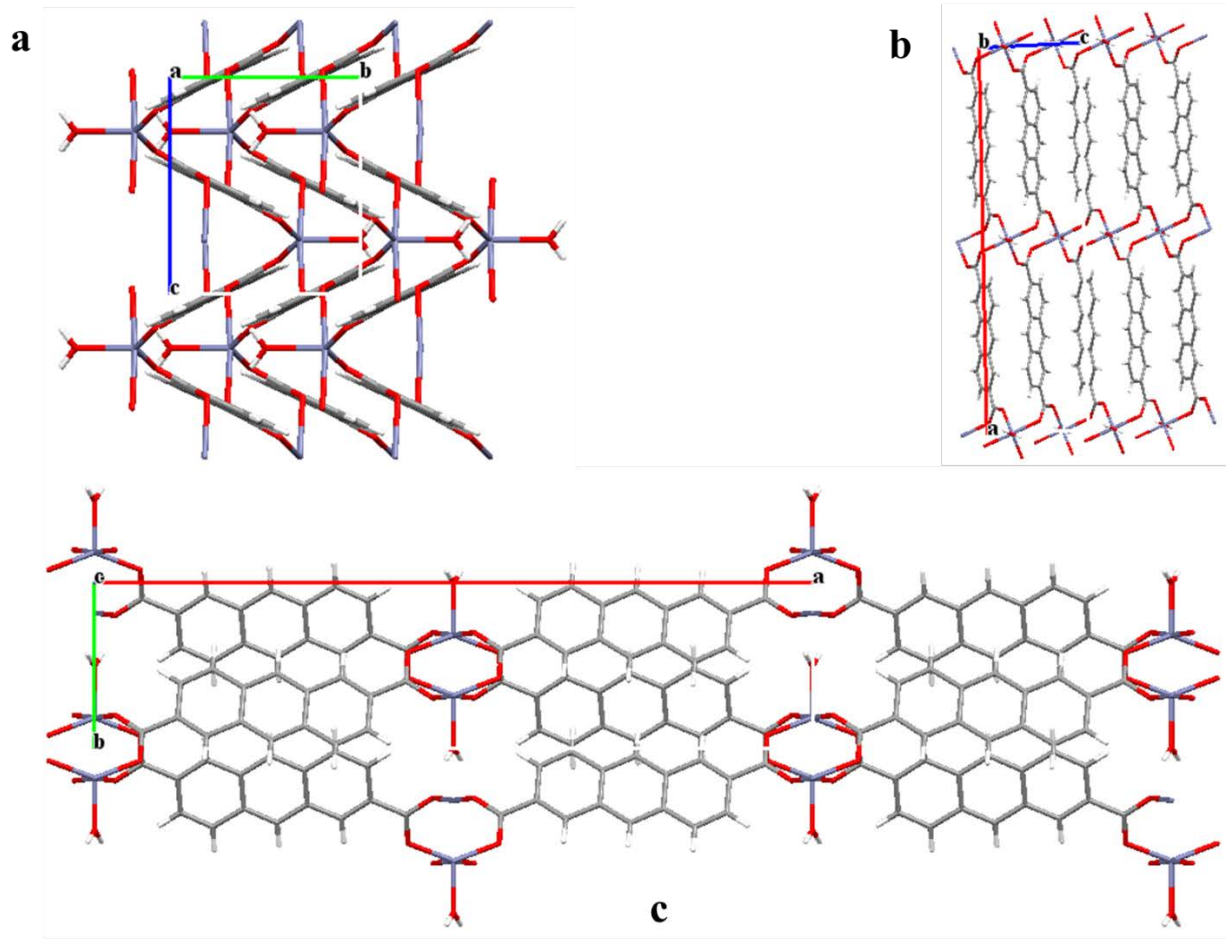

Figure 3-2. View down the crystallographic a axis (**a**), b axis (**b**), and c axis (**c**).

Crystal Structure Description of PCN-13. The crystal structure of PCN-13 has been described in the literature[14] and is presented here in Figure 3-3. The SBU of PCN-13 is formed by a $Zn_4O(H_2O)_3(COO)_6$ cluster (Figure 3-3a), where a central oxygen is connected to four Zn atoms in a tetrahedral geometry. The three of the four Zn atoms are connected to three different 9,10-ADC linkers and a water molecule and the μ^3-oxygen. The fourth Zn atom is only connected to the three 9,10-ADC linkers and the μ^3-oxygen. Each 9,10-ADC ligand is connected to two SBUs, and every SBU is connected to six different 9,10-ADC ligand, forming a 3-D framework with no possible π-π stacking (Figure 3-3b).

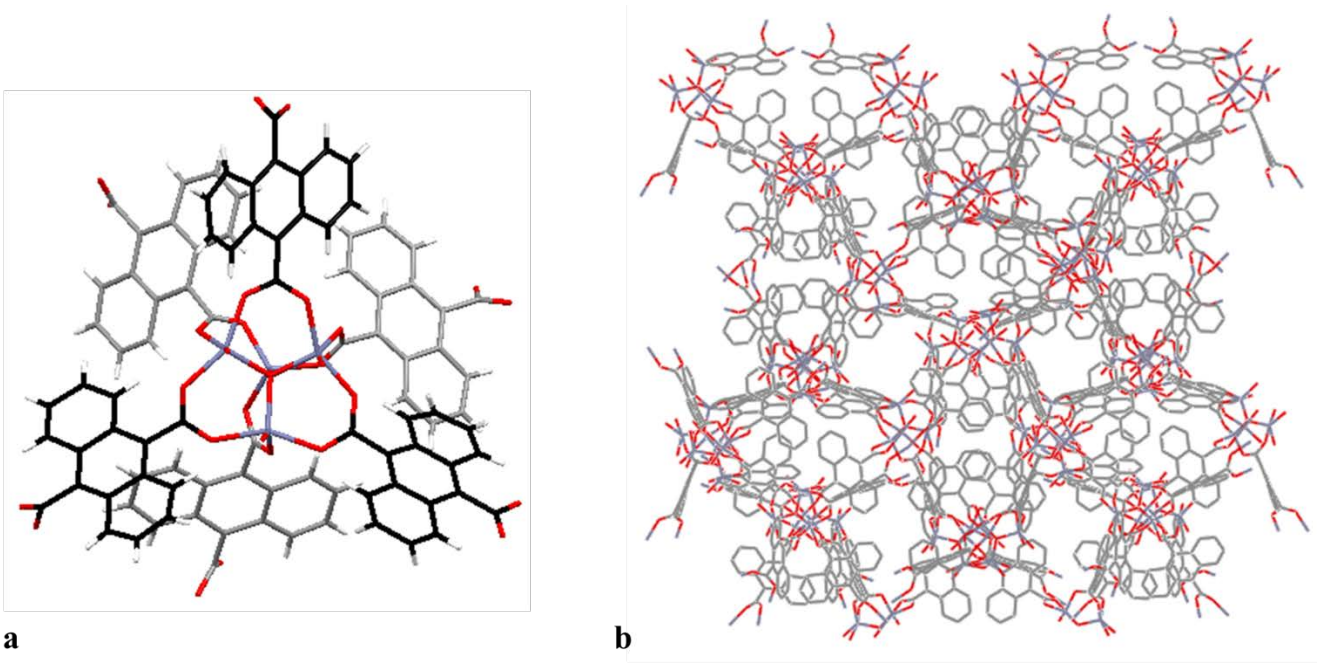

Figure 3-3. (a) $Zn_4O(H_2O)_3(COO)_6$ SBU of PCN-13. The water ligands (Hydrogens not shown for clarity) are connected to the three front-most Zn atoms. (b) View down the *a* axis of PCN-13. (carbon (grey), hydrogen (white), oxygen (red), and zinc (blue).)

*Characterization of PCN-13 and **1***. Powder x-ray diffraction (PXRD) was used to characterize the structure of PCN-13. Experimentally determined patterns were overlaid with the simulated PXRD pattern generated from the literature crystal structure using Mercury.[15] Thermogravimetric analysis (TGA) was also used for identification purposes for PCN-13, and results matched well with the TGA found in the literature. Figure 3-2 shows PXRD, comparing the simulated literature pattern to experimentally obtained pattern, and TGA data for PCN-13.

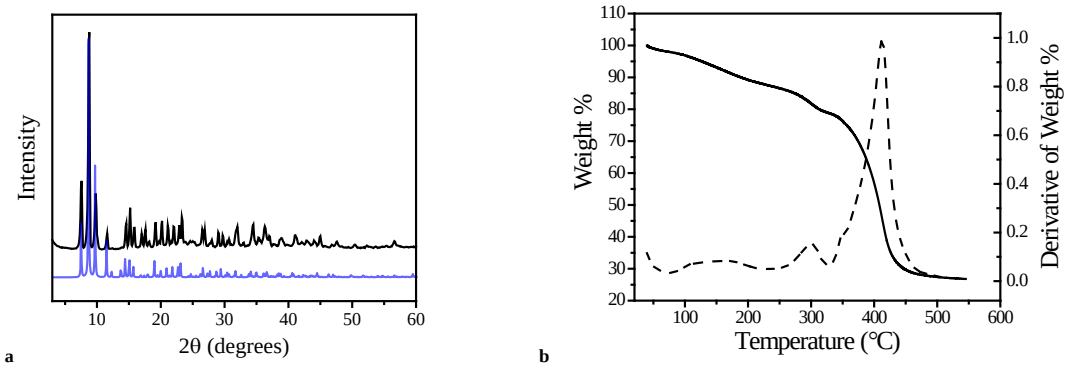

Figure 3-4. (a) PXRD of simulated literature pattern (blue) and experimentally obtained PCN-13 pattern (black). (b) TGA of synthesized PCN-13 showing the loss in weight percent (solid curve) and derivative of the weight percent (dashed curve) as a function of temperature.

The PXRD of synthesized PCN-13 matches well with the literature pattern. The TGA in Figure 3-4 shows a gradual loss in weight percent as a function of temperature. The loss of two unbound DMF molecules is observed from approximately 100 to 240 °C, resulting in a weight percent loss of 11.7 %. The loss of DMF molecules is followed by the loss of three bound water molecules from 240 to 320 °C giving a weight percent loss of 7.7 %. Degradation of 9,10-ADC is observed from 330 to 510 °C.

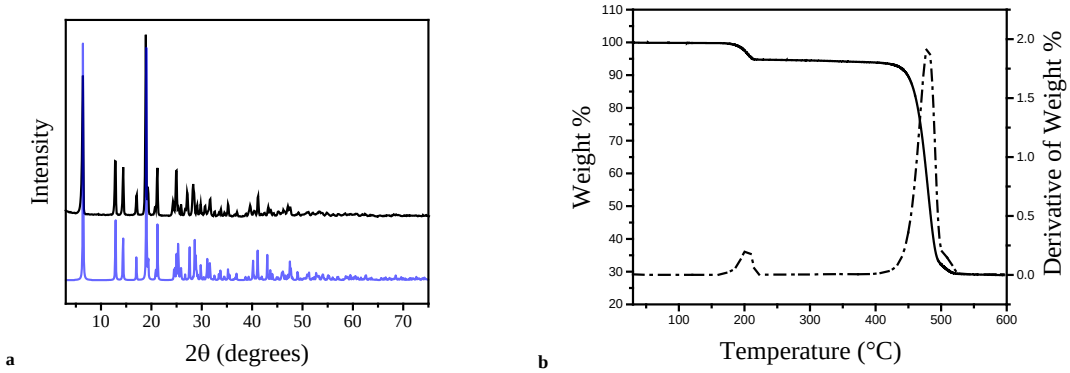

Figure 3-5. (a) PXRD of simulated pattern from crystallography data of **1** (blue) and experimentally obtained **1** pattern (black). (b) TGA of synthesized **1** showing the loss in weight

percent (solid curve) and derivative of the weight percent (dashed curve) as a function of temperature.

Other than crystal structure determination from a single crystal, PXRD was also used to confirm the synthesis of **1**, by comparing it to a simulated PXRD pattern obtained, using Mercury, from the crystallographic data obtained for **1** (Figure 3-5a). TGA was also used to confirm the makeup of the MOF. TGA shows the loss of one bound water molecule, 5.12 weight %, is observed from 160 – 230 °C, followed by the degradation of 2,6-ADC starting around 400 °C (Figure 3-5b). *Steady state absorption and emission.* Steady state luminescence spectra were obtained for the PCN-13 and **1** and 9,10- and 2,6-anthracenedicarboxylate (9,10-ADC and 2,6-ADC). Absorption spectra of the two ligands were obtained in basic DMF and both exhibit vibrational structure similar to their parent molecule, anthracene (Figure 3-6a and b). 9,10-ADC exhibits absorption maxima at 348/368/386/408 nm with spacing between bands of approximately 1560/1270/1400 cm^{-1}. The absorbance of 2,6-ADC shows maxima at 349/368/389/420 nm with approximate spacing between bands of 1480/1470/1900 cm^{-1}.

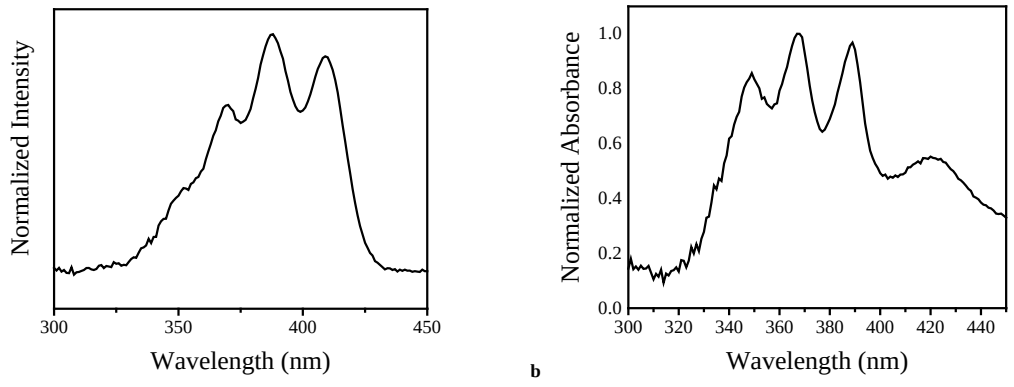

Figure 3-6. (a) Normalized absorption of 9,10-ADC and (b) 2,6-ADC in DMF.

MOFs are often not very soluble and may be degraded by various solvents, therefore, the absorption and emission of the MOFs were obtained in the solid state. A diffuse reflectance attachment was used to obtain an absorbance spectra of the two MOFs, which were recorded in the Kubelka-Monk, F(R), mode. The normalized F(R) of the MOFs and the basic form of the linkers are compared in Figure 3-7.

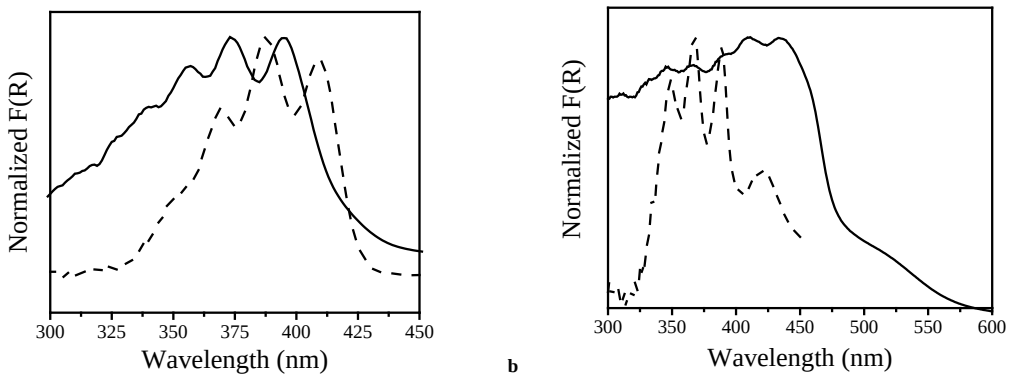

Figure 3-7. (a) Normalized absorbance of solid PCN-13 (solid line) and basic 9,10-ADC in DMF (dashed line). (b) Normalized absorbance of solid **1** (solid line) and basic 2,6-ADC in DMF (dashed line).

The absorbance spectrum of PCN-13 is broadened and blue shifted relative to the basic linker in solution. Absorbance maxima for PCN-13 were observed at 342/357/373/395 nm with spacing between bands approximately 1230/1200/1490 cm^{-1}. Despite the broadening of the absorbance spectrum of PCN-13 relative to the ligand, the anthracenic vibrational structure is still apparent, suggesting that the transitions occurring are π to π^* based. Since Zn(II) has a d^{10} electronic configuration, it is neither easy to reduce or oxidize, which further suggests that ligand to ligand electron transfer is responsible for the absorption spectra of PCN-13.[16] The broadening of the absorbance spectrum of PCN-13 relative to 9,10-ADC is due to inductive effects of the Zn

SBUs on the linkers in the MOF. Coordination to the SBUs results in perturbation of the electronic transitions occurring in the linker resulting in a more diffuse spectrum than is observed in the protonated and deprotonated forms of the linker. The blue shift observed in the absorption spectra of PCN-13 suggests that coordination to the metal ions, as well as proximity to solvent molecules within the MOF pores, results in the destabilization of the ground and/or excited state of the ligands. This destabilization of the electronic levels perturbs the electronic transitions occurring between them, resulting in higher energy transitions relative to the free based ligand.

The absorbance of **1** is broadened and red shifted with respect to 2,6-ADC in basic DMF. Vibrational structure of **1** is nearly lost and difficult to distinguish. The absorption of **1** also trails off into the UV, which is not observed in the ligand. The broadened range of absorption is attributed to greater perturbation due to inductive effects than is observed in the case of PCN-13. The crystal structure of **1** shows that the anthracene molecules are more closely packed compared to those in PCN-13. The increased density of the structure of **1** relative to PCN-13 possibly results in greater through-space interchromophore interations between anthracene units resulting in a wider range of absorption and a red shift.[14] The distance between the hydrogens of one anthracene molecule to the planar face of another anthracene molecule ranges between 4.01 - 3.70 Å, which could allow for interactions between the π-system of one anthracene ring with the σ-orbitals of the hydrogens. Such orbital interactions could explain the differences observed in the absorbance spectra of 2,6-ADC and the MOF.

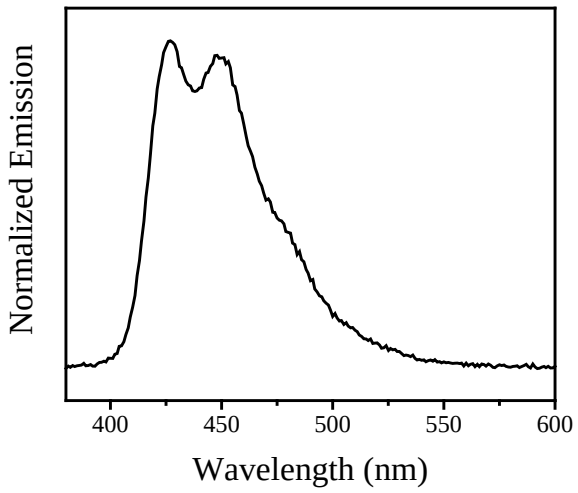

Figure 3-8. Normalized emission of 9,10-ADC in DMF, with excitation λ =370 nm.

The emission of 9,10-ADC (Figure 3-8), recorded from 380 nm to 700 nm upon excitation at λ = 370 nm, shows emission maxima at 425/447 nm, and was found to be very weak with a fluorescence quantum yield $\Phi_{fl} = 0.05 \pm 0.01$, much less than observed when fully protonated in DMF ($\Phi_{fl} = 0.39 \pm 0.07$). The protonated form of 2,6-ADC has been observed to fluoresce in DMF ($\Phi_{fl} = 0.85 \pm 0.18$), THF, and DMSO, but upon deprotonation no emission is observed. The reduced or loss of emission upon deprotonation of the linkers may result from the lowering in energy of an nπ* triplet state, allowing for intersystem crossing from the excited singlet state, S_1, to an isoenergetic triplet state, T_n. Once in the triplet state, relaxation may occur through the process of intersystem crossing to an isoenergetic vibrational level of the ground state, S_0, followed by internal conversion to the ground vibrational state of S_0.

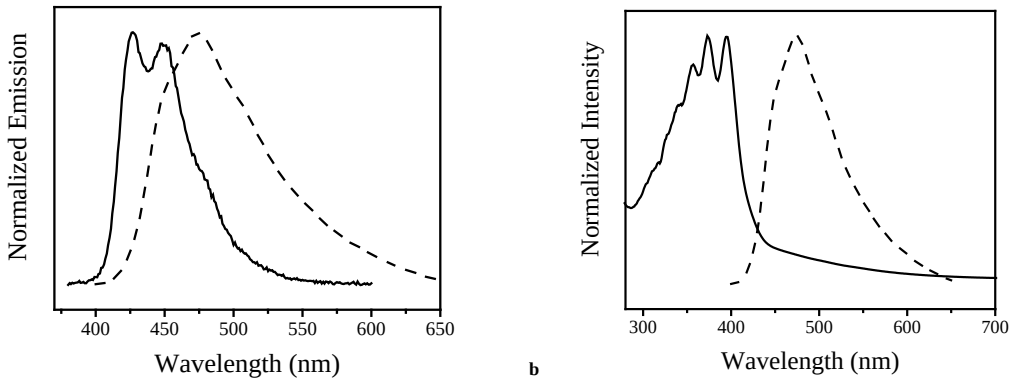

Figure 3-9. (a) Normalized emission of 9,10-ADC in basic DMF (solid line) and PCN-13 (dashed line), and (b) Normalized absorbance (solid line) and emission (dashed line), excitation at $\lambda = 374$ nm, of PCN-13.

Figure 3-9a shows the emission of PCN-13 overlayed with the emission of 9,10-ADC in DMF. Upon incorporation into the MOF, vibration structure of 9,10-ADC emission is lost and a red shift is observed. The red shift in the emission of PCN-13 relative to 9,10-ADC in solution can be attributed to inductive effects between anthracene units and the Zn metals. The broadening of the emission is likely homogeneous and due to an increased number of available vibrational sublevels as a result of coordination to Zn. Figure 3-9b shows the emission and excitation spectra of PCN-13. The energy of the 0,0 transition was determined using Planck's relation, $E(eV) = \frac{1240}{\lambda(nm)}$, where λ is the wavelength at which the absorbance and emission spectra intersect. The $E_{0,0}$ for PCN-13 was found to be 2.88 eV, which is lower than the $E_{0,0}$ observed for 9,10-ADC in DMF, 3.04 eV. A Stokes shift of 4170 cm^{-1} was observed for PCN-13, which was a good degree larger than the Stokes shift observed for 9,10-ADC in DMF (980 cm^{-1}). The larger Stokes shift suggests that there is a greater degree of reorganization of the nuclear coordinates between the ground and excited state of PCN-13 than the linker in solution. The change in nuclear configuration in the

excited state of PCN-13 may have to do with interactions between the $Zn_4O(H_2O)_3(COO)_6$ cluster and the excited anthracene molecules. Preliminary efforts have been made to calculate the fluorescence quantum yield of PCN-13, but without the use of an integrating sphere, the results may not be accurate. The experimentally determined Φ_{fl} of PCN-13 was found to be very low, approximately $0.004 \pm 1E^{-4}$, which is much lower than the Φ_{fl} of the linker in solution. If the experimentally determined yield is accurate, this suggests that additional nonradiative pathways are made available upon coordination to the Zn SBU. These additional nonradiative pathways would have rate constants greater than those for the radiative emission process, resulting in the observed reduced fluorescence quantum yield. It is possible that the inability for the acid groups to rotate into a more coplanar configuration, as is believed to occur in solution, results in a decrease in the emission of 9,10-ADC. Further studies on the lifetime of the emissive state of PCN-13 would need to be conducted to test this theory.

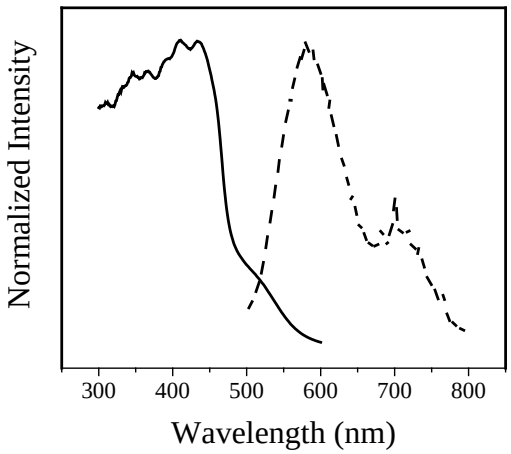

Figure 3-10. Absorption (solid line) and emission (dashed line) of **1**.

Figure 3-10 shows the absorption and emission of solid **1**. The $E_{0,0}$ energy was determined to be 2.40 eV, which is lower in energy than the $E_{0,0}$ energy observed for PCN-13. The Stokes

shift was found to be 5820 cm^{-1}. One possible cause for the emission of 2,6-ADC in the MOF but not in solution could be due to increased rigidity of the organic linker in the MOF relative to solution, as well as inductive effects due to coordination to the Zn atoms. The MOF has a very compact structure and as a result of coordinated water molecules, hydrogen bonding is also present throughout the complex. The close packing and hydrogen bonding likely leads to increased rigidity of the ligand in the MOF relative to solution. The increased rigidity reduces the number of available radiationless pathways, allowing for the competing process of emission to occur.

3.4 Conclusion

This work has shown that the location of carboxylic acid groups on anthracene perturbs the electronic transition, with dipole moments across the longitudinal and short axes of anthracene, to different extents. Positioning of the carboxylic acid group at the 9,10 positions has little influence on the absorption spectrum of anthracene other than a red shift due to inductive effects. Whereas the a slightly more perturbed spectrum, red shifted with different vibrational structure relative to anthracene, is obtained by COOH placement at the 2,6 position due both inductive and resonance effects. The functionalization of the 1,4 position on anthracene results in the most perturbation to the electronic transitions occurring in anthracene. Both high and low energy transitions of anthracene are red-shifted to a greater extent in 1,4-ADCA than either of the other two acids studied.

Carboxylic acid functionalization at the 9,10 position of anthracene had little effect on the absorption spectrum of anthracene, but the emission spectrum was greatly red shifted and void of anthracenic vibrational structure. The absorbed increase in Stokes shift and absence of vibrational structure is believed to be due to the rotation of carboxylic acid groups to a more coplanar configuration. The rotation in the excited state likely increases the overlap between the π-systems

of the anthracene rings and the carboxylic acid group, which perturbs the anthracenic $\pi \rightarrow \pi^*$ transitions and may result in charge transfer character in the excited state. Further studied in frozen solutions will need to be performed to provide further evidence for the rotation of the carboxylic acid groups in the excited state.

The addition of carboxylic acids onto anthracene resulted in an increase in fluorescence quantum yields and fluorescence lifetimes. Anthracene exhibits a Φ_{fl} of 0.27 in ethanol, whereas the dicarboxylic acids of anthracene all displayed Φ_{fl} ranging between 0.73 and 0.40 in DMSO and THF. Both the fluorescence quantum yields and lifetimes exhibit minor dependencies on solvent dielectric constant. These yields and lifetimes to not exhibit any trends with changes in other solvent parameters, but a wider range of solvents with varying in solvent parameter magnitudes are needed to fully determine if any solvochromism exhists.

A new microporous MOF (**1**) has been synthesized from $Zn(NO_3)_2$ and 2,6-anthracenedicarboxlic acid. The MOFs **1** and previously reported[10] PCN-13 have been characterized using PXRD and TGA, and the steady state luminescent properties have been studied and compared to the luminescent properties of 9,10- and 2,6-ADC in basic DMF. It has been determined that the absorption and emissive properties of the linkers are affected by coordination to metal centers and proximity to other ligands within the MOF. Metal coordination and aggregation effects result in a shift in the absorption and emission wavelengths and broadening of the spectra. In the case of **1**, incorporation of a non-fluorescent ligand, 2,6-ADC, results in a MOF with fluorescent properties. Increased rigidity of the ligand within the MOF reduces the available radiationless processes, allowing for the competing process of fluorescence to become a more dominant pathway. In the case of PCN-13, the effects of incorporating the ligand into the MOF does not have the same effects as are observed with **1**. PCN-13 is nearly non-emissive, unlike the

free based ligand, 9,10-ADC. It is possible that coordination of the ligand to the Zn SBU prohibits rotation of the acid groups to a more coplanar configuration with the ring system, thereby resulting in less intense fluorescence. This works shows that incorporation of a fluorescent ligand into a MOF may enhance the emission by reducing nonradiative processes, through rigidification of the ligand, or may actually provide additional radiationless pathways to compete with fluorescence.

3.5 References

1. Dou, Z.; Yu, J.; Cui, Y.; Yang, Y.; Wang, Z.; Yang, D.; Qian, G., Luminescent Metal–Organic Framework Films As Highly Sensitive and Fast-Response Oxygen Sensors. *Journal of the American Chemical Society* **2014,** *136* (15), 5527-5530.
2. Wang, G.-Y.; Song, C.; Kong, D.-M.; Ruan, W.-J.; Chang, Z.; Li, Y., Two luminescent metal-organic frameworks for the sensing of nitroaromatic explosives and DNA strands. *Journal of Materials Chemistry A* **2014,** *2* (7), 2213-2220.
3. Zhang, C.-F.; Qiu, L.-G.; Ke, F.; Zhu, Y.-J.; Yuan, Y.-P.; Xu, G.-S.; Jiang, X., A novel magnetic recyclable photocatalyst based on a core-shell metal-organic framework Fe3O4@MIL-100(Fe) for the decolorization of methylene blue dye. *Journal of Materials Chemistry A* **2013,** *1* (45), 14329-14334.
4. Zhou, X.-H.; Li, L.; Li, H.-H.; Li, A.; Yang, T.; Huang, W., A flexible Eu(iii)-based metal-organic framework: turn-off luminescent sensor for the detection of Fe(iii) and picric acid. *Dalton Transactions* **2013,** *42* (34), 12403-12409.
5. Pramanik, M.; Patra, A. K.; Bhaumik, A., Self-assembled titanium phosphonate nanomaterial having a mesoscopic void space and its optoelectronic application. *Dalton Trans.* **2013,** *42* (14), 5140-5149.
6. Silva, C. G.; Corma, A.; Garcia, H., Metal-organic frameworks as semiconductors. *Journal of Materials Chemistry* **2010,** *20* (16), 3141-3156.
7. Bo, Q.-B.; Zhang, H.-T.; Wang, H.-Y.; Miao, J.-L.; Zhang, Z.-W., Anhydrous Lanthanide MOFs and Direct Photoluminescent Sensing for Polyoxometalates in Aqueous Solution. *Chemistry – A European Journal* **2014,** *20* (13), 3712-3723.
8. Yuan, S.; Deng, Y.-K.; Sun, D., Unprecedented Second-Timescale Blue/Green Emissions and Iodine-Uptake-Induced Single-Crystal-to-Single-Crystal Transformation in ZnII/CdII Metal–Organic Frameworks. *Chemistry – A European Journal* **2014,** *20* (32), 10093-10098.
9. Kent, C. A.; Liu, D.; Ma, L.; Papanikolas, J. M.; Meyer, T. J.; Lin, W., Light Harvesting in Microscale Metal–Organic Frameworks by Energy Migration and Interfacial Electron Transfer Quenching. *Journal of the American Chemical Society* **2011,** *133* (33), 12940-12943.
10. Shengqian Ma, X.-S. W., Christopher D. Collier, Erika S. Manis, and Hong-Cai Zhou*, Ultramicroporous Metal-Organic Framework Based on 9,10-Anthracenedicarboxylate for Selective Gas Adsorption. *Inorganic Chemistry* **2007,** *46* (21), 8499-8501.
11. Technologies, A. *CrysAlisPro Software system, v1.171.36.28*, Agilent Technologies UK Ltd: Oxford, UK, 2013.
12. Sheldrick, G. M., A short history of SHELX. *Acta Cryst.* **2008,** *A64*, 112-122.

13. Dolomanov, O. V. B., L. J.; Gildea, R. J.; Howard, J. A. K.; Puschmann, H. , *J. Appl. Cryst.* **2009,** *42*, 339-341.
14. Bauer, C. A.; Jones, S. C.; Kinnibrugh, T. L.; Tongwa, P.; Farrell, R. A.; Vakil, A.; Timofeeva, T. V.; Khrustalev, V. N.; Allendorf, M. D., Homo- and heterometallic luminescent 2-D stilbene metal-organic frameworks. *Dalton Transactions* **2014,** *43* (7), 2925-2935.
15. Ma, S.; Wang, X.-S.; Collier, C. D.; Manis, E. S.; Zhou, H.-C., Ultramicroporous Metal−Organic Framework Based on 9,10-Anthracenedicarboxylate for Selective Gas Adsorption. *Inorganic Chemistry* **2007,** *46* (21), 8499-8501.
16. Liu, F.; Zhang, L.; Wang, R.; Sun, J.; Yang, J.; Chen, Z.; Wang, X.; Sun, D., Five MOFs with different topologies based on anthracene functionalized tetracarboxylic acid: syntheses, structures, and properties. *CrystEngComm* **2014,** *16* (14), 2917-2928.

Future Work

Photophysics of Anthracenedicarboxylic acids.

Further studies of the three acids in solvents with differing polarity will need to be performed to provide evidence for or against any solvochromatic trends. Solvochromism would be apparent in solvents of differing polarity if there exists an excited charge transfer between the π-systems of the carboxylic acid groups and anthracene. A study in solvents that vary in hydrogen bond donor, or acceptor strength could be performed to determine the effects of intermolecular forces on the rates of radiative and nonradiative decay.

To test the hypothesis that 9,10-ADCA undergoes conformational changes in the excited state, the absorbance and fluoresce should be taken in a glass matrix. A Possible solvent mixture to use for this experiment is EPA (ethanol, isopentane, and diethyl ether), which will form a glass at 5 K or less. Assuming that the ground state conformation is when the acid groups are at a dihedral angle of 60 ° to the anthracene plane, the excited state should remain in this 60 ° conformation when frozen. The emission of the frozen molecule should show similar vibrational structure to the emission of anthracene, if the acid groups of 9,10-ADCA are frozen in such a position (60 °) that overlap of the π-systems is not possible.

Photophysics of the Anthracenic MOFs.

The current data on PCN-13 suggests that incorporation of 9,10-ADC into the Zn based MOF results in an increase in the rate of nonradiative decay. The fluorescence quantum yield, obtained without the use of an integrating sphere, is much lower than the basic or acidic linker in solution, suggesting that incorporation into the MOF is “turning off” the fluorescence of the

linker. Before additional conclusions can be drawn, a more accurate determination of the fluorescence quantum yield will need to be obtained using an integrating sphere.

Incorporation of 2,6-ADC into a Zn based MOF has resulted in a MOF with emission properties that the basic form of the linker does not possess. When comparing the emission to the acidic form of the ligand, the emission of the MOF is greatly red-shifted compared to 2,6-ADCA. Lifetime measurements on the emission of the MOF will need to be conducted to determine if the emission is fluorescence or phosphorescence. Additionally, quantum yield measurements of the MOF will be required to understand further changes in the photophysics of the linker upon incorporation into a MOF.

If a the linkers exhibit solvochromatic trends in solvents with differing polarity, spectroscopic studies could be performed on the MOFs soaked in different solvents of differing polarity to determine if similar trends seen in the linkers are observed in the MOF as well.

Appendix

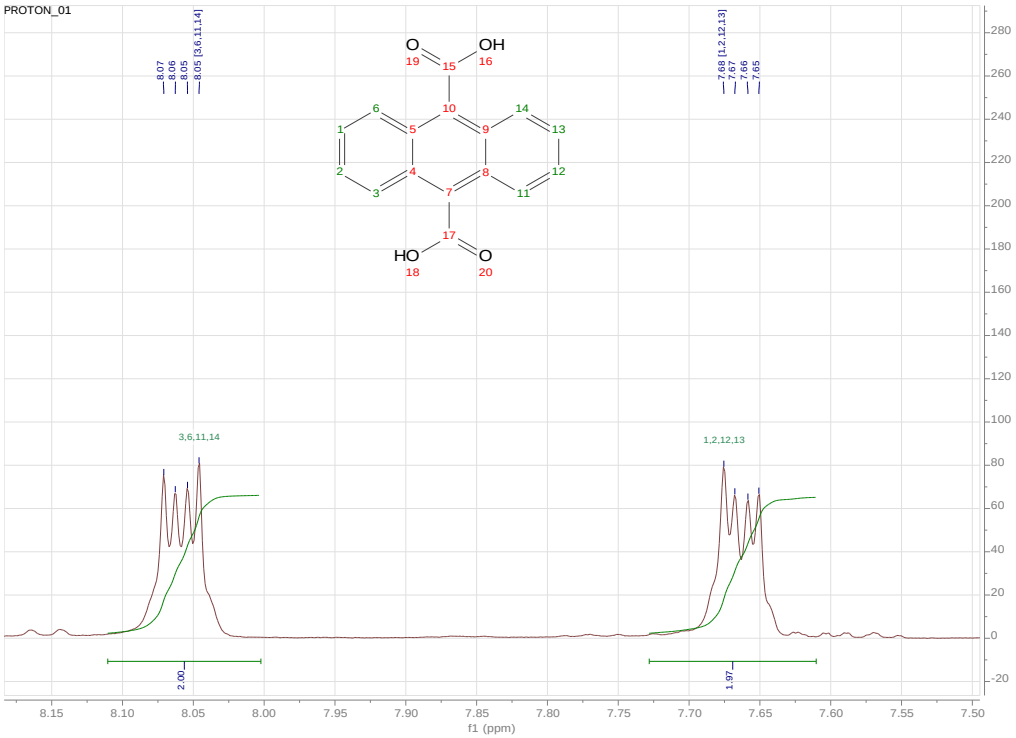

Figure A1. ^{1}H NMR of 9,10-ADCA in d-DMSO.

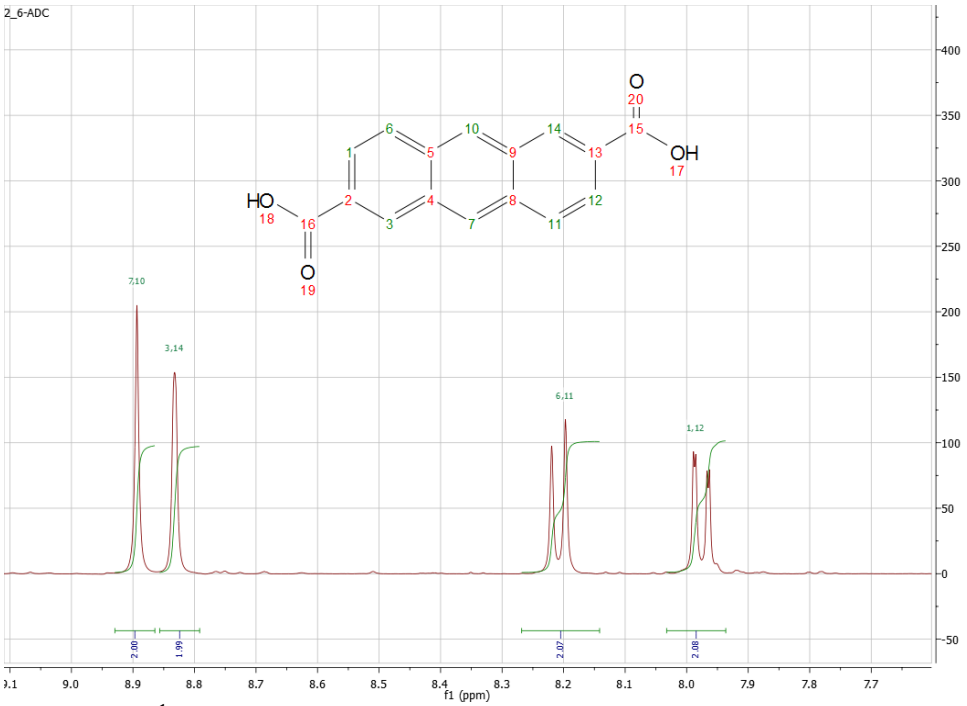

Figure A2. ^{1}H NMR of 2,6-ADCA in d-DMSO.

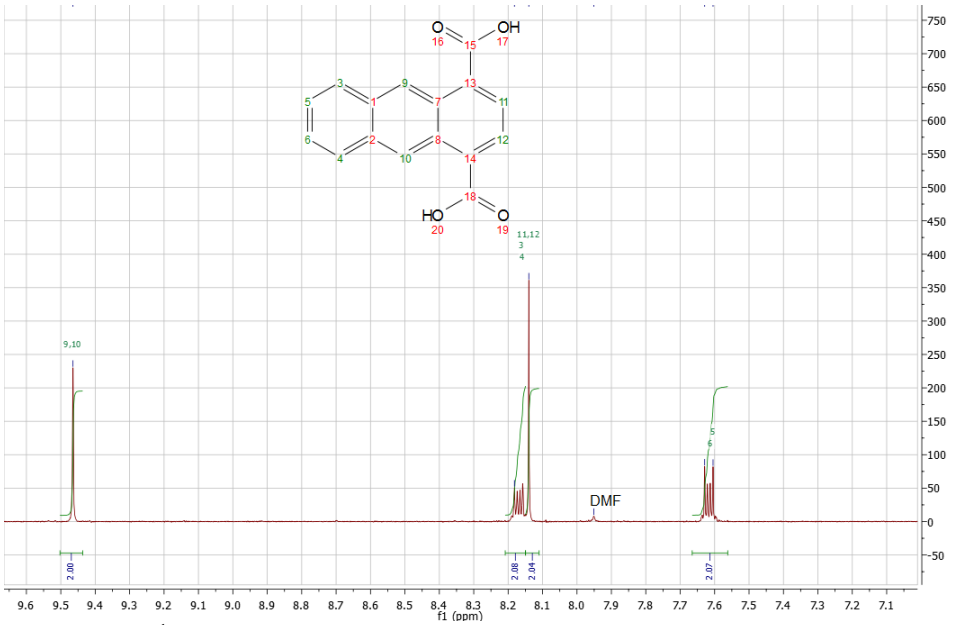

Figure A3. ^{1}H NMR of 1,4-ADCA in d-DMSO.

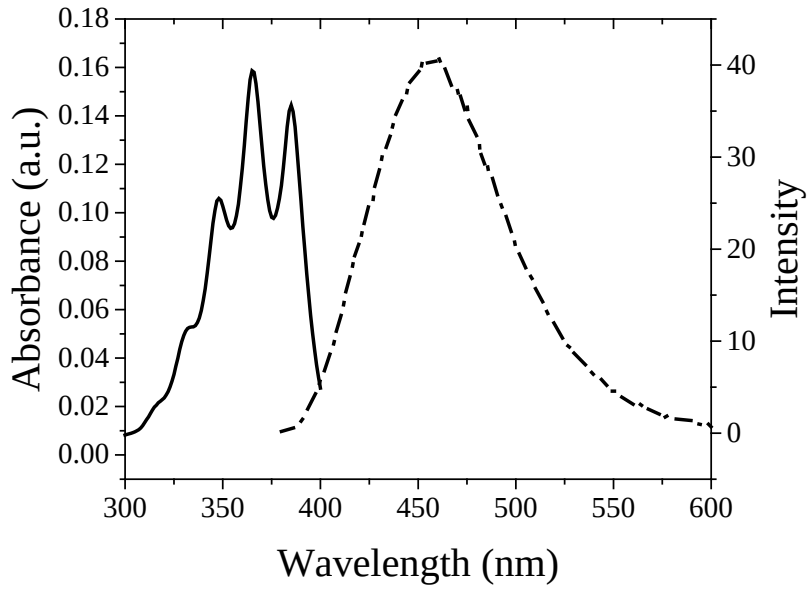

Figure A4. Absorbance (solid) and emission (dashed) of 9,10-ADCA in AcCN.

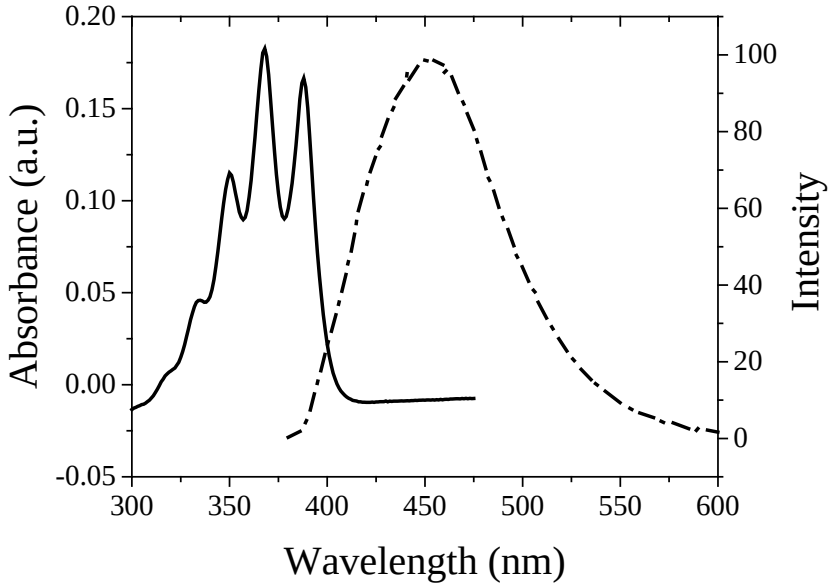

Figure A5. Absorbance (solid) and emission (dashed) of 9,10-ADCA in DMF.

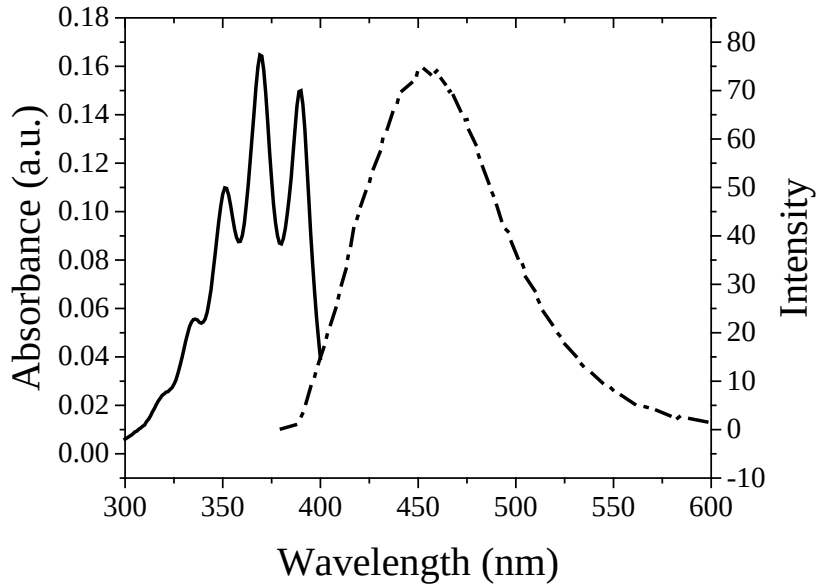

Figure A6. Absorbance (solid) and emission (dashed) of 9,10-ADCA in DMSO.

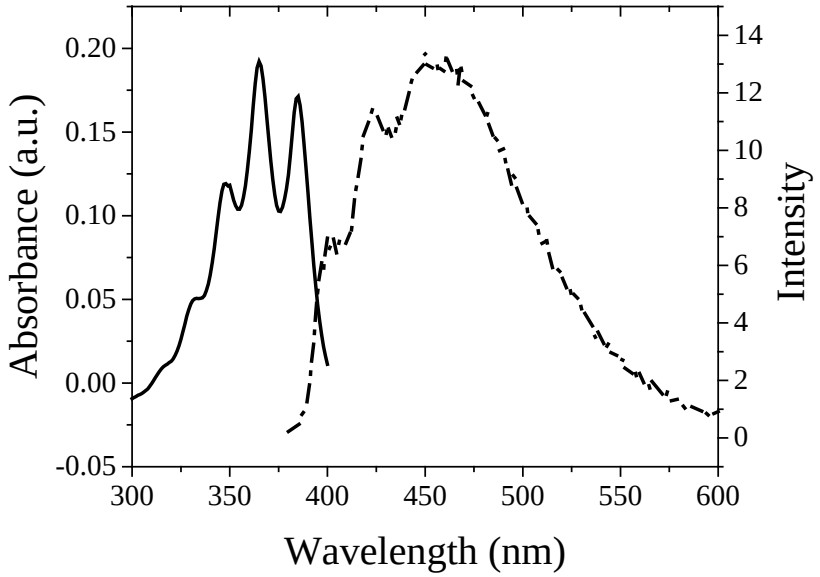

Figure A7. Absorbance (solid) and emission (dashed) of 9,10-ADCA in MeOH.

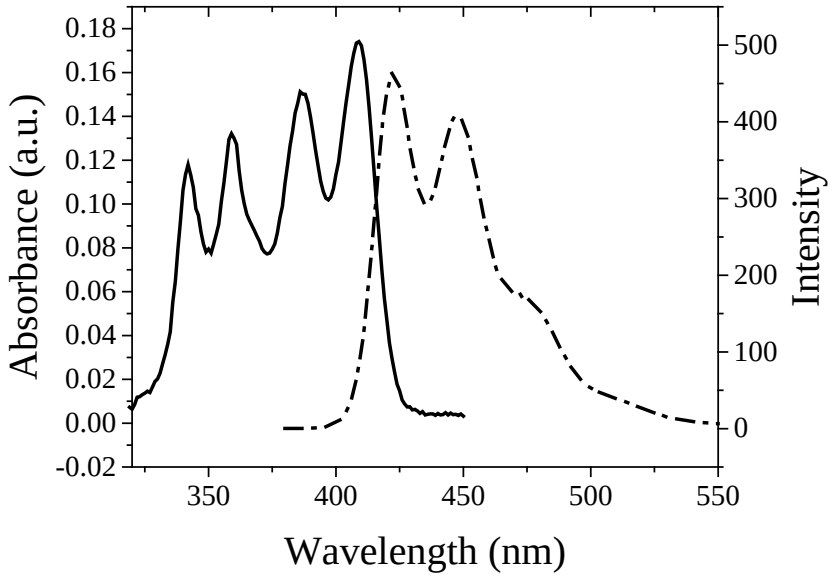

Figure A8. Absorbance (solid) and emission (dashed) of 2,6-ADCA in DMF.

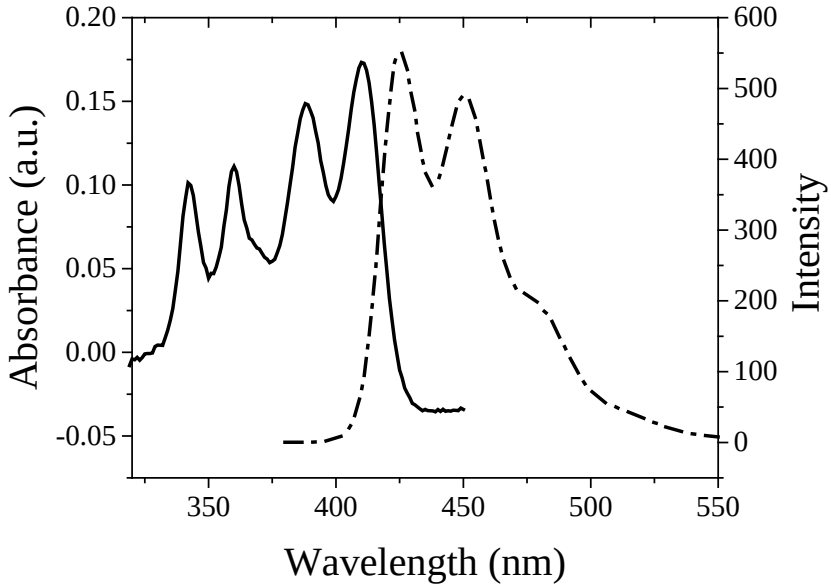

Figure A9. Absorbance (solid) and emission (dashed) of 2,6-ADCA in DMSO.

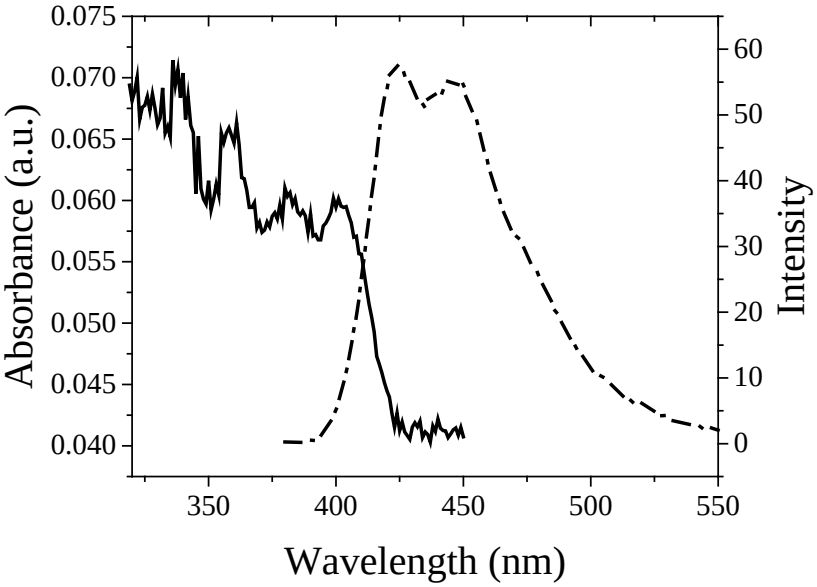

Figure A10. Absorbance (solid) and emission (dashed) of 2,6-ADCA in MeOH.

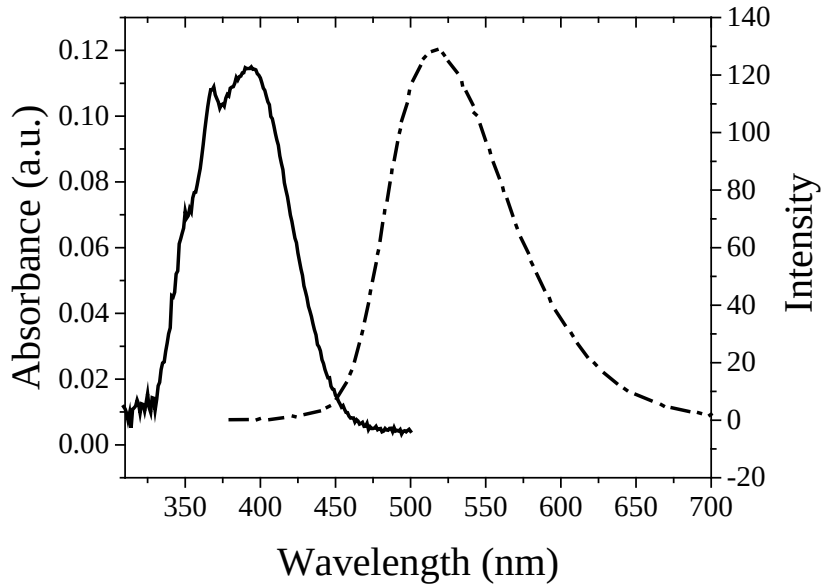

Figure A11. Absorbance (solid) and emission (dashed) of 1,4-ADCA in AcCN.

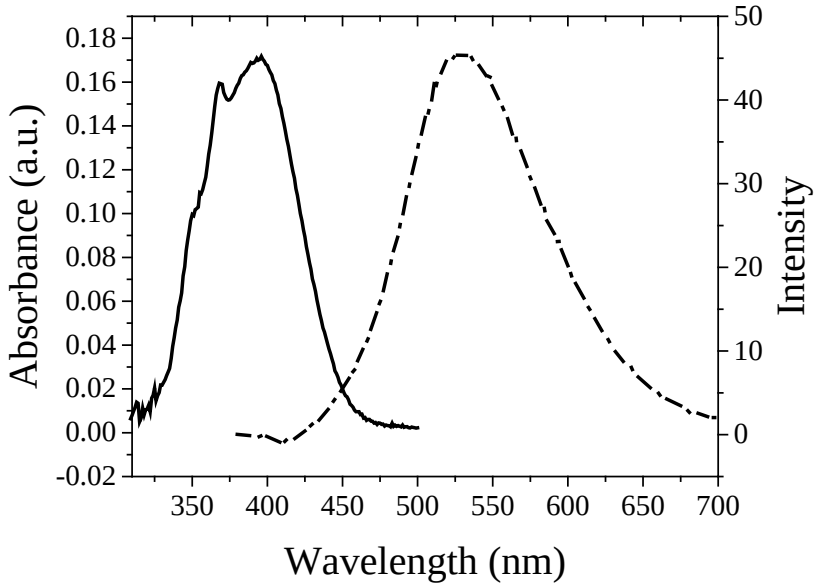

Figure A12. Absorbance (solid) and emission (dashed) of 1,4-ADCA in DMF.

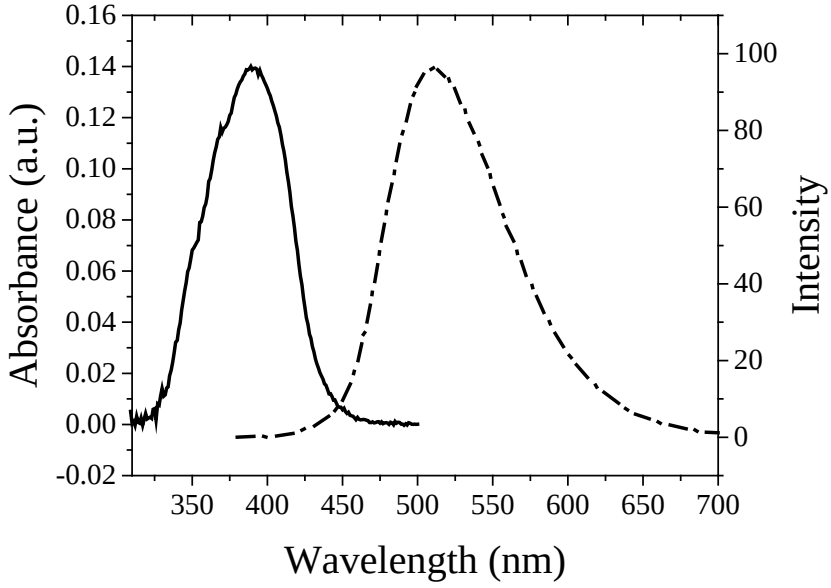

Figure A12. Absorbance (solid) and emission (dashed) of 1,4-ADCA in DMSO.

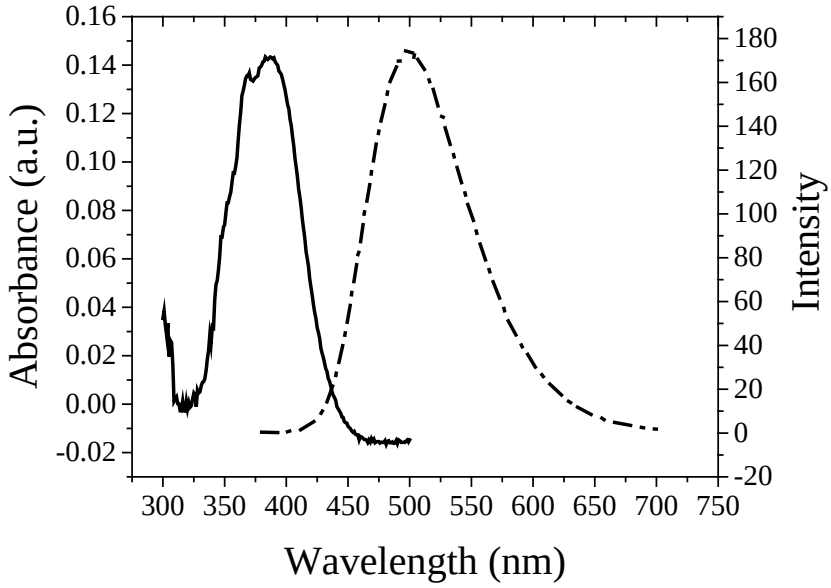

Figure A14. Absorbance (solid) and emission (dashed) of 1,4-ADCA in MeOH.

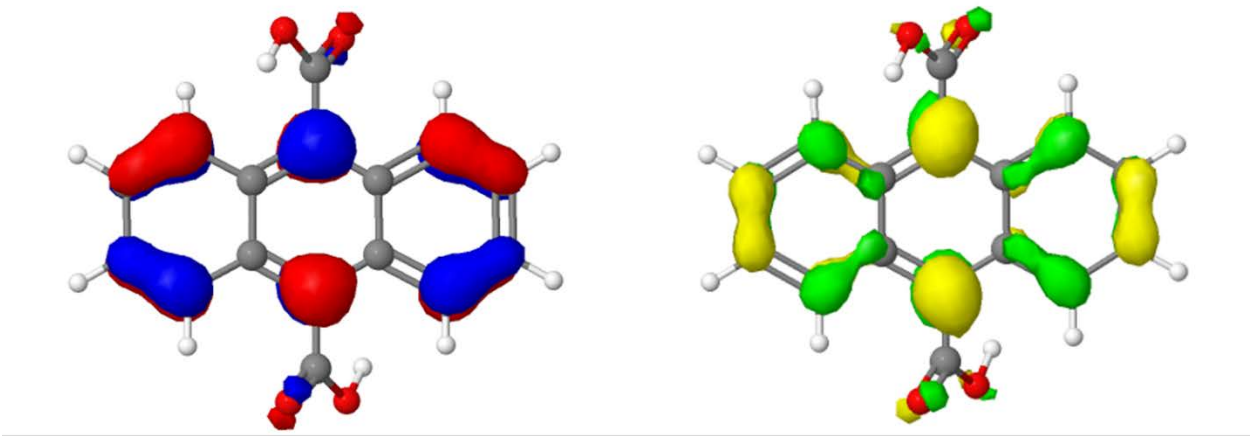

Figure A15. Frontier orbitals of 9,10-ADCA.

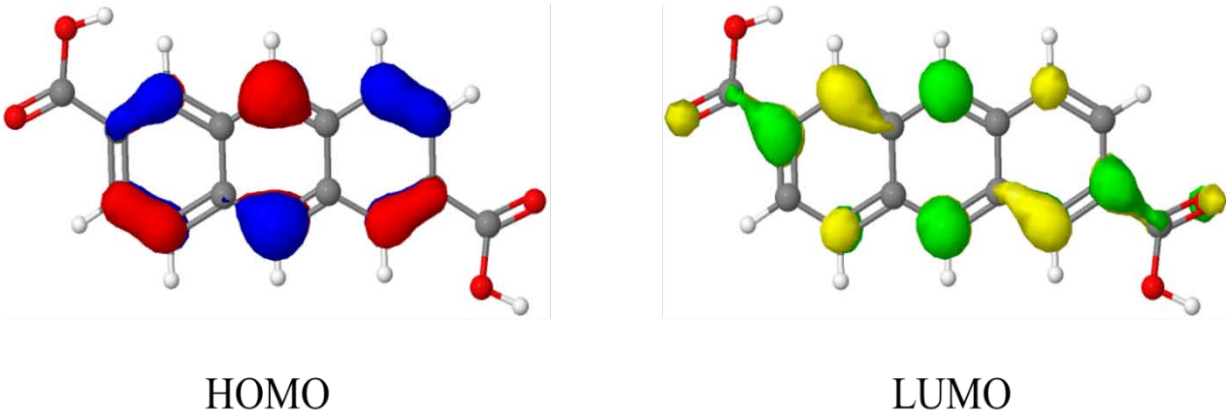

Figure A16. Frontier orbitals of 2,6-ADCA

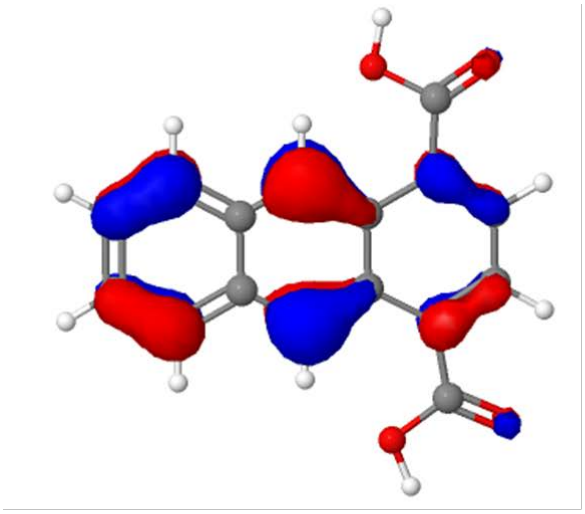

HOMO

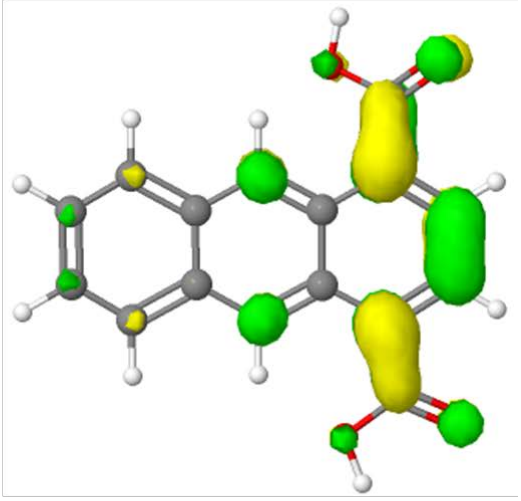

LUMO

Figure A17. Frontier orbitals of 1,4-ADCA

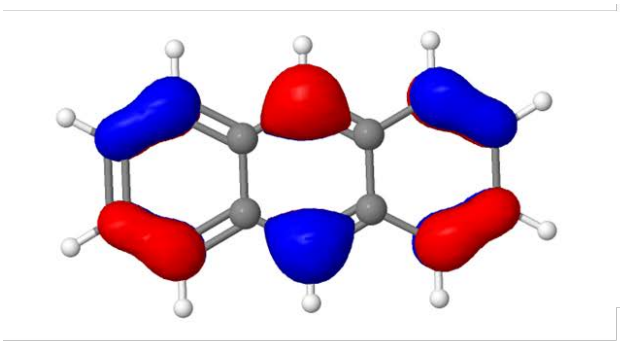

HOMO

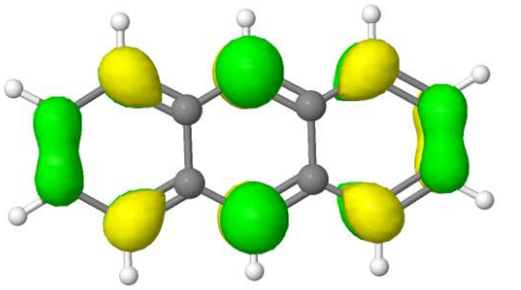

LUMO

Figure A18. Frontier orbitals of anthracene.

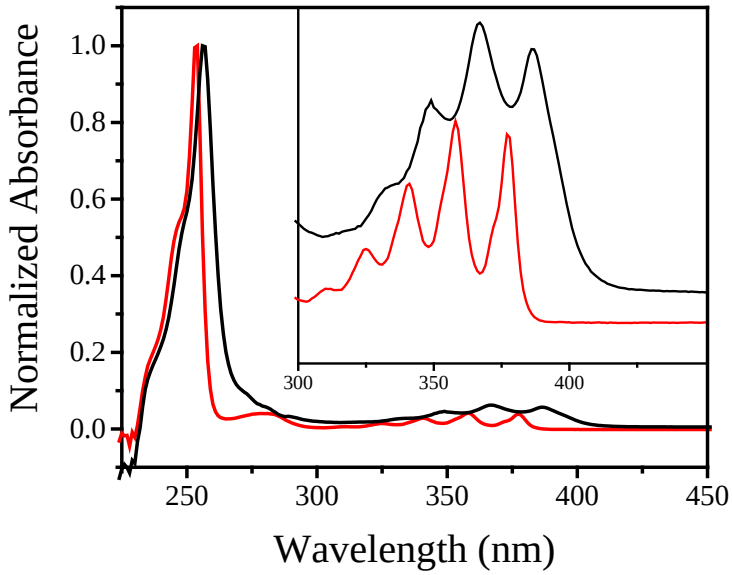

Figure A19. Normalized absorbance of 9,10-ADCA(black) and anthracene(red) in THF.

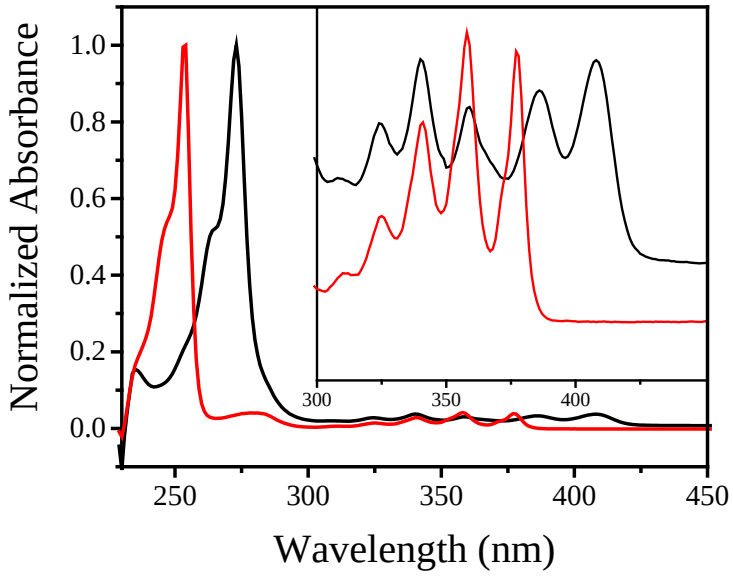

Figure A20. Normalized absorbance of 2,6-ADCA(black) and anthracene(red) in THF.

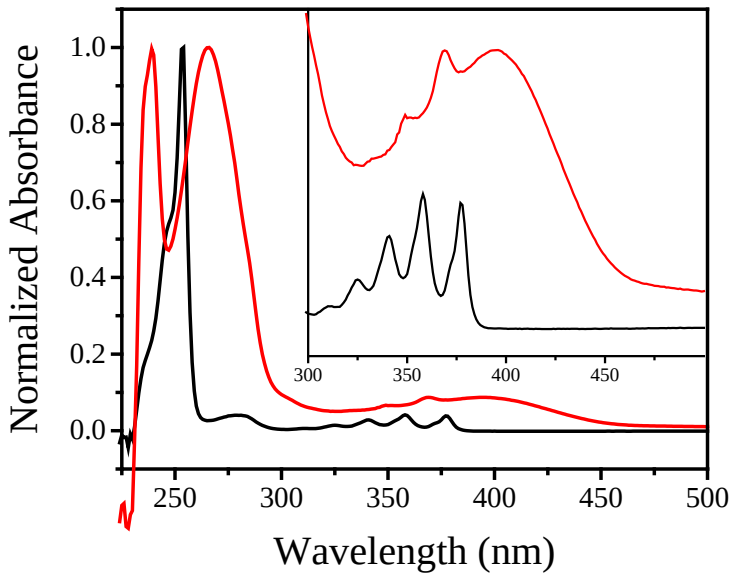

Figure A21. Normalized absorbance of 1,4-ADCA(black) and anthracene(red) in THF.

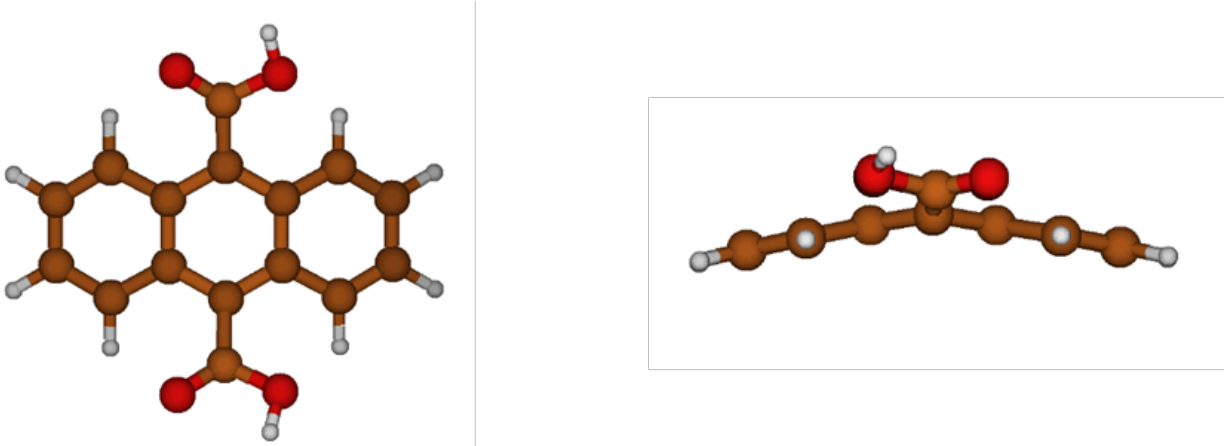

Figure A22. Highest energy conformation of 9,10-ADCA showing the distortion of the anthracene ring when the carboxylic acid groups are coplanar (0°) to the ring system.

Table A1. Polarity/polarizability solvent parameter (π) vs. k_r for 9,10-, 2,6-, and 1,4-ADCA.

	π^*	k_r		
		9,10-ADCA	**2,6-ADCA**	**1,4-ADCA**
DMSO	**1**	6.89 ± 0.77	3.85 ± 1.12	1.75 ± 0.44
DMF	**0.88**	3.24 ± 0.58	4.94 ± 1.05	0.46 ± 0.09
AcCN	**0.75**	3.95 ± 1.45		1.56 ± 0.21
MeOH	**0.6**	2.24 ± 0.59	1.16 ± 0.42	1.57 ± 0.30
THF	**0.58**	6.4 ± 0.69	3.88 ± 1.09	2.88 ± 0.43

Table A2. Index of hydrogen bond acceptor character (β) vs. k_r for 9,10-, 2,6-, and 1,4-ADCA.

	β	k_r		
		9,10-ADCA	**2,6-ADCA**	**1,4-ADCA**
DMSO	**0.76**	6.89 ± 0.77	3.85 ± 1.12	1.75 ± 0.44
DMF	**0.69**	3.24 ± 0.58	4.94 ± 1.05	0.46 ± 0.09
MeOH	**0.62**	2.24 ± 0.59	1.16 ± 0.42	1.57 ± 0.30
THF	**0.55**	6.4 ± 0.69	3.88 ± 1.09	2.88 ± 0.43
AcCN	**0.31**	3.95 ± 1.45		1.56 ± 0.21

Table A3. Index of hydrogen bond donor character (α) vs. k_r for 9,10-, 2,6-, and 1,4-ADCA.

	α	k_r		
		9,10-ADCA	**2,6-ADCA**	**1,4-ADCA**
MeOH	**0.93**	2.24 ± 0.59	1.16 ± 0.42	1.57 ± 0.30
AcCN	**0.19**	3.95 ± 1.45		1.56 ± 0.21
DMSO	**0**	6.89 ± 0.77	3.85 ± 1.12	1.75 ± 0.44
DMF	**0**	3.24 ± 0.58	4.94 ± 1.05	0.46 ± 0.09
THF	**0**	6.4 ± 0.69	3.88 ± 1.09	2.88 ± 0.43

Table A4. Refractive index (η) vs. k_r for 9,10-, 2,6-, and 1,4-ADCA.

	n	k_r		
		9,10	**2,6**	**1,4**
DMSO	**1.479**	6.89 ± 0.77	3.85 ± 1.12	1.75 ± 0.44
DMF	**1.43**	3.24 ± 0.58	4.94 ± 1.05	0.46 ± 0.09
THF	**1.407**	6.4 ± 0.69	3.88 ± 1.09	2.88 ± 0.43
AcCN	**1.344**	3.95 ± 1.45		1.56 ± 0.21
MeOH	**1.329**	2.24 ± 0.59	1.16 ± 0.42	1.57 ± 0.30